1982

Electrochemical Determination of the Heterogeneous Electron Transfer Kinetics of Soluble Spinach Ferredoxin

Charlene D. Crawley
cdcrawle@vcu.edu

College of Humanities and Sciences
Virginia Commonwealth University

This is to certify that the thesis prepared by

Charlene D. Crawley entitled Electrochemical Determination of the Heterogeneous Electron Transfer Kinetics of Soluble Spinach Ferredoxin

has been approved by her committee as satisfactory completion of the thesis requirement for the degree of Master of Science in Chemistry.

[redacted]
Director of Thesis

[redacted]
Committee Member

[redacted]
Committee Member

[redacted]
Committee Member or School Director of Graduate Study

[redacted]
Department Chairman or Representative

[redacted]
School Dean

1/22/82
Date

Electrochemical Determination of the Heterogeneous Electron Transfer Kinetics of Soluble Spinach Ferredoxin

A thesis submitted in partial fulfillment
of the requirements for the degree of
Master of Science at Virginia Commonwealth University

by
Charlene D. Crawley
Director: Dr. Fred M. Hawkridge
Professor of Chemistry
Virginia Commonwealth University
Richmond, Virginia
August, 1981

ACKNOWLEDGEMENTS

First, I'd like to thank Dr. Fred M. Hawkridge for his guidance, kindness and support. He possesses the unusual quality of both skilled researcher and respected leader. I have yet to encounter anyone in my academic career who was more understanding and inspiring.

My decision to pursue a Master's degree here has resulted in many benefits, not solely academic. I have been fortunate to have worked in an atmosphere conducive to personal as well as intellectual growth. I am indebted to Joyce Stargardt and Edmond Bowden, who were instrumental in my decision to join this research group. I am grateful for Ed's willingness to share his knowledge, time and attention. Joyce is the model of what I hope to achieve as a professional and a woman. Both she and Carl are very special people who have generously given of their hearts and lives and have been a great blessing to me.

It is a rare opportunity to work in a group with contributions from people of such diverse backgrounds. I am fortunate to have had the benefit of my interactions with James Castner, Eddie Thomas and Dave Cohen.

I'd also like to thank Dr. Henry N. Blount for his many stories of inspiration and the generous use of his home and research facilities.

Finally, I'd like to acknowledge the support of my parents, Mr. and Mrs. Frank Crawley, and family.

TABLE OF CONTENTS

TABLE OF CONTENTS (continued)

LIST OF TABLES

LIST OF FIGURES

LIST OF FIGURES (continued)

EXAFS

LIST OF ABBREVIATIONS

A	electrode area, cm^2
A_1	primary acceptor species of photosystem I
A_2	secondary acceptor species of photosystem I
Å	angstrom, 10^{-8} cm
A^D	diffusion controlled absorbance of the species monitored
A_N	normalized absorbance
A_O	absorbance of the oxidized reactant
A_R	absorbance of the reduced product
ATP	adenosine triphosphate
C^b	bulk concentration, moles/liter
$C_O(0,t)$	surface concentration of oxidized reactant
$C_R(0,t)$	surface concentration of reduced product
DC	direct current measurement
DCMU	dichlorophenyl dimethyl urea
DME	dropping mercury electrode
D	diffusion coefficient, cm^2/sec
E	applied potential, V
E_{act}	energy of activation, cal/mole deg
$E^{o'}$	formal potential, V
EPR	electron paramagnetic resonance
EXAFS	extended x-ray absorbance fine structure

LIST OF ABBREVIATIONS (continued)

$E_{1/2}$	half wave potential, V
F	Faraday constant, 96,485 coul/mol
Fd	soluble spinach ferredoxin
FNR	ferredoxin-NADP reductase
$\Delta G_c^{\ddagger}$	free energy change for the cathodic process
$\Delta G_a^{\ddagger}$	free energy change for the anodic process
HIPIP	high potential iron sulfur protein
i	current, Amp
i_a	anodic component of the current, Amp
i_c	cathodic component of the current, Amp
IHP	inner Hemholtz plane
i_k	kinetic current, Amp
i_l	limiting current, Amp
i_o	exchange current, Amp
j_o	exchange current density, Amp/cm^2
k_f	heterogeneous rate constant for the forward reaction at a given potential, cm/sec
k_b	heterogeneous rate constant for the backward reaction at a given potential, cm/sec
$k_{f,h}$	formal heterogeneous rate constant for the forward reaction at the formal potential, cm/sec
$k_{b,h}$	formal heterogeneous rate constant for the back reaction at the formal potential, cm/sec
k°	standard heterogeneous rate constant, cm/sec

LIST OF ABBREVIATIONS (continued)

M	metal
MPOTE	metallized plastic optically transparent electrode
MVMG	methyl viologen modified gold
n	number of electrons transferred in the oxidative or reductive process
$NADP_R$	nicotinamide adenine dinucleotide phosphate, reduced form
NHE	normal hydrogen electrode
OHP	outer Hemholtz plane
OTE	optically transparent electrode
ox	oxidized species in a redox couple
PC	plastocyanin
PQ	plastoquinone
PS I	photosystem I
PS II	photosystem II
P_{430}	membrane bound iron sulfur protein(s) of PS I
P_{680}	primary electron donor of PS II
P_{700}	primary electron donor of PS I
Q	primary electron acceptor of PS II
R	(a) gas constant, cal/deg mol, J/deg mol (b) resistance
RDE	rotating disk electrode
red	reduced species in a redox couple
RRDE	rotating ring-disk electrode

LIST OF ABBREVIATIONS (continued)

RSS	rapid scanning spectrometer
SnO_2	tin oxide electrode
SPSC	single potential step chronoabsorb-tometry
T	temperature, °K
t	time, sec
X	primary electron acceptor of PS I
α	electrochemical transfer coefficient
ε	molar absorbtivity, liter/mole-cm
λ	wavelength, nm
η	overpotential, V
ν	kinematic viscosity, cm^2/sec
ω	rotation frequency, sec^{-1}

ABSTRACT

The application of electrochemical techniques to biological systems has become an attractive method for characterizing the redox and electron transfer behavior of biomacromolecules. This study focuses on the role of soluble spinach ferredoxin (Fd) in photosynthesis where it functions as an electron carrier to membrane bound species in the plant chloroplast. An electrochemical model is used wherein Fd now serves as a soluble redox species which undergoes oxidation and reduction via electron transfer at an electrode. This type of model is significant in that both the membrane and electrode reactive sites are characterized by charged bilayer interfacial regions which significantly influence electron transfer rates.

The formal heterogeneous electron transfer rate constant, $k^{o'}_{f,h}$, and the electrochemical transfer coefficient, α, were determined using transient and steady state electrochemical techniques. Transient oxidative and reductive kinetic data were obtained spectroelectrochemically via single potential step chronoabsorptometry (SPSC) at three different surfaces: methyl viologen modified gold (MVMG) minigrid electrodes, tin oxide (SnO_2) semiconductor electrodes and at metallized plastic gold optically transparent electrodes (MPOTE). The steady state measurements were made via hydrodynamic voltammetry at a MVMG rotating ring-disk electrode (RRDE).

Only the modified gold surfaces resulted in behavior suitable

for the determination of heterogeneous electron transfer kinetic parameters. The transient kinetics of Fd were initially evaluated using an irreversible Butler-Volmer kinetic model descriptive of species exhibiting slow rates of electron transfer at an electrode surface. This yielded an average $k^{o'}_{f,h}$ = 6.5 (±1.3) x 10^{-5} cm/sec and α = 0.60 (±0.16) for reductive experiments performed at four different modified gold surfaces. Recently the theory for SPSC was extended to quasi-reversible systems, which undergo moderate rates of electron transfer. Since Fd exhibits quasi-reversible behavior at the MVMG grid, the transient reductive data were reanalyzed using this more exact model. The values obtained using the quasi-reversible model were $k^{o'}_{f,h}$ = 1.16 (±0.5) x 10^{-4} cm/sec and α = 0.42 (±0.06). The corresponding reductive steady state results at the modified RRDE yielded $k^{o'}_{f,h}$ = 5.9 (±0.05) x 10^{-4} cm/sec and α = 0.476 (±0.001). Oxidative experiments were only successful with transient experiments at the MVMG minigrid surface wherein $k^{o'}_{f,h}$ = 3.39 (±0.01) x 10^{-5} cm/sec and α = 1.17 (0.02).

Absorbance data also indicates protein adsorption as a prestep to electron transfer. This type of phenomenon is common to biological molecules reacting at electrodes. The behavior of Fd at these surfaces and the kinetic results are discussed in terms of mechanistic implications.

CHAPTER I

INTRODUCTION

A. Preface

The objective of this work is to characterize the heterogeneous electron transfer behavior of soluble spinach ferredoxin. Spinach ferredoxin is a non-heme iron-sulfur protein which functions as an electron transport agent in plant chloroplasts. The primary reactive sites for this protein are at cell membrane surfaces. As will be elaborated, reactions involving membrane bound species have been shown to exhibit behavior similar to that of reactions occurring at metal electrode surfaces. Electrochemical theory and models will be utilized in the analysis of the kinetic behavior of this system.

B. Background

Unlike traditional solution chemistry where reactions occur predominately between species in the same phase, biological systems are often characterized by interfacial interactions. Since many biological species coexist and react in or on insoluble membrane surfaces, there is a need to understand heterogeneous electron transfer by biological molecules (1).

The direct study of processes occurring at electrode-solution interfaces encompasses a wide area of electrochemistry. The use of electrochemical methods to characterize the electron transfer and redox behavior of biological molecules is a growing field of interest in bioelectrochemistry (2-3).

Biological systems have been predominately characterized using

classical kinetic and thermodynamic treatments. Nernstian reversibility applies to systems at equilibrium and homogeneous kinetics implies that all species involved in reactions are soluble. For many protein and/or enzyme reactions neither is the case. An excellent review on the subject of the relevance of electrodics in characterizing the behavior of biological systems has been presented by Bockris et al. (4).

Classical homogeneous kinetics is based on the premise that all species are governed by mass action theories wherein reactions are rate limited by the collisions of "free" reacting molecules. Cope (5) has shown that cytochrome c oxidase, a membrane bound enzyme which catalyzes the reduction of oxygen by the reduced form of cytochrome c does not conform to the classical mass action treatment of enzyme kinetics. He proposes that a new kinetic theory is required to describe this system as well as similar biological systems wherein the catalytic property of the enzyme is dependent upon the membrane nature of the enzyme and must be characterized using applicable heterogeneous relationships. Though spinach ferredoxin (Fd) does not exhibit enzymatic activity in itself, it catalyzes photosynthesis by channeling electrons from the bound primary electron acceptor complex to the membrane bound flavin enzyme, ferredoxin-NADP reductase, with the concurrent reversible reoxidation of Fd in stoichiometric amounts. In his analysis, Cope cites that "catalysis involves electron conduction through solids in the membrane in accordance with the laws of solid state physics and may also involve electron conduction across the liquid-solid membrane interface in accordance with the behavior of

electrodes" (5). This approach to the study of proteins and biomacromolecules was first introduced by Szent Gyorgy in the early forties (2).

There are currently two main divisions in the thermodynamic theories of biological systems in practice; theories of reversible and non-linear irreversible thermodynamics. Reversible and linear irreversible thermodynamics account for equilibrium and "near" equilibrium systems and are both well established theories. There is current debate over the applicability of linear irreversible thermodynamics in describing the function of metabolic processes in that the formalisms and assumptions are valid only under very limited conditions. A discussion on this matter has been recently reviewed by D. F. Wilson (6).

The most recent branch of thermodynamics used to characterize biological systems, non-linear irreversible thermodynamics, was developed to account for systems far from equilibrium and it is still in its developmental stages (7). However, the laws and equations are derived from classical thermodynamic equilibrium theory. Researchers in the field agree that biological systems are "open", non-equilibrium systems on a macroscopic level and do not exist in a closed environment. However, in developing the theory for non-linear irreversible thermodynamics one assumes the existence of microscopic sub-systems within the macroscopic body (e.g. a cell) which are at equilibrium (5). Therefore the formulations are extensions from classical equilibrium thermodynamics.

The first example cited for the nonapplicability of classical

thermodynamics in describing the behavior of a heterogeneous system was reported by Tafel in 1903 (4). He demonstrated that he could force reactions to occur in a selected direction by applying small currents across the interface of a gas evolving electrode thereby causing a deviation in reversible behavior. In this case, it was shown that the potential difference associated with the reaction is not only described by the concentration of reactants as stated by the Nernst equation, but that overpotential dependence is also apparent when the electrochemical potential of one phase is shifted from the reversible potential. This example becomes relevant to biological systems when one considers that many metabolic processes do not occur under equilibrium conditions and therefore cannot be characterized using Nernstian relationships. This type of "overpotential" dependence is common to electrochemical systems and can be described using Butler-Volmer formalisms which shall be outlined in detail in a later chapter.

Another feature common to the biological membrane surface and the surface at an electrode in solution is the charged bilayer structure existing at both interfaces.

Both mammalian and plant cells are enveloped by a plasma membrane consisting of a bilayer structure of mainly lipids and proteins (8). Lipids define the bilayer or membrane wall with the formation of a discontinuous layer due to the orientation of the ionic and polar lipid head groups with water molecules, that also serve to define the solution side of the bilayer. Two types of proteins are present in the membrane (8). The peripheral proteins are loosely associated with

the membrane and easily removed by extraction with aqueous non-detergent solvents. The integral proteins are more tightly bound with the membrane and can only be solubilized with the use of detergents that also disrupt the bilayer. These proteins play an important role in membrane functions since they serve as binding agents for the enzymes and other components responsible for energy producing reactions of mitochondria and plant chloroplasts.

A model of the lipid-protein membrane structure as described in general biochemistry texts is shown in Figure 1. The heavy lines represent the polypeptide chains of the integral proteins which are partially embedded in or extending out of the lipid bilayer. The bilayer is charged due to the presence of ionic residues on the surface of the protruding integral proteins. This bilayer membrane structure can be related to the double layer structure that exists at metal solution interfaces.

The inner layer of the solution double layer closest to the electrode contains tightly bound ions or "specifically adsorbed" ions (9). This layer is analogous to charged regions of the integral proteins protruding out of the lipid bilayer. The outer layer of the electrode solution double layer is called the diffuse layer and is made up of solvated ions which are not adsorbed on the surface of the electrode and interact via electrostatic mechanisms. A model of the electrode solution double layer is depicted in Figure 2.

Since anions are less apt to be hydrated by solvent molecules, they can approach the electrode surface much easier than solvated cations and are hence more open to adsorption. Therefore, inside the electrical double layer on the solution side there is a highly charged

Figure 1. Lipid-Globular Protein Mosaic Model of the biological membrane structure: a) integral protein, which extends into the bilayer, b) ionic and polar lipid headgroups, c) nonpolar hydrophobic region of the bilayer (8).

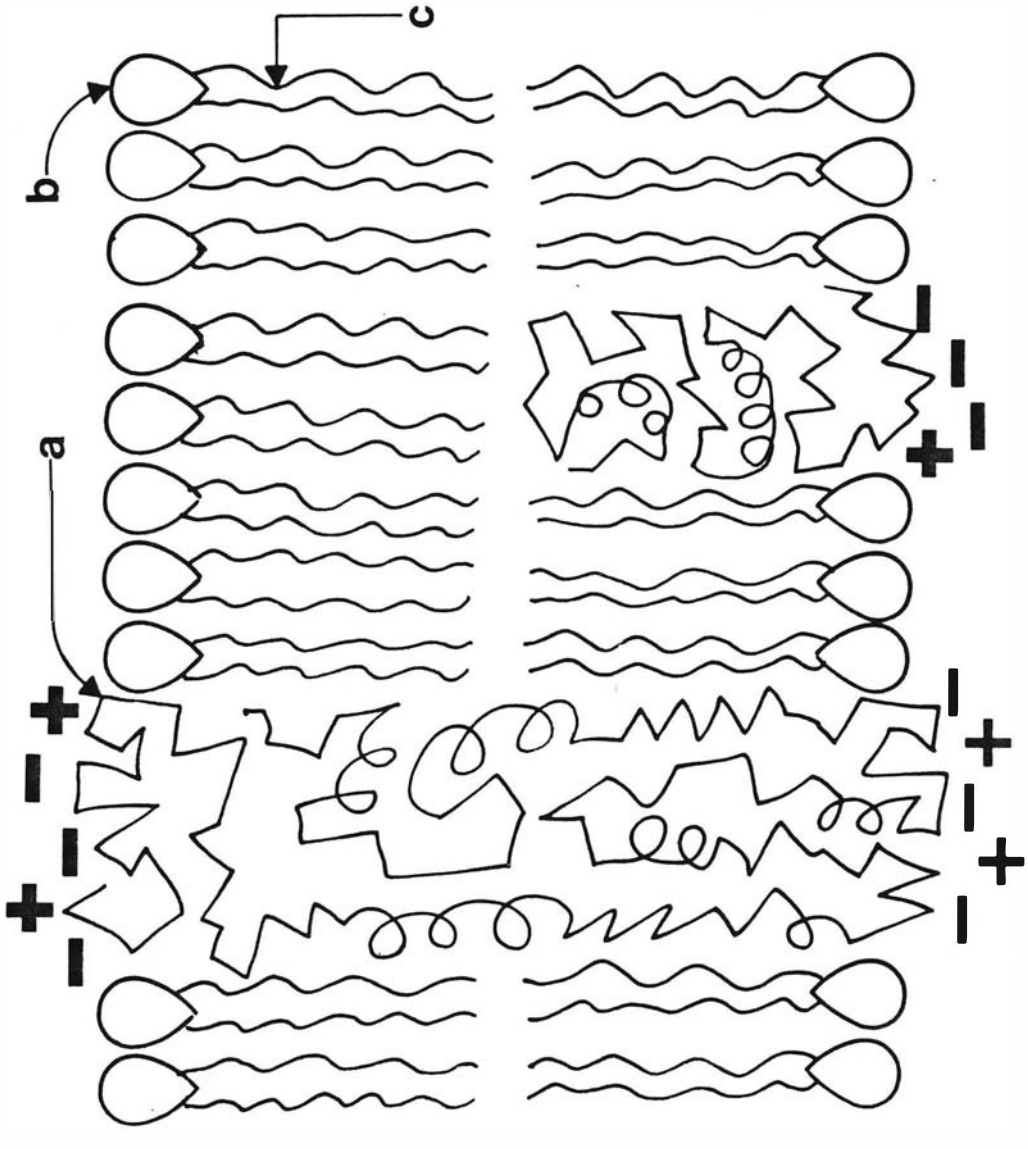
c
b
a

Figure 2. Model of the electrode-solution double layer (9).

a. M = metal electrode surface

b. IHP = inner helmholtz plane

c. OHP = outer helmholtz plane

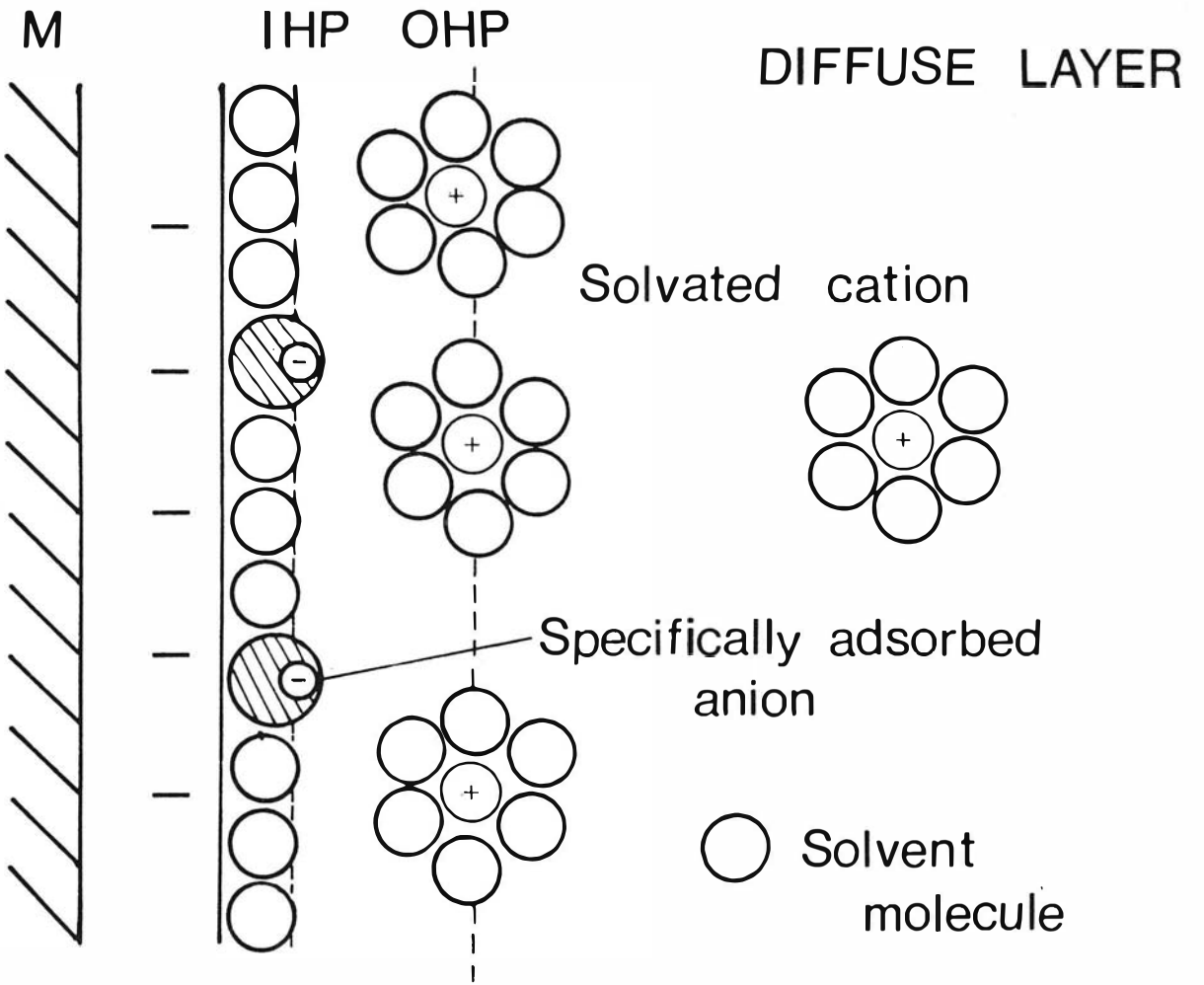
M
IHP
OHP
DIFFUSE LAYER
Solvated cation
Specifically adsorbed anion
Solvent molecule

region close to the electrode surface due to the imbalance of positively and negatively charged species (10). Further away from the electrode into the bulk of solution, this situation relaxes and the proportions become equal. This same type of charge imbalance is also exhibited at the lipid-protein membrane bilayer due to the variation of charges on the integral proteins.

As depicted in Figure 1, one side of the membrane bilayer may be cationic and the other anionic, thus allowing the formation of a membrane potential and hence a site amenable to ion transport across the membrane which form regions of high specificity and reactivity. This situation can be simulated at the electrode-solution interface by varying the potentials at the metal surface and thereby altering the charge of the electrical double layer and hence its reactivity.

Though it is known that pure soluble proteins act as insulators, these "integral" or "structural" proteins have been shown to exhibit electronic conductivity akin to electrodes. A treatise on this subject as well as the three current models for the mechanisms of charge carrier transport in these proteins is described by Simionescu and co-workers (11).

In 1941, A. Szent Gyorgyi first proposed the possibility of structural proteins having semi-conductor characteristics. Gyorgyi postulated that charge transfer interactions may occur with "impurity" molecules which are capable of donating electrons into the conduction bands of these proteins. In 1949, it was theoretically shown with molecular orbital calculations by Evans and Gergeley (12) that these conduction bands are a consequence of electronic conjugation through the π orbitals of the =C=O·····H-N= hydrogen bridges in α and β pro-

teins. This "electrode like" property of structural proteins has been supported and verified by several groups (11).

Because of the complexity of the membrane bilayer structure, the rate controlling step for many protein-enzyme reactions is the formation of the reactant complex at the surface of the membrane which is analogous to the effect of the electrical double layer structure at an electrode on the electron transfer or charge transfer reactions occurring across the metal-solution interface. A study of the reaction rate of both systems must therefore take into account the properties of the surface. Hence the biological liquid-solid interface shows similar electrical behavior to the electrode surface which should then allow for correlation between phenomena exhibited by both systems.

The work presented here is not biochemical in nature. The experiments and theory deal with electrochemical phenomena observed for a biological molecule. Reactions in living systems are much more complex than the simple electrode models chosen here to exemplify them. Nevertheless, attempts will be made to point out similar behavioral characteristics, when applicable, to clarify the theoretical considerations used. The two types of electrochemical methods used to characterize the heterogeneous electron transfer behavior of spinach ferredoxin are spectroelectrochemistry and rotating disc hydrodynamic voltammetry.

CHAPTER II

PHYSICAL CHARACTERISTICS OF FERREDOXINS

A. Role of Spinach Fd in Photosynthesis

Ferredoxin participation has been characterized in photophosphorylation (photosynthesis), nitrogen fixation and bacterial fermentation. Due to current interest in energy conversion processes the main focus presented here will be on the role of soluble spinach ferredoxin in photosynthesis. Research in the area of photosynthesis spans a period of over two centuries and a vast amount of literature has been produced on the subject. A brief outline of the most widely accepted mechanism for photosynthesis, as well as pertinent references in the area will be given.

Photosynthesis in green plants can be characterized as the light dependent reduction of carbon dioxide to the level of carbohydrates coupled to the oxidation of water to molecular oxygen (13).

$$H_2O + CO_2 \xrightarrow{h\nu} (CH_2O) + O_2 \qquad (1)$$

In green plants, this process is accomplished by very organized cell bodies called chloroplasts. Each cell may contain from 50-200 chloroplasts ranging from 3-10 μm in diameter (5). The chloroplasts are bounded by a double membrane envelope. The outer membrane envelope is a lipid bilayer. The inner membrane envelope is the permeability barrier and contains systems for the transport of certain metabolites. This barrier is impermeable to large molecules, protons, hydroxyl ions and most charged molecules (5). Within this boundary internal

membranes consisting of closed flattened sacs called thylakoids reside which in particular regions may be stacked in groups to form grana. The space between the inner membrane and the thylakoid membrane is called the stroma. Thylakoid membranes contain all of the light absorbing pigments, electron transport components and enzymes required for ATP synthesis (13). The stroma contains the enzymes of the Calvin cycle (by which CO_2 is reduced to carbohydrates) and the necessary components for protein synthesis and enzymes of other biosynthetic pathways (13).

Early research established that the thylakoid membrane of green plants contains two types of photosynthetic units known as Photosystem I (PS-I) and Photosystem II (PS-II). Via a mechanism known as noncyclic photophosphorylation these two photosystems accomplish light induced electron transport from water to evolve oxygen with the concomittant production of Adenosine Triphosphate (ATP) and nicotinamide adenine dinucleotide phosphate-reduced $(NADP)_R$ (14, 15). Figure 3 is a schematic diagram of these two photosystems and the Z scheme for photophosphorylation (16). Recent evidence has supported the possibility that yet another mechanism, cyclic photophosphorylation, which is postulated as the mechanism for ATP synthesis in bacterial species, may occur in conjunction with the Z scheme in green plants (17).

Excitation of PS II by light of ~680 nm causes the electron donor, P_{680}, which is a specialized form of chlorophyll a, to transfer an electron to an acceptor species, Q, which is a form of plastoquinone. This acceptor is a mild reductant and upon oxidation transfers electrons via a chain of electron carriers to reduce the primary

Figure 3. Z-scheme for photosynthesis in green plants presented in terms of the potential gradient (16) where: P680 is the primary donor of PS II which absorbs light of 680 nm, Q is the primary acceptor species of PS II, P700 is the primary electron donor of PS I, P430 is the bound iron sulfur proteins, which are candidates for the primary electron acceptor species, X, FD is soluble ferredoxin, FNR is ferredoxin-NADP reductase, and NADP is nicotinamide adenine dinucleotide phosphate.

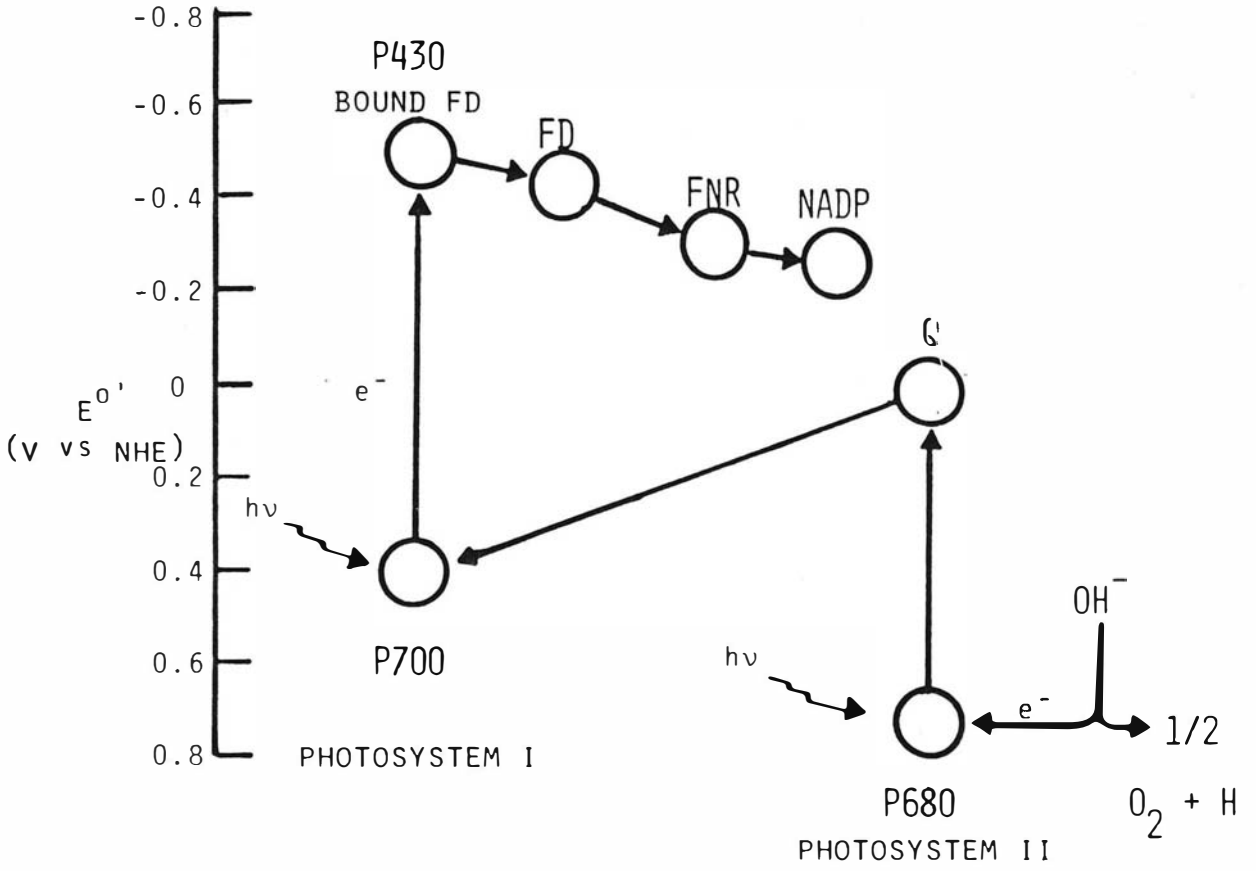

GENERAL MECHANISM FOR PLANT PHOTOSYNTHESIS

electron donor of PS-I, P_{700}. P_{700} can then be photo-oxidized by light of 700 nm after which it donates an electron to the primary electron acceptor complex.

To date, it has been postulated that this complex is comprised of four different membrane bound acceptors (18):

(1) A_1 primary acceptor, a photo-reducible chlorophyll

(2) A_2 secondary acceptor, (possibly component X)

(3) Centers A and B - two iron-sulfur proteins which are also referred to as P_{430}

There is discrepancy in the literature as to which of these species is actually the primary electron acceptor of PS-I which is designated as component X (18, 19). It has recently been proposed that P-430 might also function as such (20, 21). However the majority of researchers do agree that component X is a membrane bound iron-sulfur protein. Soluble ferredoxin then mediates electron transfer from the bound acceptor to a membrane bound enzyme, ferredoxin-NADP reductase (22) resulting in the re-oxidation of ferredoxin and the reduction of NADP (See Figure 4). The reduced NADP then initiates a set of dark reactions, namely the Calvin cycle, in which CO_2 is reduced to carbohydrates. Therefore the reduction of ferredoxin is the terminal photochemical event occurring in the conversion of radiant energy into chemical energy (23-26).

The ability of chloroplasts to reduce ferredoxin in the light initiated reactions is of interest to researchers in the field of energy conversion processes. Ferredoxin has a potential very near that of the H^+/H_2 couple at pH 7 ($E^{\circ\prime}$ Fd = -423, (27)), therefore from a thermodynamic viewpoint photosynthesis can also facilitate

Figure 4. Photosynthetic electron and proton movement across the thylakoid membrane in green plants (14) where: Mn is manganese, P680 is the primary donor of PS II, Q is the primary acceptor species of PS II, PQ is plastoquinone, DCMU is dichlorophenyl dimethyl urea, which is a herbicide and inhibitor to PS II, cyt f is cytochrome f, PC is plastocyanin, P700 is the primary electron donor of PS I, X is primary electron acceptor of PS I, fd is soluble ferredoxin, reductase is fd-NADP reducing enzyme, and NADP is nicotinadmie adenine dinucleotide phosphate.

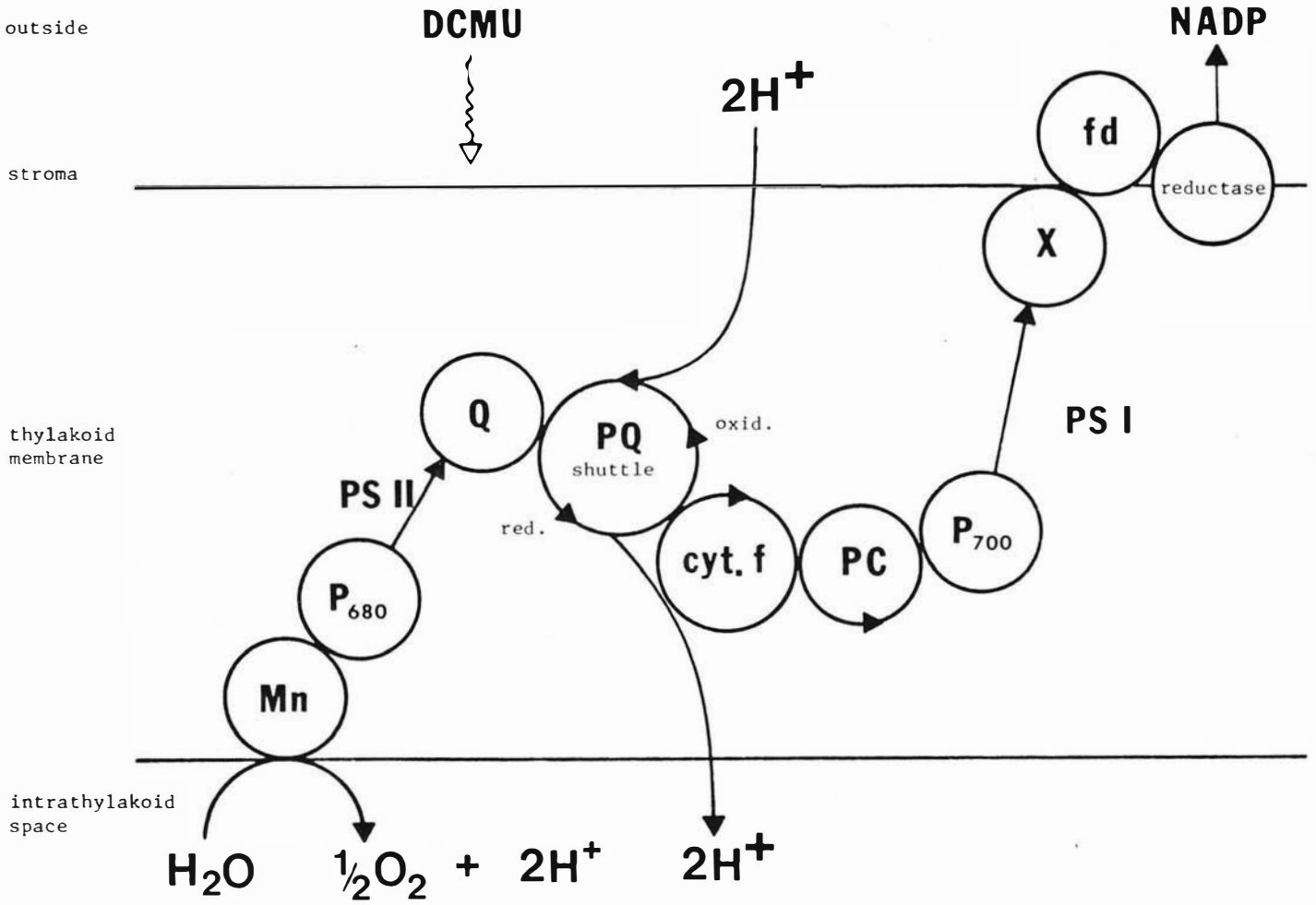
outside
DCMU
NADP
2H+
stroma
fd
reductase
X
thylakoid membrane
Q
PQ
shuttle
oxid.
red.
PS II
PS I
cyt. f
PC
P700
P680
Mn
intrathylakoid space
H2O
½O2 + 2H+
2H+

the decomposition of water to produce molecular hydrogen, which is a potential source of fuel. A knowledge of the detailed mechanism should then allow researchers to mimic this process synthetically and produce devices for fuel production that simulate photosynthetic quantum conversion (14).

B. Classification of Spinach Ferredoxin

Iron containing proteins can be broadly classified into two main categories: (1) heme-type proteins which contain the Fe-porphyrin ring as the prosthetic group, and (2) non-heme-type proteins wherein the class of iron-sulfur proteins is included. Iron-sulfur proteins are characterized generally as iron-containing proteins having the Fe-S chromophore as the prosthetic group. These proteins can be further specified by exhibiting one or more of the following properties (28): (a) acid-labile sulfur, (b) absorption bands between 350 and 600 nm, (c) capability of transferring electrons at a low oxidation-reduction potential, and (d) paramagnetism as detectable by EPR in one or more oxidation states.

Ferredoxins are iron-sulfur proteins that function primarily as electron-carriers in various metabolic processes. They are distinguished from other iron-sulfur proteins by their ability to interchangeably catalyze the photoreduction of NADP by isolated chloroplasts. Other inherent features include (29): (a) characteristic composition and sequence of amino acids, (b) low molecular weight (6000 - 13,000 daltons), and (c) redox potentials close to that of hydrogen gas (E° = -420 mV (NHE)). They are further divided into subclasses depending upon the systems in which they transfer elec-

trons, i.e. bacterial, plant and others. A review of the characteristic properties of ferredoxin has been reported by Malkin and Rabinowitz (30). Table I shows the nomenclature of the three classes as initially designated by Buchanon and Arnon in a review of the chemistry and function of ferredoxins (31). This system has since been modified as its widespread use is only valid in literature appearing before 1973. Since then more recent guidelines for the classification and nomenclature of iron-sulfur proteins has appeared (see Table II (32)). Notably, the Fe-S chromophore is now designated as an iron-sulfur cluster.

C. Physical Properties

Spinach ferredoxin contains the 2Fe-2S iron cluster and functions as a one electron carrier. It was first isolated and characterized by Tagawa and Arnon in 1962 (33). The charge on the cluster is +2 in the oxidized form $[2Fe\text{-}2S]^{+2}$, and +1 in the reduced state $[2Fe\text{-}2S]^{+1}$.

The two iron atoms in the active site are antiferromagnetically coupled and each one is coordinated to four sulfur ligands in a distorted tetrahedral configuration (34). A bridge between the two iron atoms is formed via two inorganic sulfur ligands and each iron is also coordinated to two cysteinyl sulfur atoms (see Figure 5). In the oxidized form both iron atoms are high spin, ferric; upon reduction one of the irons is converted to high spin ferrous (35).

Due to the antiferromagnetic coupling interaction the unpaired electron on one Fe atom has opposite spin orientation to the unpaired electron on the second Fe atom which is manifest in the diamagnetism exhibited in both the oxidized and reduced forms of the molecule at

TABLE I (31)

System of Nomenclature for Various Types of Ferredoxins

Class	Occurrence	Representative Type	Characteristics
Ferredoxin a	Fermentative (nonphotosynthetic) and photosynthetic green anaerobic bacteria	Clostridium pasteurianum	Contains more than 2 (Fe-S) clusters per molecule; molecular weight ~6000
Ferredoxin a_1	Photosynthetic purple sulfur anaerobic bacteria	Chromatium strain D	Contains 7-8 (Fe-S) clusters; molecular weight ~10,000
Ferredoxin b	Algae and higher plants	Spinach chloroplast	Contains 2 (Fe-S) clusters; molecular weight ~12,000
Ferredoxin c	Aerobic nitrogen-fixing bacteria	Azotobacter vinelandii	Contains 6 (Fe-S) clusters; molecular weight ~120,000

TABLE II (32)

Classification of Iron-sulfur Proteins

I. Simple iron-sulfur proteins

A. Rubredoxins (Rd) - This group contains iron-sulfur proteins without acid-labile sulfur

1. 1-center Rd

2. 2-center Rd

B. Ferredoxins (Fd) - This group comprises iron-sulfur proteins that contain an equal number of iron and labile-sulfur atoms

1. 2 iron Fd

a. 1-cluster Fd (2Fe/cluster)

b. 2-cluster Fd (2Fe/cluster)

2. 4 iron Fd

a. 1-cluster Fd (4Fe/cluster)

b. 2-cluster Fd (4Fe/cluster)

C. Other (simple) iron-sulfur proteins - This group includes all simple iron-sulfur proteins that are neither rubredoxins or ferredoxins

II. Complex iron-sulfur (IS) proteins

A. IS Flavoproteins

B. IS Molybdenum proteins

C. IS hemoflavoproteins

D. Others

Figure 5. Structure and properties of soluble spinach ferredoxin (42)

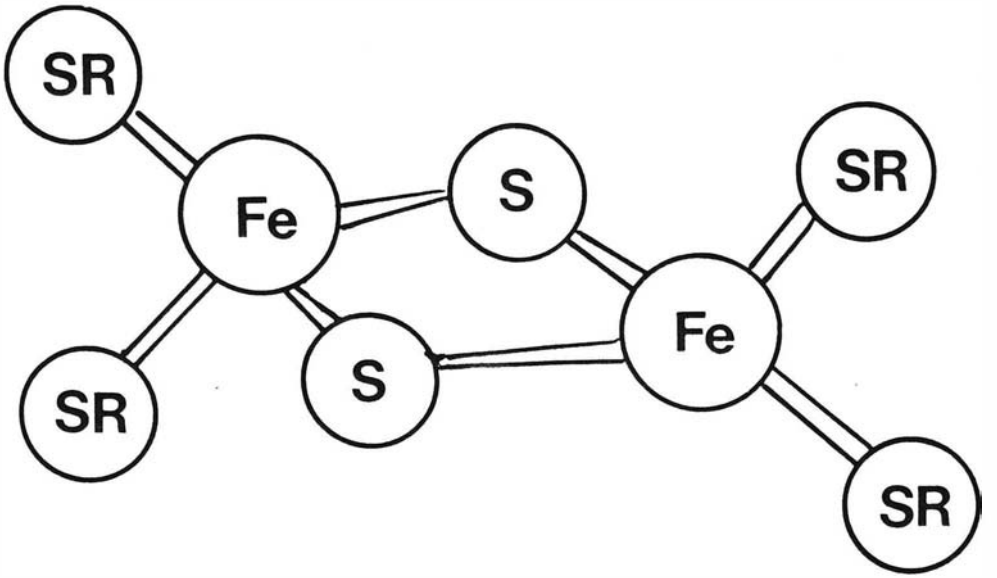

SPINACH FERREDOXIN

Molecular Wt	11,000 ± 1000
$E^{o'}$	−428 mv vs NHE
λ_{max}	420 nm
$\Delta\varepsilon$	5130 $M^{-1} cm^{-1}$

low temperatures (e.g., 77° K) (36). Reduced spinach ferredoxin is paramagnetic at room temperature and is characterized by exhibiting an EPR signal with g_x = 1.89, g_y = 1.96, g_z = 2.05 (37). A molecular orbital schematic diagram of the probable configuration of the Fe-Fe spin coupled system in a tetrahedral environment, which is analogous to the active center of Fd is depicted in Figure 6.

According to this scheme an electron would be placed into the $d^*_{z^2}$ antibonding molecular orbital upon reduction of the molecule, which would then cause it to be paramagnetic. If the $d^*_{z^2}$ level was very strongly antibonding reduction would be predicted to occur at low potentials. The antibonding effect of this orbital can be lessened by a slight elongation of the Fe-Fe distance and by a slight bending of the Fe_2S_2 center across the S-S bond upon reduction which would allow reduction to occur at more positive potentials (37). X-ray crystallographic data on the active site of the Hi-potential iron sulfur proteins (HIPIP) has shown that the Fe-S cluster expands significantly upon acceptance of an electron (38). One distinguishing feature of these proteins is their relatively positive redox potentials. However, plant ferredoxins have not been shown to undergo such a significant conformational change in the active site upon reduction which is postulated as one reason for its low reduction potential.

Each Fe atom in the cluster is attached to the protein portion which consists of 97 amino acid residues via two cysteine groups (39). The content of acidic amino acids is higher than that of basic amino acids (40) and the total charge on the protein is calculated to be as large as -17 at pH 7 (41). The molecular weight as determined by

Figure 6. Schematic diagram of Fe-Fe molecular orbitals in a ferredoxin model compound (37).

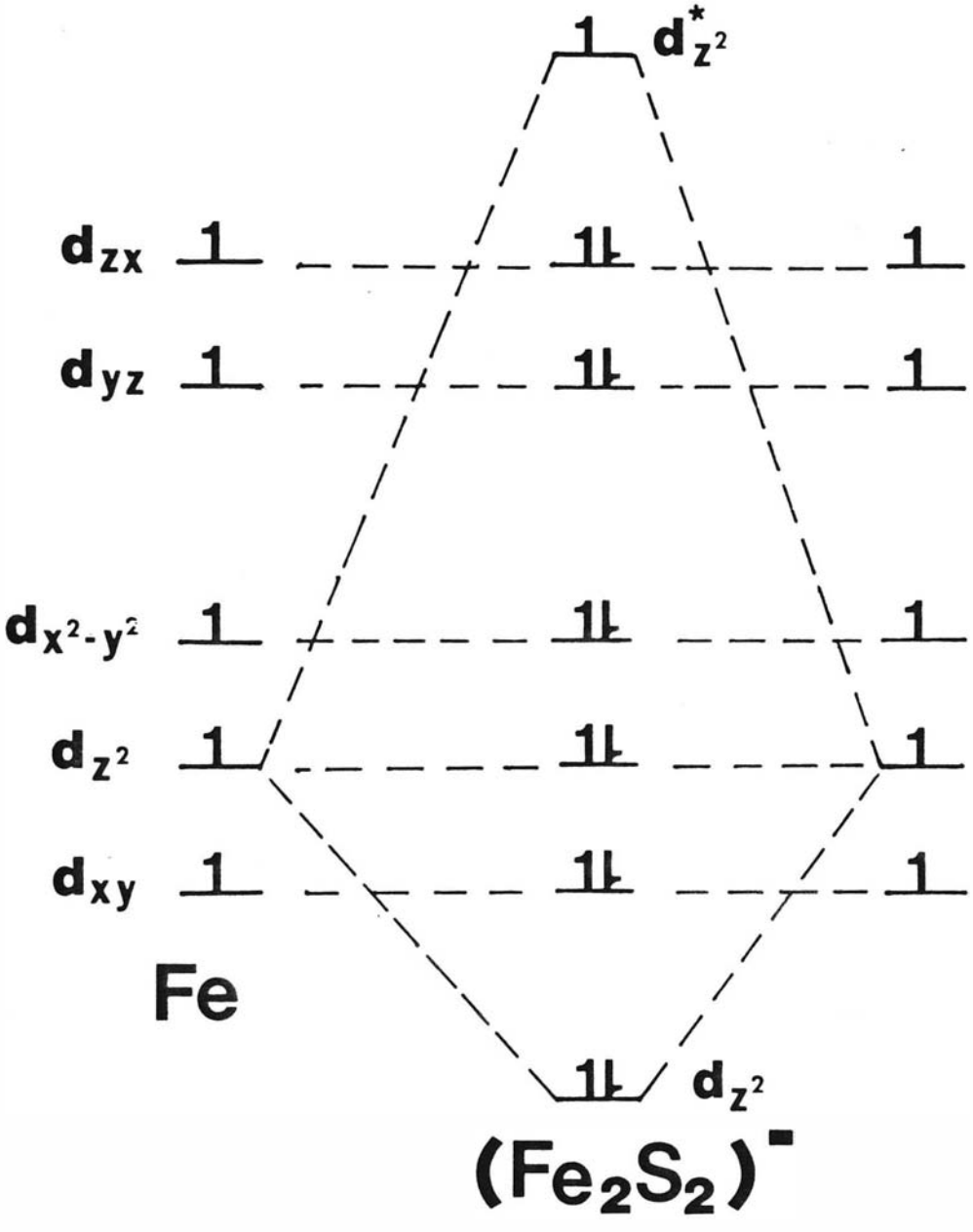
$d^*_{z^2}$
d_{zx}
d_{yz}
$d_{x^2-y^2}$
d_{z^2}
d_{xy}
Fe
d_{z^2}
$(Fe_2S_2)^-$

Tagawa and Arnon is 11,640 (42) and the formal potential ($E^{\circ\prime}$) is -420 mV vs. NHE at pH 7.5.

D. Absorption Spectrum

Spinach ferredoxin, like all oxidized iron sulfur proteins, is characterized by distinctive absorption maxima of low molar absorptivity superimposed on a broad background absorbance which increases progressively from 700 nm to 300 nm (43). The spectrum of the reduced species is characterized by a marked peak in the UV region at 267 nm, a shoulder at 312 nm and a broad shoulder between 450 and 470 nm. The oxidized form exhibits absorption maxima at 463, 420, 325 and 274 nm (33).

Reduction causes a loss in absorbance at all wavelengths longer than 300 nm. Protein denaturation also results in the loss of the 420 and 465 nm bands. Ferredoxins are sensitive to oxygen and will readily denature under aerobic conditions at relatively low salt concentrations (44, 45).

In a study of the near IR spectrum of non-heme proteins by Wilson (43), it was proposed that the 714 nm band of spinach ferredoxin may be sensitive to protein conformational changes occurring in the molecule. Band assignments and IR spectra for the 1200-600 nm regions have been reported for the oxidized and reduced forms by Rawlings *et al.* (46).

E. Structure-Function Relationship

To date no X-ray crystallographic structure has been determined for spinach ferredoxin. However, a 3.5 Å resolution X-ray analysis was performed on a similar plant-type ferredoxin, *spirulena platensis*

(47). This protein contains the familiar 2Fe-2S cluster, has 98 amino acid residues and a molecular weight of 10,890. An electron density map revealed the iron cluster to be 8 Å from the surface of the protein matrix with the probability that portions of it might be exposed. A similar study on another chloroplast type of ferredoxin from blue green algae, aphanothece sacrum, which is characterized by having 96 amino acid residues and a molecular weight of 10,480, also indicated that the iron cluster was located near the surface of the molecule (48).

Detailed X-ray analyses have been performed on synthetic analogues of the 2Fe-2S chromophore (49). The presence of the chromophore in the model compound was substantiated by the similarity of the electronic spectrum to that of native plant ferredoxins; (small differences were attributed to solvent effects since analogues were only soluble in non-aqueous solvents).

Polarographic studies revealed that reduction of the analogue occurs at much more negative potentials than that of the 2Fe-2S species in the protein matrix of the native ferredoxin. This implies that the protein seems to cause electron transfer to be more "energetically" feasible. A detailed review of the structure-function relationship of proteins that exist in electron transfer biomolecules has been presented by Adman (50). From results of a theoretical study by Sarai (51) on the role of the protein matrix in controlling the rate of electron transfer in electron transport agents, it was postulated that the "protein environment is important in controlling the irreversibility of electron transfers and minimizing the energy

dissipation due to back reactions".

Extended X-ray absorbance fine structure (EXAFS) spectroscopic studies on a 2Fe-2S plant type ferredoxin (rhubarb) and a corresponding synthetic analog were performed by Teo and co-workers (52) to discern the effect of the protein on the active site as well as to determine structural parameters for the prosthetic group.

In monitoring changes in bond length in the Fe-S and Fe-Fe bonds upon reduction of the protein and its synthetic analog, they attempted to correlate the effect of strain energy at the active site on the redox reactions. They found that there were small, though significant changes upon reduction of the model compounds that were comparable to analogous changes detected in the native protein species. EXAFS results were reported to be accurate to better than 0.02 Å in Fe-S and 0.03 in Fe-Fe bond distances for the model compounds. The average Fe-S and Fe-Fe distances were determined to be 2.234 Å and 2.704 Å in both the analog and the plant species, respectively. Upon reduction the Fe-S distance in plant Fd changes from 2.23 to 2.24 Å, and the Fe-Fe distance changes from 2.726 to 2.762 Å. From these results it was concluded that if there was any strain energy present in the native species it would be "manifest" within the polypeptide region rather than being stored in the redox center. Therefore only small changes were detected in the geometry and bond lengths upon reduction.

To summarize the results of the studies presented (i.e. polarographic vs. structural changes) on the synthetic analogs versus native protein species, one could postulate that the protein seems to enhance

electron transfer at the active site in a manner which is not attributable to or manifest by changes in the Fe-S, Fe-Fe bond lengths. One should note, however, that studies involving X-ray methods can only determine the static structure of the molecules. Therefore, the role of the protein in enhancing the electron transfer behavior of electron carrier molecules may be more complex than effects postulated from merely structural arguments. Other studies are necessary wherein features of the molecule are monitored concomittantly with the redox reactions.

Cowan et al. (53) measured the electrical conductivities of a ferredoxin model compound in comparison with other active system models in studying its electron transfer behavior and concluded that rate enhancement is a function of the nature of the active center in conjunction with the effects of the polypeptide portion.

For the simple inorganic Fe^{2+}/Fe^{3+} reaction in solution:

$$Fe^{2+}(H_2O)_6 + Fe^{3+}(H_2O)_6 \rightarrow Fe^{3+}(H_2O)_6 + Fe^{2+}(H_2O)_6 \qquad (2)$$

the rate constant is 10^{-3} to 10^{2} $M^{-1}sec^{-1}$ compared with 10^{4} to 10^{8} $M^{-1}sec^{-1}$ for iron containing biological electron carrier molecules. Cowan attributes this large difference in rate constants to a combination of two factors: (1) the lack of short range order in the simple inorganic system which can be achieved in biological systems via the membrane structure, and (2) large bond length and geometrical changes required in the hydration sphere of the aquated species.

Since electron transfer is fast compared to nuclear motions

(Franck-Condon Principle) rapid electron transfer reactions require the initial and final states to have similar geometries and bond lengths (53). Slow electron transfer in the aquation reaction is attributed to the fact that reorganization of the surrounding ligands is required either before, during or after electron transfer.

In addition Cowan observed that the electrical conductivity, hence rate of electron transfer, was larger in a mixed valent organometallic compound biferrocene (Fe(II)-Fe(III)) picrate I

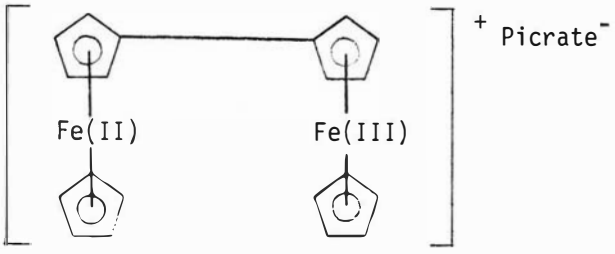

which was attributed to a short range electron hopping mechanism occurring between the two centers. In this study they compared electronic measurements of a number of inorganic model centers and found that the overall conductivity of the ferredoxin model was larger. The Fe atoms in the model were bound tetrahedrally to sulfur and the Fe-Fe interatomic distance was 2.7 Å. Cowan summarized a number of factors which would contribute to the rapid rates of electron transfer exhibited by biological carrier molecules (53): (1) short range order (membrane structure), (2) mixed valence compounds or mixed valence arrays of carriers, (3) little required geometrical or bond length changes in going from the initial to the final state, (4) linear pathway, (5) small changes in spin quantum number, (6) exo-

thermic reactions, (7) low charged complexes to reduce coulombic repulsions, (8) matched redox potential of donor and acceptor, and (9) delocalized or highly polarizable ligands.

F. Redox Characteristics

The unique feature of ferredoxins is their ability to transfer electrons of strong reducing power as indicated by their low negative redox potentials. Therefore it is apparent that a knowledge of the stoichiometry and energetics of these proteins is crucial in discerning their function as electron transport agents. One of the major problems encountered in determining these parameters is the availability of reagents capable of reducing them quantitatively in the presence of oxygen. As previously mentioned, reduced ferredoxins are inherently unstable under aerobic conditions (45).

Photochemical reduction is accomplished *in vivo* by isolated chloroplasts and intact thylakoid fragments. Plant chloroplasts in the presence of light of appropriate wavelengths are capable of generating more than adequate reducing power to completely titrate stoichiometric amounts of ferredoxin at native pH. The extent of reduction is measured spectroscopically. However, since ferredoxins typically exhibit absorbance maxima of low molar absorptivity in the visible region, highly absorbing electron carriers and/or enzymes present in the chloroplast may interfere with the signal of interest. This problem can be alleviated, however, with the use of physiological or chemical reagents.

Physiological enzyme systems such as hydrogenase in the presence of equally negative redox couples are commonly used to re-

duce low potential biological redox molecules. The most common method involves equilibration of the H_2-hydrogenase system with the protein. However, the extent of reduction is pH dependent. Reduction greater than 90% can only be achieved above pH 8 (42) and precise environmental control over such variables as temperature and pressure is crucial. Stombaugh and co-workers (54) measured the formal potentials and number of electrons transferred for a number of low potential iron sulfur proteins using the H_2-hydrogenase reductant under varying solution conditions. This system was amenable to spectroscopic detection without the interference of intermediates. However, loss of chromophore during the course of the experiment was a major source of error. Denaturation and loss of activity was attributable, in part, to inactivation at the gas-liquid interface from bubbles formed during phase equilibration. This resulted in erroneous ferredoxin concentration measurements which were manifest in the calculated E°'. They found that attempts to reoxidize the protein with oxygen to determine the true final ferredoxin concentration would cause further denaturation due to the instability of the reduced species to oxygen. Re-oxidation by evacuation of the H_2 in the system would result in an increase in the concentration of the protein due to the evaporation of solvent during evacuation.

The most commonly used methods of chemical titration of low potential proteins use sodium dithionite under anaerobic conditions. Dithionite is popular due to its low redox potential, high reactivity and transparency in the visible region of the spectrum

(55). The Fd concentration is then amenable to detection by absorption or EPR spectroscopic (56, 57) measurements.

However, dithionite is unstable at low pH and auto-oxidizable. Therefore its use is restricted to above pH 6.5 (55) and strict anaerobic conditions must be maintained in order to accurately determine the concentration of dithionite consumed by reactant (57). It has been suggested that dithionite is recommended only in stoichiometric determinations, unless its concentration has been accurately determined (56). Also, as with hydrogenase, the redox potential of dithionite is pH dependent and governed by the Nernst relation.

$$E = -0.059\ pH, \qquad (3)$$

for a one electron transfer process.

G. Electrochemistry

Electrochemical titrations of low potential proteins are particularly attractive in that quantitative reduction can be achieved at native solution pH depending on the electrode material used and/or availability of an appropriate mediator.

Biological redox molecules do not commonly react directly at metal electrodes (59). Though the prosthetic group may react readily, the protein moity often couples poorly to the electrode surface and may result in protein denaturation and/or deactivation of the enzyme. Because of this most electrochemical analyses of biological systems have been conducted in the presence of exogenous "mediators". These mediators can achieve rapid equilibration

between the electrode and the biological molecule without chemical interaction or interference with the measurements of interest. A list of commonly used mediators and their sources has been tabulated by Kuwana (59). A study on the potential use of viologen compounds as mediators in biological systems has recently been reported (60).

Mediated electrochemical titrations are advantageous due to their ability to accurately titrate small volumes of solution repetitively in the absence of additional chemical titrants. A discussion of additional attractive features of this technique has been outlined (42). The E°' and n values for spinach ferredoxin have been measured electrochemically in the presence of mediators and detected by potentiometry (42), EPR (54), circular dichroism (56) and coulometry (61).

Direct electrochemical reduction of ferredoxins has been studied most commonly at mercury electrodes via polarographic techniques.

Weitzman et al. (62) first reported the electrolytic reduction of Clostridial ferredoxin at the dropping mercury electrode (DME). They compared polarograms of ferredoxin reduced by Hg with the corresponding polarograms obtained by reduction via the physiological reductant, H_2-hydrogenase. They concluded from the results that the direct polarographic reduction was analogous to the biological reduction process. This assumption was later refuted by Kuznetsov (63). Direct polarographic analysis of other ferredoxins have been reported using DC and cyclic polarography at the DME and the hanging mercury drop electrode respectively (64, 65, 66), differential pulse polarography (67) and ac polarographic techniques (56, 63,

67-69). Kiselev et al. (64) also reported voltammagrams obtained for several plant ferredoxins at platinum electrodes.

Several authors have suggested that ferredoxins adsorbed strongly to mercury surfaces (62, 63, 64). However, as cited by Senda and co-workers (69), they did not consider the effects of adsorption on the measured polarographic half wave potential, $E_{\frac{1}{2}}$. It was experimentally observed by Kuznetsov et al. (63) that electrochemical reduction resulted in the destruction of the active center and release of the S-H group as demonstrated by the shift in the half wave potential. They also attributed the decrease in current of these species at Hg to protein unfolding and coverage of the electrode surface. This behavior has been shown to be characteristic of many proteins (70). Ikeda et al. (68) experimentally observed the irreversible adsorption of Clostridial ferredoxin on the surface of a mercury electrode. Cyclic voltammograms were recorded on a Hg drop which had been previously immersed in protein solution and washed afterward in distilled H_2O that were the same as the voltammagrams obtained in protein solution. They postulated that the adsorption is a diffusion controlled process for low concentrations of protein and results in denaturation of the surface product to form the "apo" species (loss of active site).

Rickard et al. (61) have monitored the behavior of spinach ferredoxin directly at plain gold, antimony doped SnO_2 and Hg-Au minigrid electrodes. They reported slow reduction, on the time scale of the experiment, at the first two surfaces and protein denaturation at the Hg-Au surface as detected from absorbance measurements.

Relatively fast heterogeneous oxidation and reduction does occur, however at gold electrodes which have been electrochemically modified with methyl viologen via a procedure first reported by Landrum et al. (71). These surfaces have been utilized in this work to study the direct electron transfer behavior of Fd, and have also been effective in reducing myoglobin (72) and cytochrome c (73). The formal heterogeneous electron transfer rate constant, k^o, and the electrochemical transfer coefficient, α, have been determined at the methyl viologen modified gold minigrid and rotating ring disc electrode.

CHAPTER III

THEORY

A. Butler-Volmer Theory (9, 10, 74)

In a homogeneous system the reaction rate is solely a function of the concentrations of the reactants or products at some specified temperature and pressure. For the simple reaction:

$$A \xrightarrow{k} B \tag{4}$$

the rate law is described by, rate = k[A], where the first order rate constant k is the proportionality factor. Qualitatively for such a homogeneous system the rate constant is proportional to the number of collisions occurring between the reacting molecules having energy greater than the energy of activation, E_{act}. This rate constant varies with temperature in a manner as described by the Arrhenius equation

$$k = Ae^{-E_{act}/RT} \tag{5}$$

where k = first order homogeneous rate constant, sec^{-1}, A = frequency factor, E_{act} = energy of activation, R = gas constant and T = temperature, °K. The constant A, the frequency factor, represents the number of collisions occurring between reacting molecules and the exponential term incorporates the number of collisions having sufficient energy to result in a net reaction at some temperature.

In developing a kinetic theory for heterogeneous reactions, one

must consider contributions from more than one phase, particularly the electrode surface which is exposed to the reaction mixture. For an electrode reaction the rate is a function of the nature of the electrode surface and the magnitude of the electric field at the reacting interface.

At the instant of immersion of an electrode into electrolytes, the metal-solution interface is uncharged and the rate of charge transfer is governed only by chemical kinetics. Within a few microseconds (74) a dynamic equilibrium is reached wherein both sides of the interface become charged due to the transfer of electrons between the electrode and solution and the subsequent migration of ions to the interface forming the charged double layer structure as depicted in Figure 2. The electrical double layer is formed at the outer helmholtz plane (OHP) and is the environment in which redox processes occur across the interface.

The electric field developed at the interface may hinder further ion movement and charge transfer depending on the magnitude of the field and the charge on the ion. An additional potential or source of activating energy must then be supplied to move an ion from its initial state across the interface to its final state. Therefore, the movement of a charged species to the surface of the electrode is influenced by both the sign and the magnitude of the potential field existing between the bulk of solution and the OHP. The rate of electron transfer then becomes a function of the potential gradient existing at the interface as well as the surface concentrations of reactants and products.

An electrochemical system can be described by the same type of potential energy-distance profile reflecting atomic movements of reactants and products as is typical of chemical systems. However, the electric field produced by the charged double layer now serves to modify the potential energy barrier in a manner which is dependent on the applied potential. The modification is such that only a fraction of the input energy appears in the change of activation energy and therefore in the rate expression (74) (see Figure 7).

The reaction scheme for an oxidized species, O, undergoing reduction at the electrode surface to form the reduced species, R, is as follows:

$$O + ne \underset{k_b}{\overset{k_f}{\rightleftharpoons}} R \tag{6}$$

where k_f and k_b are the heterogeneous rate constants for the forward and backward reactions in dimensions of cm/sec. The exponential term in the Arrhenius type formulation for the heterogeneous rate constant now incorporates a term (αE) which is the fraction of the electrode potential effective in accomplishing the forward reductive reaction and ($1-\alpha$)E is the fraction needed to facilitate the reverse reaction (9). The following equations incorporate what is known as the Butler-Volmer theory of kinetics:

$$k_f = k^\circ e^{\frac{-\alpha nF(E - E^\circ)}{RT}} \tag{7}$$

$$k_b = k^\circ e^{\frac{(1 - \alpha)nF(E - E^\circ)}{RT}} \tag{8}$$

Figure 7. Diagram of potential energy barrier for an electrodic reaction (9): E = applied potential, n = number of electrons transferred, F = Faraday constant, α = electrochemical transfer coefficient, $\Delta G^{\ddagger}_{Oc}$ = cathodic free energy change at E = O, $\Delta G^{\ddagger}_{Oa}$ = anodic free energy change at E = O, $\Delta G^{\ddagger}_{c}$ = cathodic free energy change at E = E, $\Delta G^{\ddagger}_{a}$ = anodic free energy change at E = E.

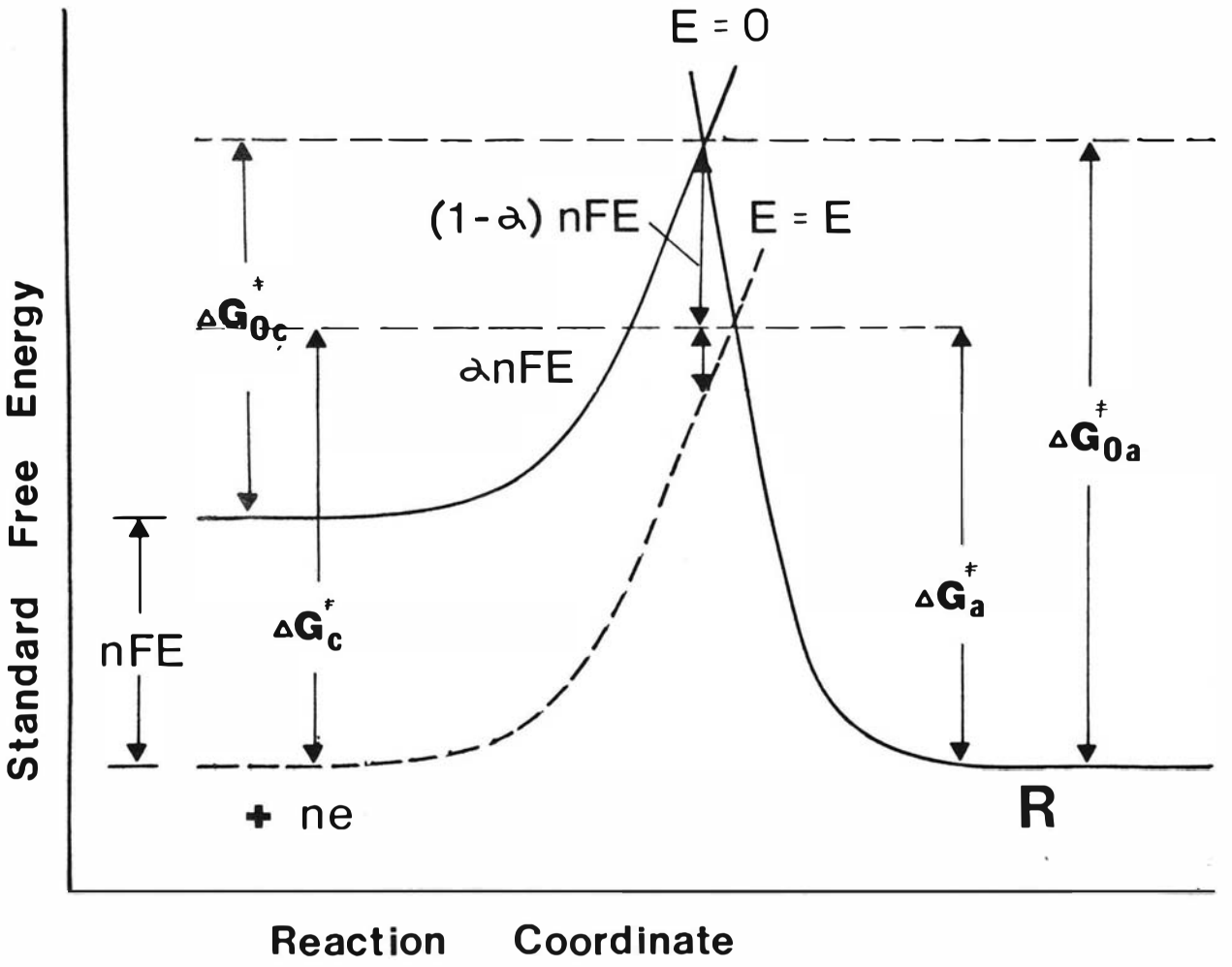
E = 0
(1-a) nFE
E = E
$\Delta G^{\ddagger}_{0c}$
anFE
$\Delta G^{\ddagger}_{0a}$
nFE
$\Delta G^{\ddagger}_{c}$
$\Delta G^{\ddagger}_{a}$
+ ne
R
Standard Free Energy
Reaction Coordinate

where E° is the formal potential, E is the applied potential, k° is the standard rate constant and is defined as the value of k_f and k_b at the formal potential of the system, n is the number of electrons transferred, F is the Faraday constant, and α is the transfer coefficient or symmetry factor. The standard heterogeneous rate constant, k°, can be qualitatively described in terms of the time it takes for a system to attain equilibrium. It is independent of potential and a characteristic of the system at equilibrium.

$$k^\circ = Ae^{-E_{act}/RT} \tag{9}$$

It may cover ten orders of magnitude ranging from 10 to 10^{-9} cm/sec. The transfer coefficient, α, has been defined by Bockris as representing the fraction of the electrical energy by which the electrical part of the activation energy decreases and thus the net rate of the reaction increases (74). α is an intrinsic property of a given electrode reaction interface and converges to about 0.5 for a simple one electron transfer process.

For an electrode reaction the rate of electrolysis is directly proportional to the faradaic current as expressed in moles/sec per unit area:

$$\text{Rate} = \frac{i}{nFA} \tag{10}$$

where i is current in amperes, n is the number of electrons transferred, F is the Faraday constant, 9.648×10^4 Coulombs/equivalent, A is area of electrode (cm^2). The reaction rate in the forward direction is then proportional to the surface concentration of the

oxidized species denoted by $C_o(0,t)$ and produces a net cathodic current:

$$\text{Rate}_f = \frac{i_c}{nFA} = k_f C_o(0,t) \tag{11}$$

Likewise the reoxidation of R yields a net anodic current

$$\text{Rate}_b = \frac{i_a}{nFA} = k_b C_R(0,t) \tag{12}$$

The net rate of exchange across the interface yields a net current

$$i_{net} = i_c - i_a = nFAK_f C_o(0,t) - nFAK_b C_R(0,t) \tag{13}$$

At equilibrium the net current is zero and no net change in potential difference exists across the interface. The magnitude of the current is then termed the exchange current, i_o, and is a measure of the rate of the reaction that occurs in opposite directions at equal rates across the interface at equilibrium:

$$j_o = \frac{i_o}{A} \tag{14}$$

where j_o is the exchange current density.

The exchange current is a measure of the activation energy that must be put into the system to cause a net current to flow across the interface. If the exchange current is small then a large energy of activation must be put into the system such that the extent of reaction will predominate in the desired direction. A small exchange current corresponds to a small standard rate constant. The

exchange current density, j_o, may range in magnitude from 10 A/cm^2 to less than 10^{-12} A/cm^2.

Substitution of 7 and 8 into 13 yields the current-potential expression in terms of the k°.

$$i_{eq} = nFAk^\circ \left[C_o(0,t) e^{\frac{-\alpha nF(E - E_{eq})}{RT}} - C_R(0,t) e^{\frac{(1 - \alpha)nF(E - E_{eq})}{RT}} \right] \quad (15)$$

This equation can also be expressed in terms of the exchange current (9)

$$i = i_o \left[\frac{C_o(0,t)}{C_o^b} e^{\frac{-\alpha nF\eta}{RT}} - \frac{C_R(0,t)}{C_R^b} e^{\frac{(1 - \alpha)nF\eta}{RT}} \right] \quad (16)$$

where C^b is the bulk concentration of the species indicated and $\eta = E - E_{eq}$ is the overpotential. This dependence of exchange current on overpotential, η, is depicted in Figure 8 where curves represent the anodic and cathodic currents. One can force the system to deviate from equilibrium in either the cathodic or anodic direction depending on the sign and magnitude of the applied overpotential. This relation predicts an exponential dependence of the current on the overpotential up to the limiting case of extreme overpotentials afterwhich the current is no longer a function of potential or electron transfer kinetics, but is governed solely by mass transfer effects.

At equilibrium the net current is zero. Therefore the concen-

Figure 8. Effect of exchange current density, j_o, on overpotential for the reaction:

$$O + ne \rightleftharpoons R$$

where $\alpha = 0.5$ for all cases.

a) $j_o = 10^{-3}$ A/cm^2

b) $j_o = 10^{-6}$ A/cm^2

c) $j_o = 10^{-9}$ A/cm^2

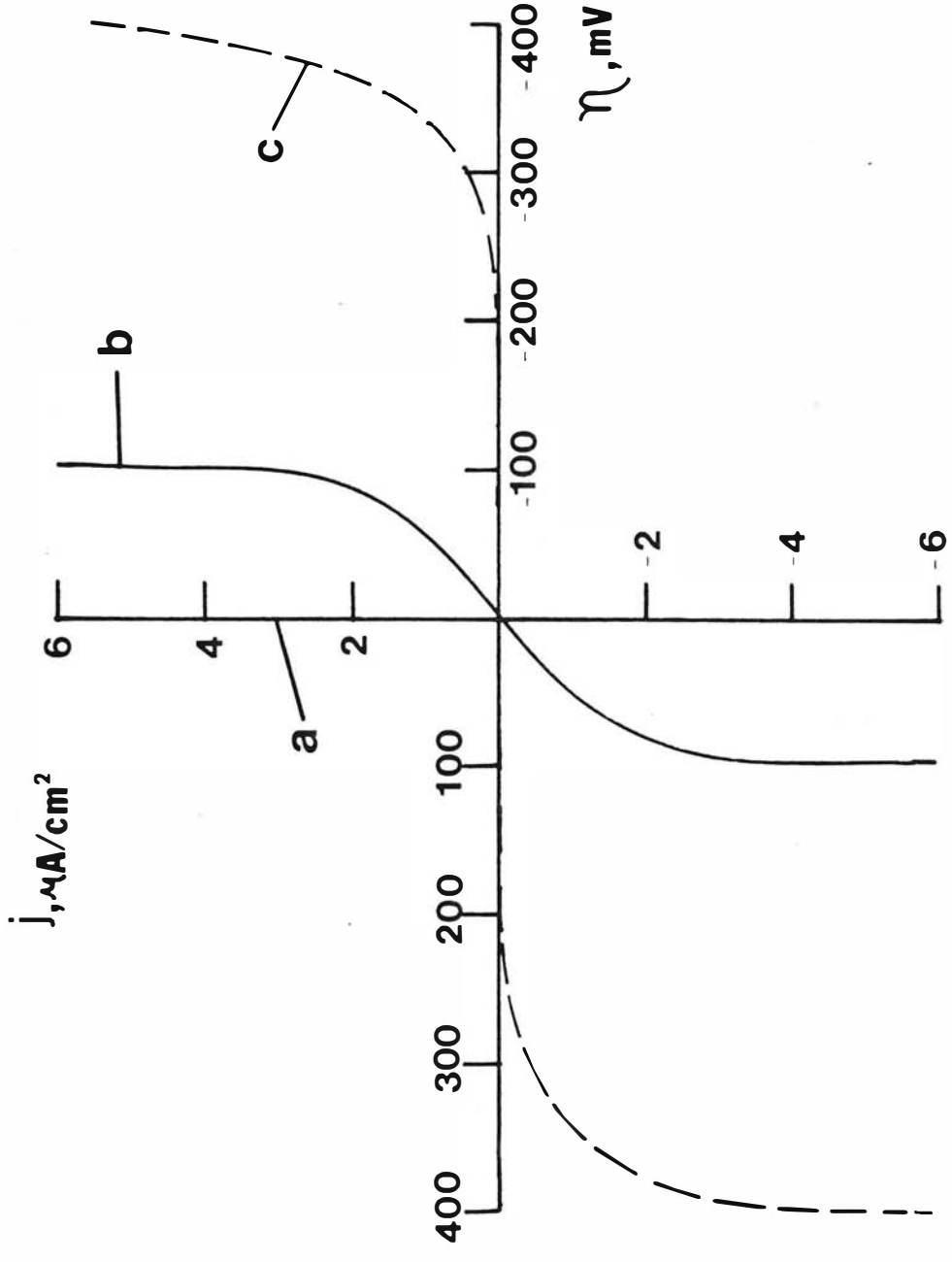
j, мА/см²
η, mV
a
b
c
6
4
2
100
200
300
400
-100
-200
-300
-400
-2
-4
-6

trations of species at the electrode are approximately the same as bulk values. In this instance Equation (16) reduces to:

$$i = i_o \left[e^{\frac{-\alpha n F \eta}{RT}} - e^{\frac{(1-\alpha) n F \eta}{RT}} \right] \tag{17}$$

which is known as the Butler-Volmer Equation.

For reversible systems no over-potential is necessary to force the system to attain the surface concentration ratio of oxidized to reduced species to conform to the thermodynamic values predicted by the Nernst Equation.

$$E = E^\circ + \frac{RT}{nF} \ell n \left[\frac{C_o^b}{C_R^b} \right] \tag{18}$$

Hence, charge transfer for these systems is rapid and the surface concentrations and applied potentials are always at equilibrium. The kinetics are so fast that the system is governed only by mass transfer effects on the time scale of the experiment.

At low overpotentials very near E_{eq} Equation (17) can be approximated by the linearized relation:

$$i = i_o \left(\frac{nF\eta}{RT} \right) \tag{19}$$

This equation predicts behavior which is characteristic of systems which, though not reversible, exhibit relatively fast heterogeneous kinetics. For η up to 100 mV, however, both anodic and cathodic processes will contribute to the measured current, and Equation (17) cannot be approximated. A significant η is still

required to drive a net current across the interface and these systems are termed to be "quasi-reversible".

When large cathodic or anodic overpotentials must be applied to the system to effect electron transfer, then the system exhibits slow kinetics and current will flow only in the cathodic or anodic direction depending on the applied potential. For these systems, the current will depend only on one of the terms in Equation (17) at any particular time. The system is said to exhibit Tafel behavior and is indicative of irreversible kinetics.

$$i = i_o e^{\frac{-\alpha n F \eta}{RT}} \tag{20}$$

when η is negative. Current attributed to solely mass transfer effects occur only at extreme overpotentials.

Hence one can classify the kinetic behavior of electrochemical systems in terms of the magnitude of the overpotential which must be applied to effect mass transfer controlled reactions. Electrode systems are thus characterized as reversible when $\eta = 0$; quasi-reversible when $0 < \eta < 100$, or irreversible when $\eta = 100$.

In summary Butler-Volmer theory describes systems that are characterized by exhibiting exponential i-E dependence. The principal requirement for such systems is the existence of a potential energy barrier (at least in one direction) that hinders the movement of charged species across the interface and which can be modified in height by the interfacial potential difference (74). Such an interface exists at biological membrane surfaces.

Electrode reactions are often complex and the potential energy supplied to a system may be utilized to initiate several electrode processes which may occur simultaneously. A summary of factors governing the rate and hence the magnitude of the faradaic current are described below (9):

(1) mass transfer of the reactant species to the electrode surface due to an electrochemical potential gradient which may arise from three factors:

   (a) diffusion - transport caused by concentration gradient

   (b) convection - transport via mechanical stirring or hydrodynamic forces

   (c) migration - transport of charged species under the influence of an electric field.

   Contributions to migration effects can often be eliminating by addition of an excess supporting electrolyte.

(2) Electron transfer across the electrode - electrolyte interface

(3) Presence of homogeneous chemical reactions preceeding or following electron transfer

(4) Other complicating surface reactions such as adsorption-desorption processes.

To study any one factor one must exclude contributions from the other processes such that the rate controlling step involves the reaction of interest. Given a system uncomplicated by factors (3)

and (4), the faradaic current will only be attributed to mass transport processes or electrode kinetics. For the system observed in this work the effects of mass transfer and electron transfer predominate. Of primary interest in this work is the rate of heterogeneous electron transfer of spinach ferredoxin at various electrode surfaces. The effects due to mass transfer must first be separated or delineated.

The flux of reactant to the electrode via mass transport will determine the magnitude of the observed faradaic current regardless of potential, given that electron transfer across the interface is fast. If the rate of electron transfer is slow, which is often the case with biological redox molecules, then sufficient overpotentials may be applied to drive electron transfer at a diffusion controlled rate such that only mass transport is rate limiting. Upon successive reduction of the applied potential such that electron transfer becomes rate limiting, then the observed faradaic current will become a function of the overpotential in a manner as described by the Butler-Volmer relations. Hence one can now extract kinetic parameters.

This method of discerning kinetic contributions is only possible because the flux attributed to mass transport phenomena has been mathematically well characterized such that contributions from both factors can be separated. However mass transport via diffusion to a stationary electrode is only defined and controlled for a short period, up to 10^2 sec (63). At longer times, effects from various convectional forces may disrupt the diffusion layer in a manner

which cannot be theoretically described.

Potential step chronoabsorptometry monitors the flux of species via absorbance measurements at a stationary electrode. Hence kinetic parameters can only be extracted on a short time scale, in this case 0-60 sec. This method then, affords a transient measurement of the kinetic behavior of the system and the extracted parameters are only descriptive of processes that occur during the perturbation. For complex molecules such as ferredoxin, conformational changes at the reactive site may be necessary before electron transfer can be accomplished which will now be manifest in the observed rate parameters.

The alternate technique utilized, hydrodynamic voltammetry, involves a steady-state process. As will be discussed, the theoretical relations describing mass transport do not break down at short times but are maintained via controlled convective forces (75). This allows the observation and comparison of the kinetic behavior of the molecule after the system has relaxed.

B. Spectroelectrochemistry

Single potential step chronoabsorptometry is a spectroelectrochemical technique wherein the absorbance of a species reacting at an electrode surface is monitored as a function of time upon application of a potential sufficient in magnitude to cause a reaction to occur (76, 77). For the reaction in question:

$$Fd_{ox} + ne \underset{k_{b,h}}{\overset{k_{f,h}}{\rightleftharpoons}} Fd_{red} \qquad (21)$$

where Fd_{ox} and Fd_{red} represent the oxidized and reduced forms of ferredoxin, respectively, and $k_{f,h}$ and $k_{b,h}$ are the forward and backward formal heterogeneous electron transfer rate constants. The absorbance is monitored at a wavelength which is characteristic of either the formation or disappearance of the product.

This technique is amenable to studying both irreversible and quasi-reversible systems as long as the following criteria are attained:

(1) an electrode surface at which the redox species of interest can couple without the use of a mediator is available,

(2) sufficient over-potential to electrolyze the species at a diffusion controlled rate can be achieved, and

(3) an optical signal which is characteristic of the process of interest is detectable on the time scale of the experiment.

The underlying theory for this technique was developed and first utilized to extract heterogeneous kinetic parameters for irreversible systems by Albertson et al. in 1979 (76). Since then it has recently been extended to quasi-reversible systems by Bancroft et al. (77).

1. Irreversible Case

As discussed earlier irreversible systems exhibit Tafel behavior in that significant overpotentials can be supplied to drive the reaction in only one direction before limiting mass transfer controlled rates predominate. For the reaction described by Equation (6) a negative overpotential is applied such that reduction occurs

at a diffusion controlled rate and contributions from the back reaction are neglibible. The time dependent absorbance relation for the product species, R, is given by

$$A_R^D(\lambda,t) = \frac{2}{\pi^{\frac{1}{2}}} \varepsilon_R(\lambda)\, D_O^{\frac{1}{2}} C_O^b\, t^{\frac{1}{2}} \qquad (22)$$

where $\varepsilon_R(\lambda)$ is the molar absorptivity of R, M^{-1} cm^{-1}, D_O is the diffusion coefficient of O, cm^2/sec, C_O^b is the bulk concentration of O, moles/liter, and t is the time, sec. If the magnitude of the applied potential is reduced then the kinetic dependence on potential becomes apparent and can be expressed in terms of the chronoabsorptometric relation of the product species.

$$A_R(\lambda,t) = \frac{\varepsilon_R(\lambda) C_R^b D_O}{k_{f,h}} \left[\frac{2k_{f,h} t^{\frac{1}{2}}}{\pi^{\frac{1}{2}} D_O^{\frac{1}{2}}} + \exp\left(\frac{k_{f,h}^2 t}{D_O}\right) \operatorname{erfc}\left(\frac{k_{f,h} t^{\frac{1}{2}}}{D_O^{\frac{1}{2}}}\right) - 1 \right] \qquad (23)$$

The absorbance is then normalized by dividing (23) by the diffusion controlled chronoabsorptometric expression (22).

$$A_N(\lambda,t) = 1 + \frac{\pi^{\frac{1}{2}}}{2\zeta} [\exp(\zeta^2)\operatorname{erfc}(\zeta) - 1] \qquad (24)$$

wherein the rate constant is now manifest in the argument

$$\zeta = \frac{k_{f,h} t^{\frac{1}{2}}}{D_O^{\frac{1}{2}}} \qquad (25)$$

Figure 9 shows the plot of the working curve which is the normalized

Figure 9. Working curve for irreversible electron transfer case.

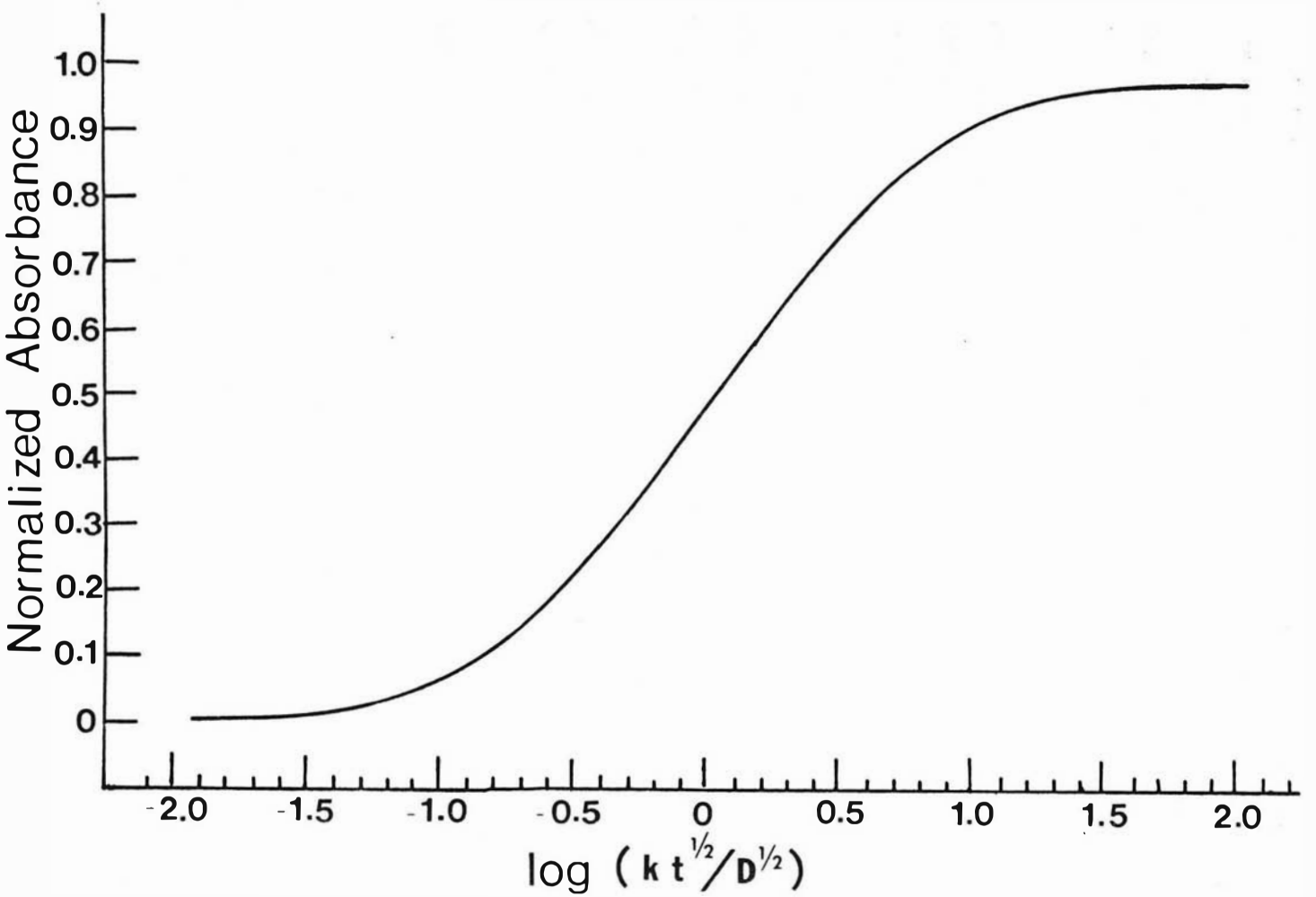
Normalized Absorbance
1.0
0.9
0.8
0.7
0.6
0.5
0.4
0.3
0.2
0.1
0
-2.0
-1.5
-1.0
-0.5
0
0.5
1.0
1.5
2.0
log (k t^1/2 / D^1/2)

absorbance versus the log of the argument from which the rate constant $k_{f,h}$ can be extracted at various overpotentials.

The standard heterogeneous rate constant, k°, can now be obtained from the linearized Butler-Volmer relation from (7).

$$\log k_f = \log k^\circ - \frac{\alpha nF}{RT}(\eta) \tag{26}$$

where $\frac{nF}{RT} = 0.059$ for n = 1 at 25°. A plot of the calculated rate constant, k_f, versus η yields a straight line where k° is the intercept and α can be extracted from the slope.

2. Quasi-Reversible Case

Quasi-reversible systems are characterized by faster kinetics such that contributions from both the forward and reverse reactions are inherent in the observed time dependent absorbance signal.

In this case the absorbance time expression is now a function of $k_{f,h}$, $k_{b,h}$, and also the magnitude of the overpotential for each potential step.

For reaction (6) the chronoabsorptometric response for the product now becomes:

$$A_R(\lambda,t) = \frac{\varepsilon_R(\lambda) C_o^b k_{f,h}}{\left(\frac{k_{f,h}}{D_o^{\frac{1}{2}}} + \frac{k_{b,h}}{D_R^{\frac{1}{2}}}\right)^2} \left[2\left(\frac{k_{f,h}}{D_o^{\frac{1}{2}}} + \frac{k_{b,h}}{D_R^{\frac{1}{2}}}\right) \frac{t^{\frac{1}{2}}}{\pi^{\frac{1}{2}}} + \right.$$

$$\left. \exp\left[\left(\frac{k_{f,h}}{D_o^{\frac{1}{2}}} + \frac{k_{b,h}}{D_R^{\frac{1}{2}}}\right)^2 t\right] \operatorname{erfc}\left[\left(\frac{k_{f,h}}{D_o^{\frac{1}{2}}} + \frac{k_{b,h}}{D_R^{\frac{1}{2}}}\right) t^{\frac{1}{2}}\right] - 1 \right] \tag{27}$$

Therefore the normalized absorbance $\frac{A_R(\lambda,t)}{A_D(\lambda,t)}$ is described by

$$A_N(\lambda,t) = \frac{\zeta\pi^{\frac{1}{2}}}{2\xi^2}\left[\frac{2\xi}{\pi^{\frac{1}{2}}} + \exp(\xi^2)\operatorname{erfc}(\xi) - 1\right] \tag{28}$$

where

$$\xi = \left[\frac{k_{f,h}}{D_o^{\frac{1}{2}}} + \frac{k_{b,h}}{D_R^{\frac{1}{2}}}\right] t^{\frac{1}{2}} \tag{29}$$

An expression relating ξ and ζ to the overpotential can be obtained from the following mathematical manipulations.

(a) Divide ξ by ζ to yield

$$\frac{\xi}{\zeta} = 1 + \left[\frac{k_{b,h}\, D_o^{\frac{1}{2}}}{k_{f,h}\, D_R^{\frac{1}{2}}}\right] \tag{30}$$

(b) From the Butler-Volmer equations (7) and (8), solve for $k_{b,h}$ and $k_{f,h}$ and substitute into (30) such that

$$\xi = \zeta[1 + (D_o^{\frac{1}{2}}/D_R^{\frac{1}{2}})\exp\{nF\eta/RT\} \tag{31}$$

where η is positive in an anodic direction and η is negative in a cathodic direction. Because of the dependence of the normalized absorbance on the functions of ξ and ζ a family of working curves must be calculated at each overpotential to account for the effects of the back reaction on the overall process. A working curve can now be obtained for the normalized absorbance as a function of the

argument ζ for each overpotential applied up to a limiting overpotential wherein the curve is indistinguishable from the irreversible curve. This limiting overpotential has been determined as $\eta \leq \pm 160$ mV. Figure 10 shows a plot of the family of working curves for the quasi-reversible case from η = -26 to -160 mV.

C. Hydrodynamic Voltammetry (9, 78, 79)

The steady state technique used to study kinetic behavior in this case is rotating disk voltammetry. Although a ring-disk electrode was used, only the disk was effective in this study. Therefore only the theory at the disk will be discussed.

For a rotating disk electrode mass transport is accomplished via both diffusive and convective forces. Convective forces predominate up to a small region very close to the electrode called the hydrodynamic boundary layer wherein mass transport is controlled by diffusion. The theory describing hydrodynamic transport to a rotating disk has been well characterized and discussion of the theoretical derivations has been presented (9, 78, 79) from which equations derived herein are referenced.

Qualitatively upon rotation of the disk, solution is forced axially upwards in a direction normal to the disk. Fluid close to the surface of the disk acquires its rotational motion and centrifugal force drives the solution outwards from the center of the disk in a radial direction (Figure 11). The liquid directed radially outwards is continuously replenished by the fluid forced axially upwards towards the disk. Therefore mass transport is accom-

Figure 10. Family of working curves for the Fd quasi-reversible model of electron transfer. Curves are increasing negative overpotentials up to the irreversible case.

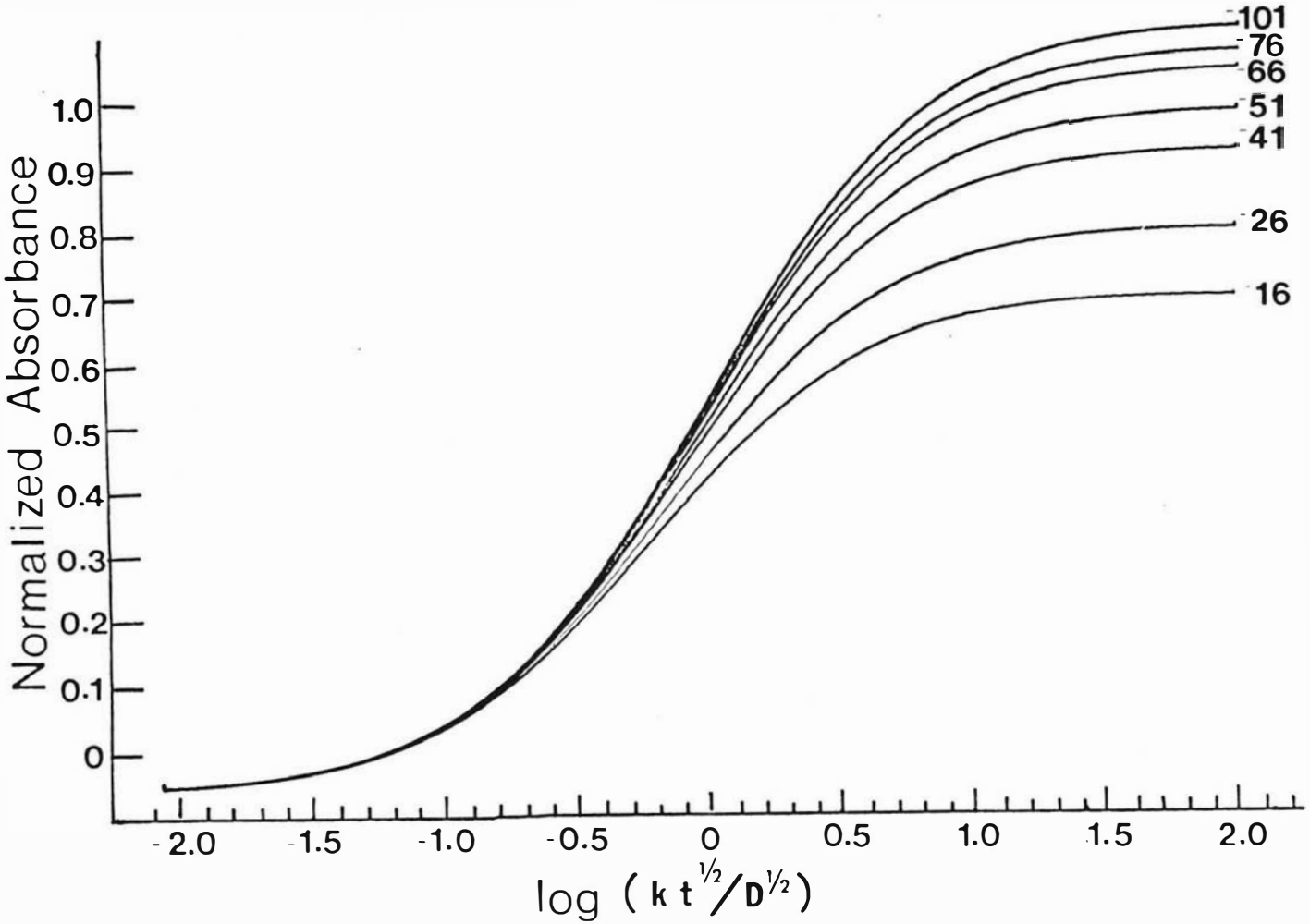
Normalized Absorbance
1.0
0.9
0.8
0.7
0.6
0.5
0.4
0.3
0.2
0.1
0
-2.0
-1.5
-1.0
-0.5
0
0.5
1.0
1.5
2.0
log (k t ½ / D ½)
101
76
66
51
41
26
16

Figure 11. Schematic diagram of solution flow to the surface of a rotating disk electrode.

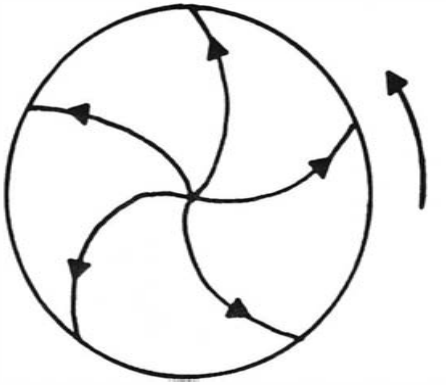

Near
Disk Surface

Below
Disk Surface

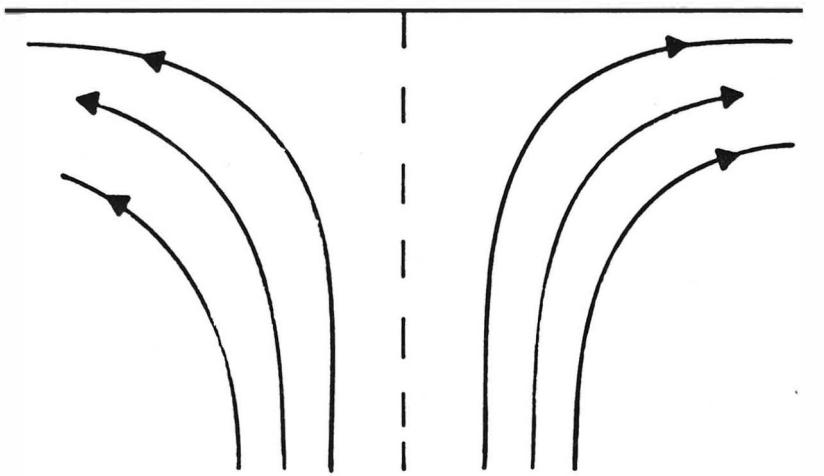

plished solely by convection up to the hydrodynamic boundary layer and can be controlled by rotation rates. Within this hypothetical layer which extends approximately 10^{-2} to 10^{-3} cm from the surface of the disk, mass transport occurs via diffusion. However, now the thickness of this layer is well defined and stable due to the constant flux of fresh sample from convective forces.

The process is steady state because the thickness of the diffusion layer does not change with time and can be maintained and controlled by the rate of rotation. As the rotation rate is varied the current will rapidly relax to a corresponding steady state value.

The relation predicting the magnitude of the limiting faradaic current from mass transfer effects only is given by the Levich equation:

$$i_\ell = 0.62nFAC^bD^{2/3}\nu^{-1/6}\omega^{1/2} \qquad (32)$$

where i_ℓ is the mass transfer limiting current (milliamperes), ω is the angular velocity of disk (sec^{-1}) where $\omega = 2\pi f$, f = frequency of rotation (rpm), ν is the kinematic viscosity (cm^2/sec) and C^b is the bulk concentration of electroactive species in moles/liter. All other variables are as previously defined. This equation then predicts linear behavior of i_ℓ with $\omega^{\frac{1}{2}}$. A deviation in this linear relationship would suggest effects from electron transfer kinetics.

The limiting or diffusion controlled faradaic current at the disk for an irreversible reaction as described by Equation (11) is

$$i_\ell = nFADk_f C_o(0,t)$$

where again $C_o(0,t)$ = concentration of electroactive species at the electrode surface. The current at the disk at any time under mass transfer via diffusion controlled conditions is a function of the concentration gradient.

$$i = i_\ell\left[\frac{C^b - C(0,t)}{C^b}\right] \tag{33}$$

where C^b and $C(0,t)$ are as previously defined. Solving for $C(0,t)$ in (33) and inserting into (11) for the kinetically controlled case yields

$$i = nFADk_f C^b\left[1 - \left(\frac{i}{i_\ell}\right)\right] \tag{34}$$

Defining the kinetic current as

$$i_k = nFADk_f C^b \tag{35}$$

then the measured current now becomes

$$i = i_k - \frac{i(i_k)}{i_\ell} \tag{36}$$

Upon rearragement

$$\frac{1}{i} = \frac{1}{i_k} + \frac{1}{i_\ell} \tag{37}$$

If the kinetics are fast then i_k will be large and Equation (37) reduces to Equation (32) where i becomes the limiting current i_ℓ. Substituting (37) with the equivalent relation in the Levich equation yields

$$\frac{1}{i} = \frac{1}{i_k} + \frac{1}{0.620nFAC^b D_o^{2/3} \nu^{-1/6}} (\omega^{-\frac{1}{2}}) \qquad (38)$$

so that now a plot of $1/i$ vs $1/\omega^{\frac{1}{2}}$ should be linear and i_k can be determined from the intercept. Since i_k is related to k_f from Equation (35), the rate constant can be calculated for each successively applied overpotential. Using the linearized Butler-Volmer relation (26) one can now plot log k_f vs. η to calculate the standard rate constant, k°, and transfer coefficient, α.

CHAPTER IV

EXPERIMENTAL

A. Reagents and Materials

Type III spinach ferredoxin was purchased from Sigma and used as received in 0.15 M Trizma buffer, pH 7.5, 0.2 M NaCl. The concentration was determined spectroscopically using $\varepsilon(420\ nm) = 9{,}680\ M^{-1}\ cm^{-1}$ (42). Methyl viologen (1,1'-dimethyl-4,4'-bipyridinium dichloride) was obtained from K & K Laboratories and used without further purification. Trizma buffer was from Sigma. A 0.15 M, pH 7.5 (0.1 M NaCl) solution was prepared when dilution of ferredoxin samples was desired for use as a supporting electrolyte, and as the background solvent for current and optical measurements. Titrisol (phosphate) buffer, pH 7.0 was obtained from E. Merck Co. Inorganic salts and other chemicals were of reagent grade and were prepared in doubly distilled water. Prepurified nitrogen gas was obtained from Airco and was passed over hot copper turnings and bubbled through distilled water before use. Grade A alumina (0.3 microns) and Gamal polishing cloth were used to polish the ring-disk electrodes and were obtained from Fisher Scientific Company.

Gold minigrid electrodes, 67% optical transparency, 200 lines per inch were obtained from Buckbee-Mears, St. Paul, Minnesota. Fluoride doped tin oxide ($SnO_2(F)$) semi-conductor electrodes (20Ω/square) were obtained from PPG Industries. Metallized plastic optically transparent electrodes (MPOTE), trade name Intrex-G (gold) as obtained from Sierracin/Sylmar was a kind gift from Dr. Neal

Armstrong. Teflon tape (2 mil) was obtained from Dilectrix Corporation. Gold mini-grid electrodes were pre-treated using a Harrick Plasma Cleaner.

B. Apparatus and Instrumentation

All spectroscopic concentration measurements were taken with a Beckman Acta MVII Spectrophotometer. Absorbance-time transients on ferredoxin were measured either with the Acta MVII at a fixed wavelength in time drive or with a Harrick Scientific Corporation Rapid Scanning Spectrometer (RSS) operating in the fixed wavelength mode. Current and/or absorbance data were recorded with a Hewlett-Packard 7015B X-Y recorder or on a Houston Strip Chart Recorder. Potentials were monitored with Keithley 178 or Digitec 262 digital voltmeters.

Voltammograms were obtained either using a Princeton Applied Research (PAR) 174 polarographic analyzer or with a potentiostat of conventional design using operational amplifiers. Single and double working electrode potentiostats were constructed in-house from conventional operational amplifier circuitry using either Teledyne-Philbrick 1009 and 1026 op-amps or a McKee Pederson 1026A op amp. A schematic of the bipotentiostat circuit (80) used is given in Figure 12.

Rotating disk experiments were conducted using an ASR2 rotator and Model DT gold disk and ring-disk electrodes manufactured by Pine Instruments Company.

Spectroelectrochemical experiments were taken using a quartz rod optically transparent electrochemical (OTE) cell which was con-

Figure 12. Schematic of bipotentiostat circuit used in the rotating disk experiments.

$R = 1 \times 10^{4}$ Ω

$C = 1 \times 10^{-12}$ F

Operational amplifier circuits are as follows: PC is the control amplifier for the auxiliary electrode, F1 is the voltage follower for the reference, CF1 is a current follower for the disk electrode, 1, CF2 is the current follower for the ring electrode, 2, DA is a differential amplifier circuit for floating input from CF2, Z2 is a zero shifting amplifier and I2 is an inverting amplifier.

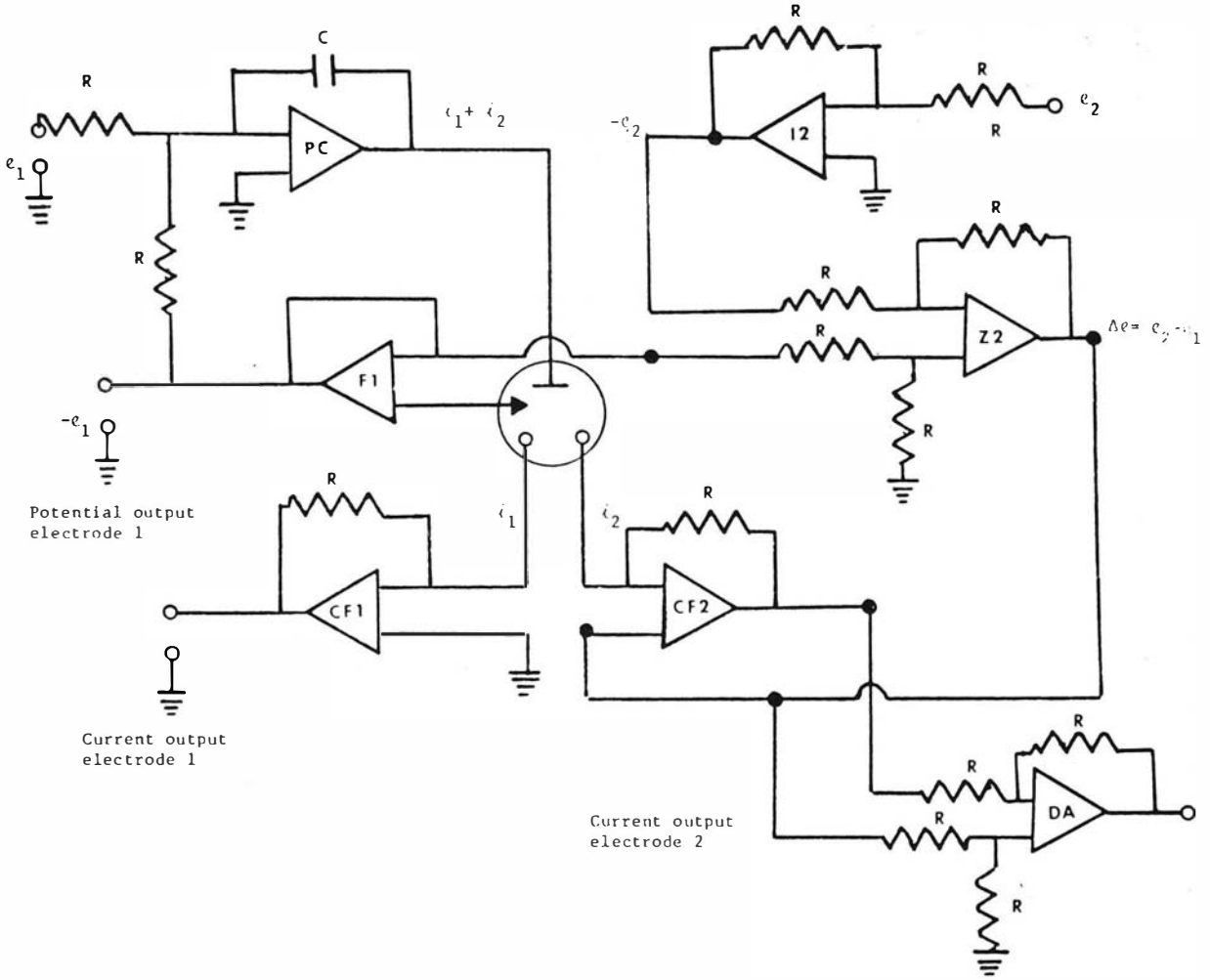
C
R
PC
$i_1 + i_2$
e_1
R
F1
$-e_1$
Potential output electrode 1
R
CF1
i_1
Current output electrode 1
R
I2
$-e_2$
R
e_2
R
R
Z2
$\Delta e = e_2 - e_1$
R
i_2
R
CF2
R
R
R
DA
R
Current output electrode 2

structed of lucite based on the design of Hawkridge and Kuwana (81). The quartz rod was implemented in accordance with an analogous cell published by Wilson and Shu (82) (See Figure 13). The quartz rod served to reduce the volume of sample required and minimized the background absorbance. The first point is of concern when considering the expense of purchasing ferredoxin ($106/10 mg (5 ml)). Also, upon reduction ferredoxin exhibits a decrease in absorbance. Due to the small dimensions of the electrochemical diffusion layer (10^{-3} cm) a short pathlength is required to reduce the background attributed to the absorbance of the unreduced bulk sample. Conventional spectroelectrochemical studies generally involve monitoring an increase in absorbance in order to improve the signal to noise ratio. Absorbance changes measured were in the range of 0.005 absorbance units.

C. Procedures

1. Calibration of Reference Electrode

Ag/AgCl (1.0 M KCl) reference electrodes were calibrated versus the normal hydrogen electrode (NHE) by equilibration with saturated solutions of quinhydrone at pH 7. The quinhydrone electrode acts as a hydrogen ion indicating electrode for pH values up to 8 (83).

$$Q + 2H^+ + 2e \rightleftharpoons QH_2$$

where Q = quinone and QH_2 = quinhydrone.

$$E_{equil} = E^\circ (Q, QH_2) - 0.059\ pH$$

Figure 13. Quartz rod optically transparent electrochemical cell.

(Reprinted with permission from Crawley, C. D.; Hawkridge, F. M., Biochem. Biophys. Res. Comm. 1981, 99, 516. Copyright 1981, American Chemical Society. Reference (92)).

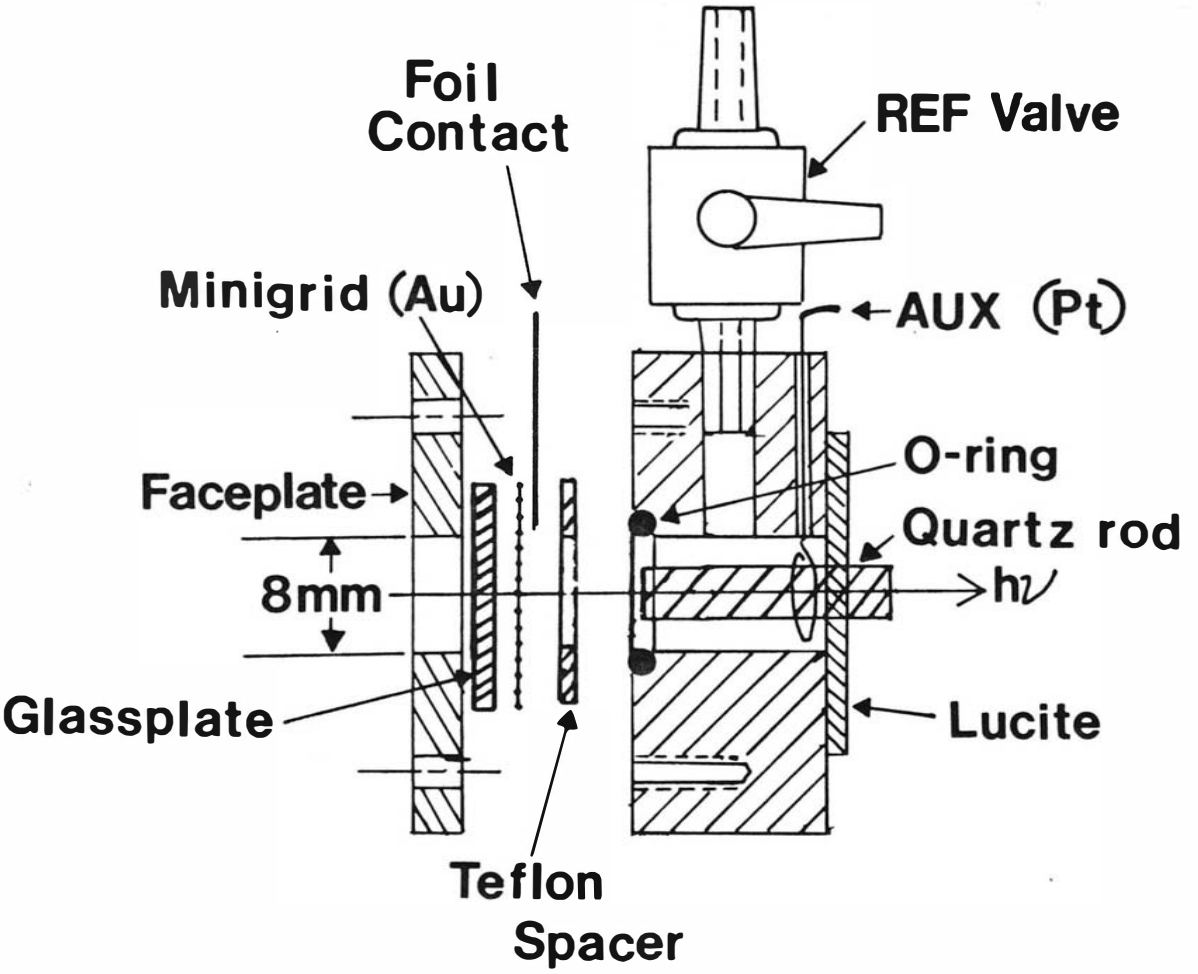
Foil
Contact
REF Valve
Minigrid (Au)
AUX (Pt)
O-ring
Faceplate
Quartz rod
8mm
hν
Glassplate
Lucite
Teflon
Spacer

where E° (Q, QH_2) = 0.699 mV. The potential difference between the reference electrode and the platinum electrode was measured potentiometrically.

$$E_{ref} = E_{equil} - \text{Reading (mV)}$$

(E_{ref} = 0.225 V ± 0.005 V)

2. Electrode Pre-treatment

Gold minigrid electrodes - before use electrodes were plasma cleaned for approximately 15 minutes (RF, 3-4 range).

Intrex-G electrodes (84) - electrodes were washed in Alconox solutions, immersed in warm HNO_3 three times (ca. 5 sec each) followed by sonicating 3-5 min in 50/50 EtOH/H_2O mixture. Afterwards they were repeatedly rinsed with distilled H_2O and dried lightly with a Kimwipe.

SnO_2(F) electrodes - electrodes were initially washed in Alconox, sonicated 15 minutes in 2X distilled H_2O, rinsed with isopropanol and dried with a Kimwipe.

Au disk and ring-disk electrodes - Prior to each experiment electrodes were polished with alumina on a gamal polishing cloth followed by Sonicating in 2X distilled H_2O. Immediately afterwards electrodes were cycled repeatedly throughout the potential range of interest in buffered solutions until reproducible voltammagrams free of surface contaminated peaks, were obtained.

3. Cell Assembly and Preparation

Spectroelectrochemistry

A diagram of the disassembled and assembled bulk cell is shown in Figures 14 and 15. When the gold grid or Intrex-G electrodes were used an aluminum foil contact was used in place of the brass shim depicted in the diagram. The gold was taped (dull side up for grid) onto a quartz or glass backplate with teflon tape. A circular hole was punched through the tape beforehand, which defined the area of electrode exposed to solution as well as an optical window through the cell. The cell was then screwed together securely. In all cases the auxiliary and reference electrodes were Pt and Ag/AgCl (1.0 M KCl) respectively.

Solution was introduced into the cell via vacuum/nitrogen procedures which have been previously published in more detail (81). For aqueous solutions, three cycles consisting of 20 seconds vacuum followed by 5 seconds nitrogen pressure were applied before filling the cell and reference compartment. Afterwards the conductance was checked with an ohmmeter between the reference, auxiliary and working electrodes to ensure good contact. For protein solutions numerous short cycles (ca. 5 sec) of N_2/vacuum were applied to prevent excessive agitation and foaming. All solutions were degassed and stored in sealed vials during cell assembly and concentration measurements were made on solution left in the degassing bulb. Ferredoxin solutions stored below 0°C were thawed prior to each experiment. The presence of the 420 and 450 nm bands, monitored spectroscopically before and after each experiment provided assurance that

Figure 14. Diagram of quartz OTE disassembled cell where: a) backplate, b) OTE, c) contact, d) Viton "o" ring, e) cell body, and f) quartz disc.

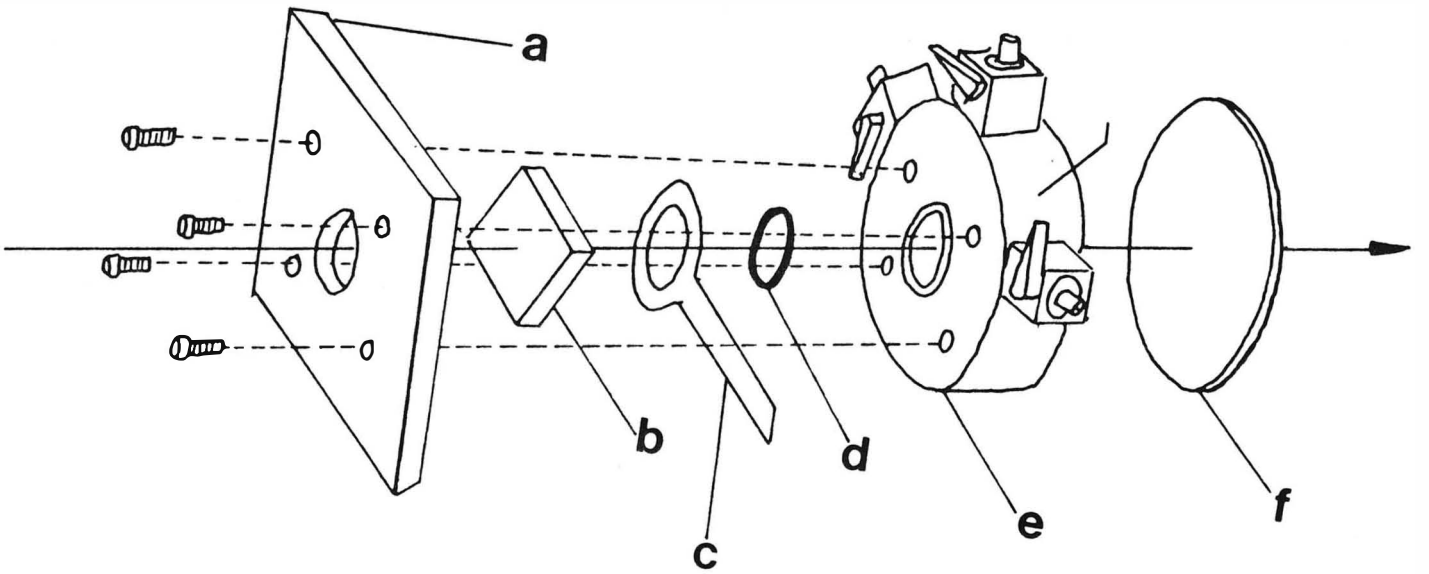
a
b
c
d
e
f

Figure 15. Back view of assembled OTE cell.

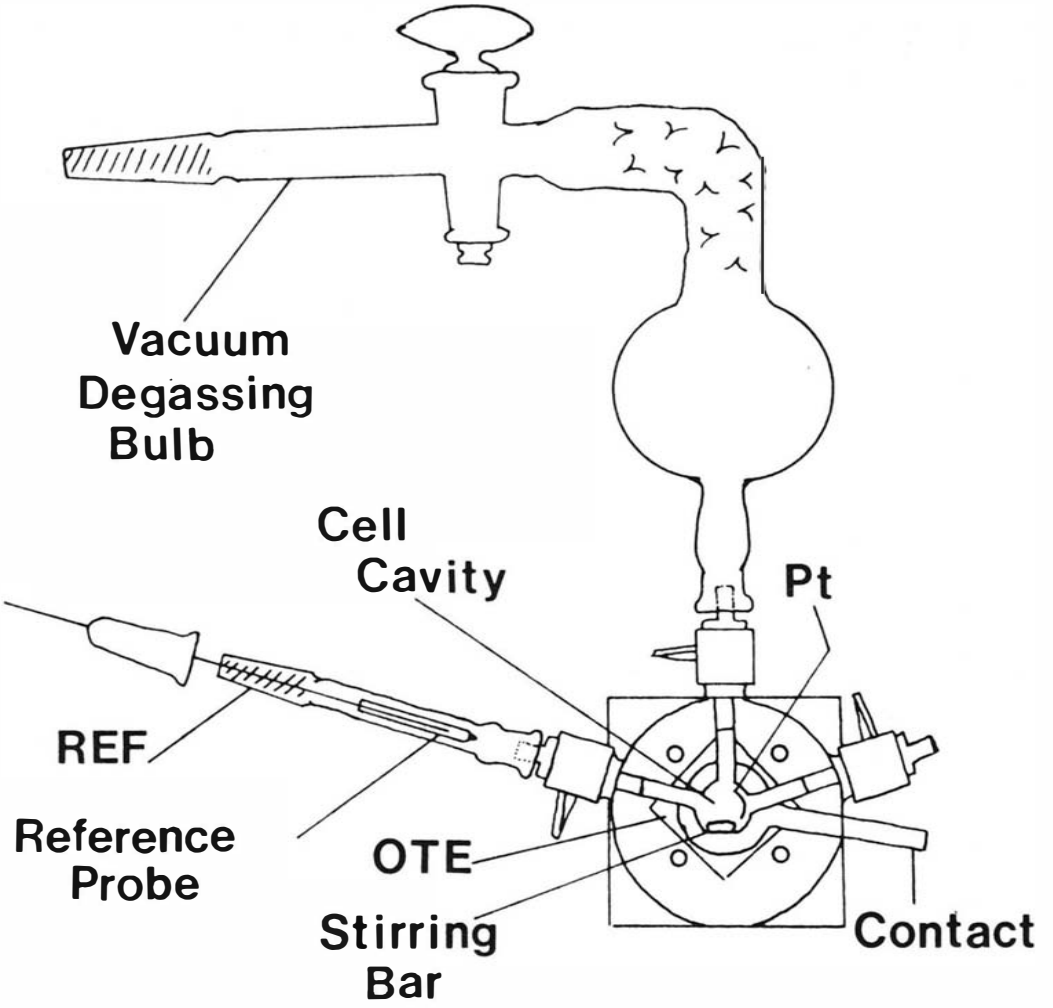
Vacuum
Degassing
Bulb
Cell
Cavity
Pt
REF
Reference
Probe
OTE
Stirring
Bar
Contact

the ferredoxin had not denatured.

Rotating Disk Voltammetry

A diagram of the cell used for disk experiments is shown in Figure 16. The glass cell (which is also jacketed for controlled temperature studies) has been fitted with a lucite cover which fits over the cell body and is held firmly in place at both ends by rubber bands. This insured that air or N_2 could only enter or escape through the top of the cell. The N_2 inlet tube served to degas the solution when immersed or to maintain a positive N_2 blanket about the peripheral of the cell when withdrawn.

The Ag/AgCl (1.0 M KCl) reference electrode consists of a u-shaped glass tube with a porous glass frit, Corning #210035, annealed into the tip. The auxiliary electrode consists of a platinum wire inserted into a glass tube which is coiled at the end and epoxied in a tube of larger diameter with a porous vycor cap epoxied to the bottom. The auxiliary electrode was filled with degassed phosphate buffer during electrode modification and Trizma buffer during the ferredoxin experiments.

4. Modification Procedures

Gold Minigrid, ring-disk and SnO_2 electrodes were electrochemically modified prior to each experiment with 1 mM methyl viologen solution. All potentials are referenced to the normal hydrogen electrode (NHE).

Gold minigrid (85)

Solution conditions: 0.067 M Phosphate (Titrisol) buffer, pH

Figure 16. Diagram of cell assembly for rotating disk experiments:

a) Au ring-disk electrode, A_{disk} = 0.458 cm^2

b) Ag anodized wire

c) Ag/AgCl reference electrode in 0.1 M KCl

d) N_2 bubbler and degassing tube

e) lucite cell cover

f) Pt wire auxiliary electrode

g) glass jacketed cell

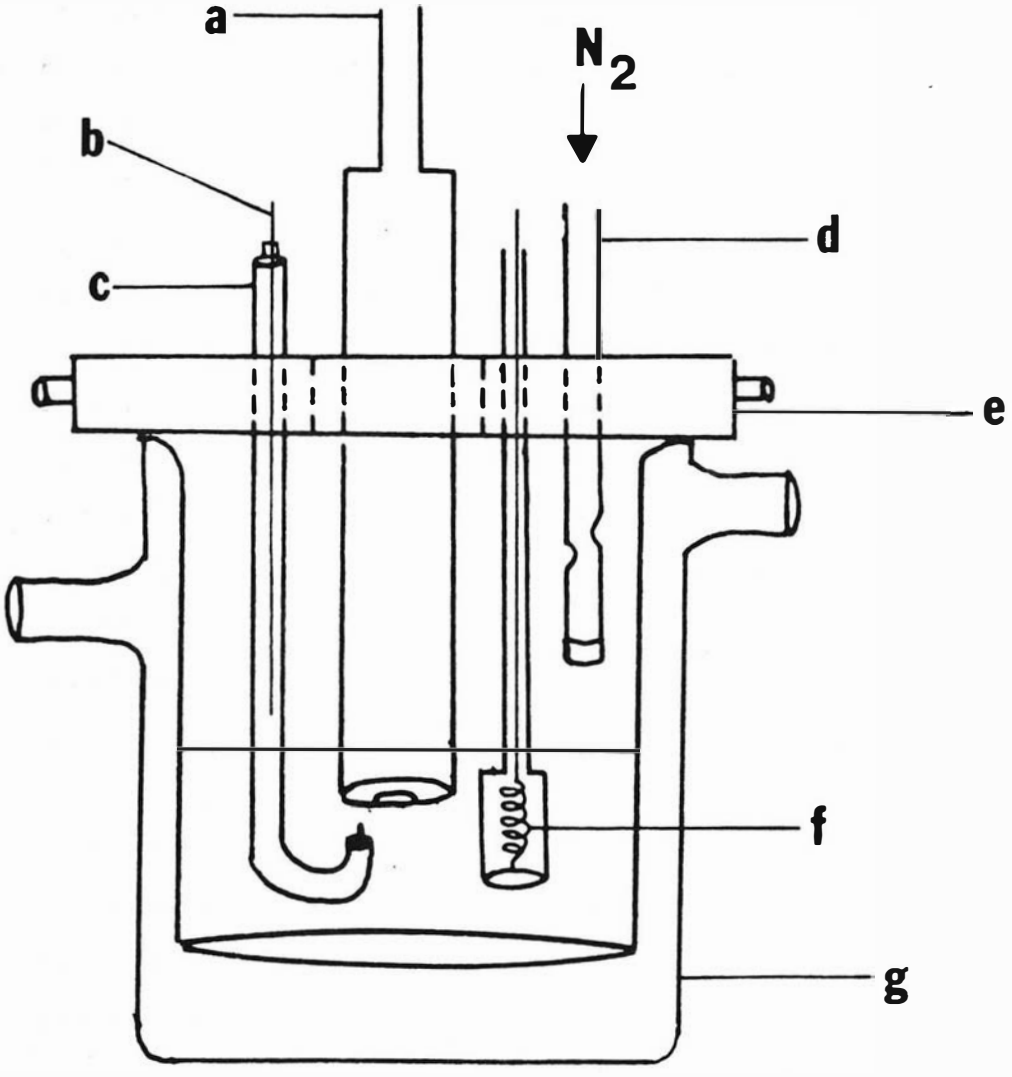
a
N2
b
d
c
e
f
g

7.0, 0.1 M NaCl.

Modification: After filling the cell with methyl viologen, a potential of -725 mV NHE was applied from open circuit for 5 minutes which produced the blue color characteristic of the cation radical $MV^{\cdot +}$. The potential was then stepped to +425 mV for an additional 10 minutes.

SnO_2(F) semiconductor electrode

Solution conditions: 1 mM methyl viologen, 0.4 M glycine/HCl buffer, pH 3.0.

Modification: Applied -750 mV for 2.5 minutes from open circuit followed by stepping to +425 mV for an additional 5 minutes. For both electrodes after modification the cell was rinsed intact with several hundred milliliters of 2X distilled water to remove the methyl viologen solution and dried on the vacuum train for approximately two hours. The reference compartment was also removed, washed and refilled with fresh degassed KCl solution before the cell was filled with ferredoxin.

Gold-ring disk electrode

Solution conditions: Same as for minigrid.

Modification: The same procedure as used for the minigrid. Modification was performed at the stationary disk and the ring and disk were each modified separately. Afterwards the electrode was rinsed and immersed in distilled water while the cell was being washed. Reference and auxiliary electrodes were washed and refilled with fresh degassed solutions.

5. Chronoabsorptometry Experimental Procedure

Reductive Kinetics

Potentials were applied from rest potential, +425 mV in all cases. Various reductive potential steps were applied and the absorbance decrease was recorded up to 60 seconds for gold, 36 seconds for SnO_2. The potential was then returned to +425 mV for 20 minutes before the next transient was taken.

Oxidative Kinetics

A small stir bar was inserted into the cell cavity during assembly. The solution was then bulk reduced at -505 mV while stirring for 80 minutes. The current was monitored until a steady state was reached, ca. 5 μA. Afterwards the cell was placed in the spectrometer. A potential of -525 mV was applied and the absorbance was monitored at 420 nm for 35 minutes until no additional absorbance changes were detectable. The resting potential throughout the experiment was -525 mV. Oxidative potentials successively more positive were then applied up to diffusion control.

6. Rotating Ring-Disk Voltammetry Experimental Procedure

Reductive Kinetics

Limiting (diffusion controlled) currents were initially recorded at -525 mV for various rotation rates. Kinetic experiments involved detecting the steady state currents for successively more positive potentials at each rotation rate. At the end of the ferredoxin experiment, background currents were measured at the same disk surface in Trizma buffer only.

Oxidative Kinetics

The limiting current at the ring and the disk was measured at -525 mV for different rotation rates. Afterwards the disk potential was set at -525 mV for diffusion controlled reduction and the ring potential was varied to successively more positive potentials. The current at the ring was then monitored at varying rotation rates to observe the oxidative behavior. Hence ferredoxin was reduced at the disk and re-oxidized at the ring.

CHAPTER V

RESULTS

Initial experiments consisted mainly of testing the reactivity of ferredoxin (Fd) at the methyl viologen modified gold (MVMG) minigrid electrode to determine the optimum potentials for diffusion controlled oxidation and reduction. Spectra of 118 μM Fd in the oxidized and reduced forms are shown in Figure 17. The arrow shows the relatively small band monitored at 420 nm. Figure 18 is a representation of the exhaustive oxidation and reduction of Fd in the quartz rod cell. The cell pathlength was calculated from Beer's Law to be ca. 0.06 cm. Reduction and oxidation were each complete in a period of approximately 40 minutes. There also did not appear to be any detectable contribution from edge diffusion within that time period. The absorbance in both cases maintained a steady state value before any increase was noted. Exhaustive oxidation and reduction could be effected for over a period of six hours without any substantial degradation of the absorbance response.

Though each surface is probably not reproduced exactly, each electrode modified according to the previously established procedure (85) was effective in electrolyzing ferredoxin. Individual electrodes did differ, however, in the lifetime of their activity. When the cell was subjected to vacuum overnight, the electrode performance was impaired though this procedure was not repeated to

Figure 17. UV-visible spectrum for 117.8 x 10^{-6} M ferredoxin solution. The solid curve represents the oxidized form and the dashed curve represents the reduced form of the molecule.

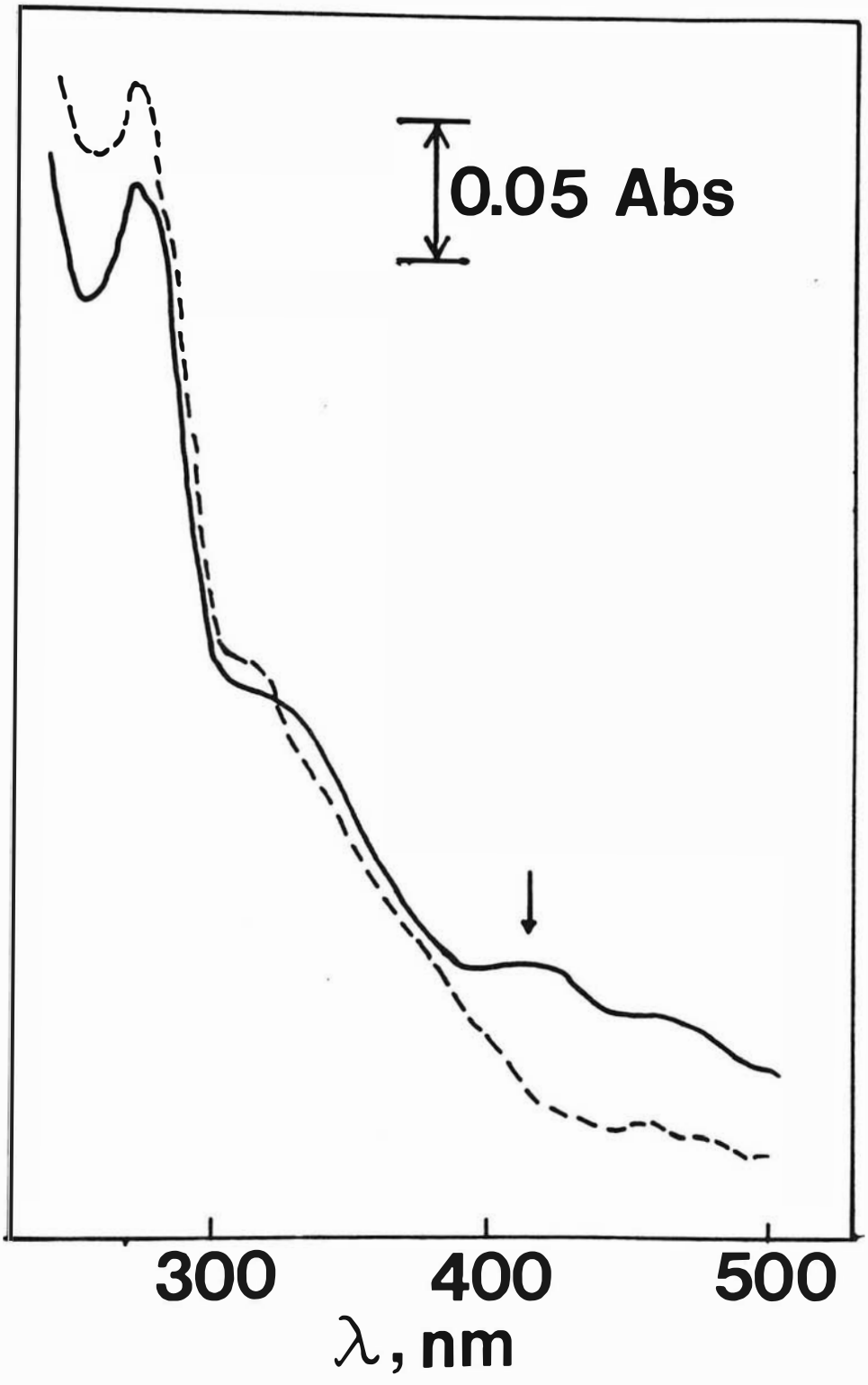
0.05 Abs
300
400
500
λ, nm

Figure 18. Absorbance indicative of the exhaustive oxidation and reduction of ferredoxin in the bulk OTE cell.

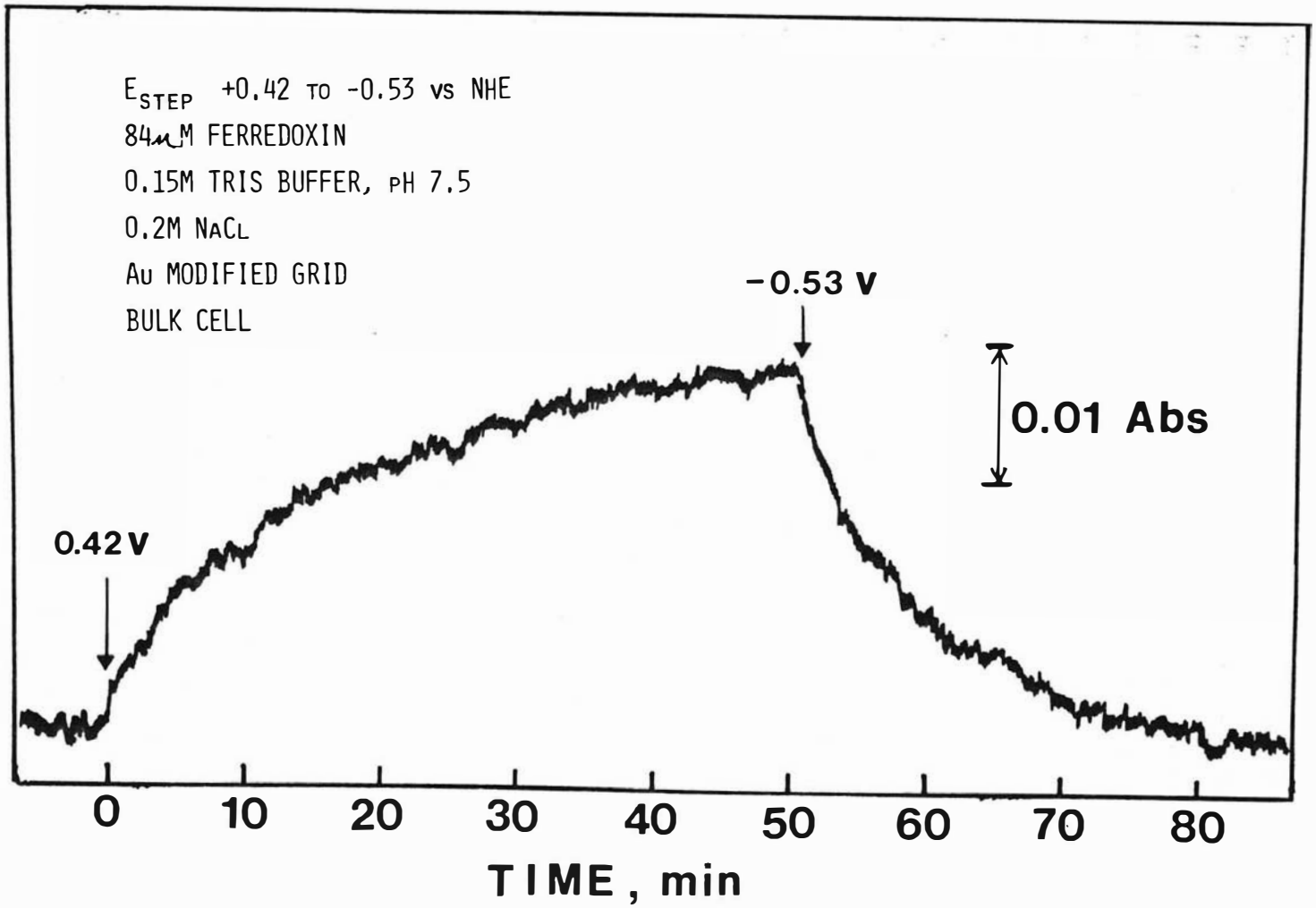
E_{STEP} +0.42 TO -0.53 vs NHE
84μM FERREDOXIN
0.15M TRIS BUFFER, pH 7.5
0.2M NaCl
Au MODIFIED GRID
BULK CELL
-0.53 V
0.01 Abs
0.42V
0
10
20
30
40
50
60
70
80
TIME, min

substantiate the effect. It also appears that cycling of the potentials before the potential step experiment in the presence of the protein results in a detectable decrease in lifetime and response. As a general rule, though, the modified grid electrodes are amenable for electrolyzing Fd for a period of at least 12 hours or more.

Figure 19 shows the absorbance versus $t^{\frac{1}{2}}$ results for two different concentrations of Fd at different newly modified electrodes. For a diffusion controlled transient as described by Equation (22), A vs $t^{\frac{1}{2}}$ should be linear over the applicable range of interest and the diffusion coefficient can be calculated from the slope. These conditions are exhibited in the experimental results. This is supportive evidence that sufficient overpotentials can be applied at this electrode to effect mass transfer limited electrolysis which is a criterion that must be fulfilled in order to extract kinetic parameters.

A. Reductive Kinetics

1. MVMG grid

Representative chronoabsorptometric results for the reduction of 118 μM Fd are given in Figure 20. Transients are shown for the application of three different overpotentials where c represents the diffusion controlled case. Because of the high level of noise apparent at this level of sensitivity, a solid line was drawn to approximate each transient. Signal averaging was not viable due to the 20 minute equilibration period required between each poten-

Figure 19. Linear dependence of absorbance versus $t^{\frac{1}{2}}$ behavior as shown for two different concentrations of ferredoxin at the MVMG minigrid electrode.

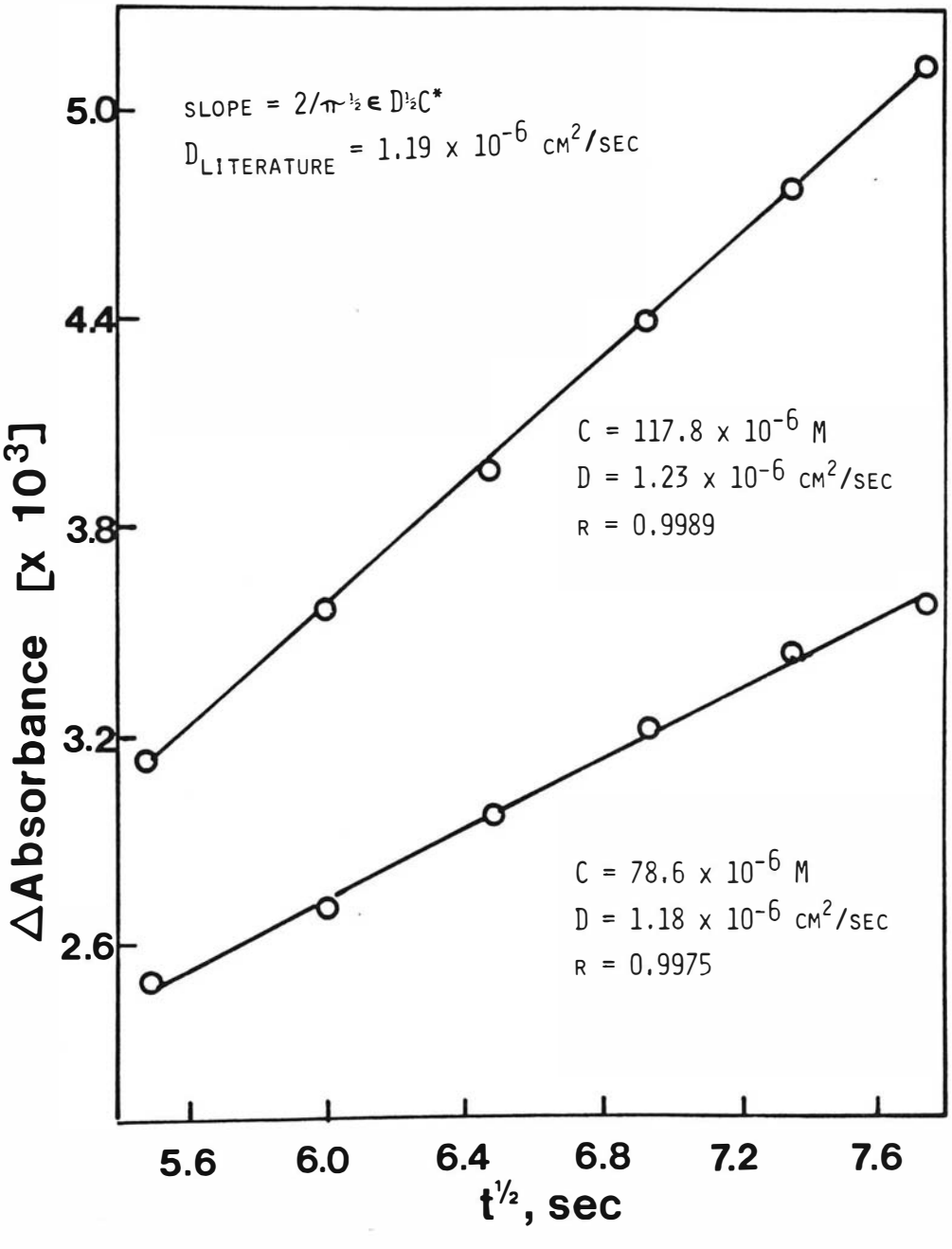
SLOPE = $2/\pi^{1/2} \in D^{1/2}C^*$
$D_{LITERATURE}$ = 1.19 x 10^{-6} cm^2/sec
C = 117.8 x 10^{-6} M
D = 1.23 x 10^{-6} cm^2/sec
R = 0.9989
C = 78.6 x 10^{-6} M
D = 1.18 x 10^{-6} cm^2/sec
R = 0.9975
ΔAbsorbance [x 10^3]
5.0
4.4
3.8
3.2
2.6
5.6
6.0
6.4
6.8
7.2
7.6
$t^{1/2}$, sec

Figure 20. Theoretical and experimental absorbance versus time behavior of spinach ferredoxin at a modified gold minigrid electrode. Solution conditions: 117.8 μM ferredoxin in 0.15 M tris buffer, pH 7.5, 0.2 M NaCl. Trace, potential step (mV vs. NHE) and overpotential, η, (mV vs. NHE).

(a) -439 mV, 16 mV

(b) -489 mV, 66 mV

(c) -524 mV, 101 mV

(Reprinted with permission from Crawley, C. D.; Hawkridge, F. M., Biochem. Biophys. Res. Comm. 1981, 99, 516. Copyright 1981, American Chemical Society. Reference (92)).

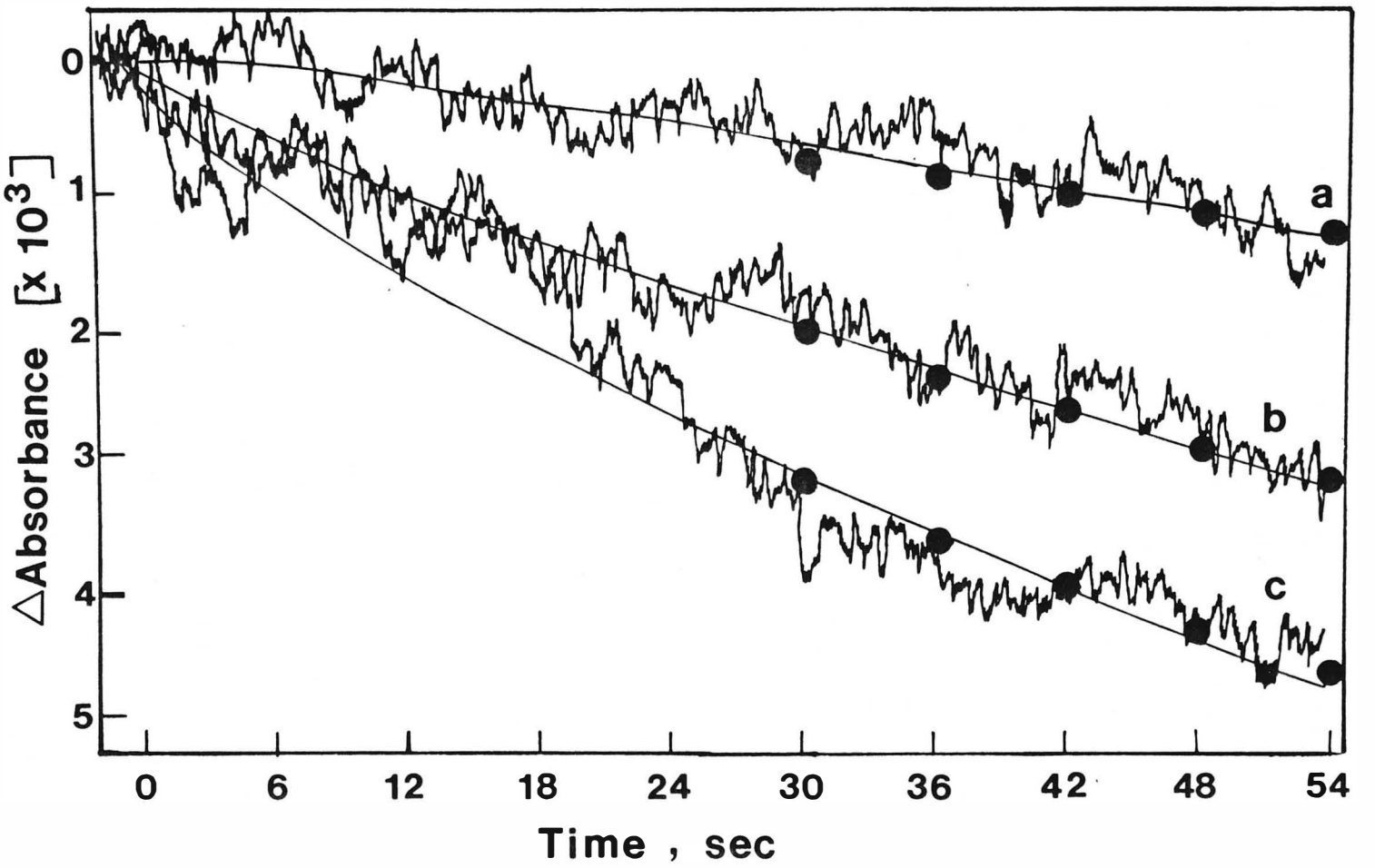
△Absorbance [x 10³]
0
1
2
3
4
5
0
6
12
18
24
30
36
42
48
54
Time , sec
a
b
c

tial step application. Solid circles represent the calculated theoretical chronoabsorptometric relations given in Chapter 3. The diffusion controlled transient is simulated by substituting the appropriate time increments, in seconds, into Equation (22) to cover the 30 to 60 second time period. For kinetically controlled cases, the average rate constant at each overpotential, as calculated from the normalized absorbance working curve, is input into Equation (23) for each time increment. This rate constant can be graphically evaluated by overlaying a plot of the experimental normalized data vs. log $(t^{\frac{1}{2}}/D^{\frac{1}{2}})$ onto the working curve. The value for $k_{f,h}$ can now be calculated from the difference in abscissa log values, where log $(k_{f,h})$ = log $(k_{f,h}t^{\frac{1}{2}}/D^{\frac{1}{2}})$ - log $(t^{\frac{1}{2}}/D^{\frac{1}{2}})$. The same process can be more conveniently achieved via computer generated A_n vs. log $(k_{f,h}t^{\frac{1}{2}}/D^{\frac{1}{2}})$ tables where D_{Fd} = 1.19 x 10^{-6} cm^2/sec (45). A program developed by D. Albertson (89) was utilized to generate the working curve file and extract rate constants using a standard searching routine for the input experimental absorbance-time file. The results are presented in Table III. As discussed in Chapter III, a plot of log $k_{f,h}$ vs η should be linear wherein log $k_{f,h}$ can be attained by extrapolating to η = 0 and α is calculated from the slope. Results from Table III are graphically presented in Figure 21, where $\eta = E_{applied} + E_{ref} - E^{\circ\prime}$. Selected transients have been overlayed onto the working curve (Figure 22) to show adherence of the experimental Fd data to the theoretical model.

As can be seen from the range of overpotentials applied, -16 to

TABLE III

Heterogeneous Electron Transfer Rate Constants for the Reduction of Spinach Ferredoxin at a Methyl Viologen Electrochemically Modified Gold Minigrid Electrode

η (mV)	$k_{f,h}$ (cm/s)
-16	$7.8\ (\pm 0.1) \times 10^{-5}$
-26	$1.1\ (\pm 0.2) \times 10^{-4}$
-41	$1.4\ (\pm 0.1) \times 10^{-4}$
-51	$1.7\ (\pm 0.1) \times 10^{-4}$
-66	$2.0\ (\pm 0.3) \times 10^{-4}$
-76	$3.9\ (\pm 0.3) \times 10^{-4}$
-101	$4.7\ (\pm 0.2) \times 10^{-4}$

Solution contained 117.6 M ferredoxin, pH 7.5 tris buffer, 0.2 M NaCl. Rate constants are mean values of at least 3 transients at each overpotential. Rate constants for individual transients are mean values of six observations over the 30 to 60 second time domain. Parentheses contain one standard deviation.

Figure 21. Dependence of $k_{f,h}$ on overpotential. Linear regression slope = 7.8 (±0.1) x 10^{-3} mV^{-1}; intercept = -4.20 (±0.06) cm/sec; correlation coefficient = 0.945.

(Reprinted with permission from Crawley, C. D.; Hawkridge, F. M., Biochem. Biophys. Res. Comm. 1981, 99, 516. Copyright 1981, American Chemical Society. Reference (92)).

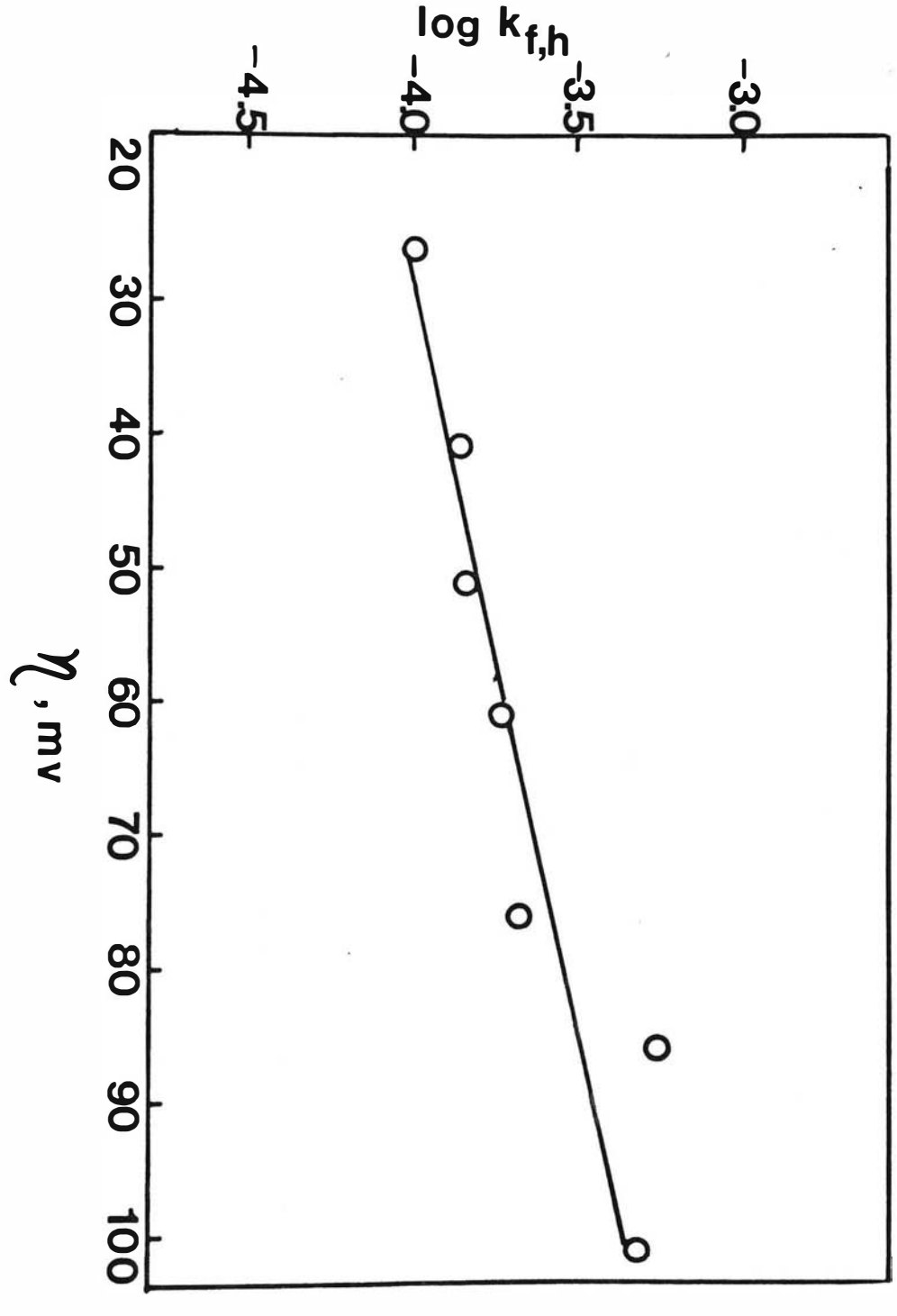
log $k_{f,h}$
-4.5
-4.0
-3.5
-3.0
20
30
40
50
60
70
80
90
100
η, mv

Figure 22. Normalized absorbance versus log ($k_{f,h}\, t^{1/2}/D^{1/2}$) working curve for the reduction of spinach ferredoxin at a modified gold minigrid electrode.

Same solution conditions as in Figure 21. Calculated log $k_{f,h}$ and transient number given in parentheses; , η = 86 (-3.34, 20); , η = 101 (-3.49, 2); , η = 66 (-3.68, 32); , η = 51 (-3.82, 25); , η = 26 (-4.17, 35); , η = 16 (-4.29, 9).

(Reprinted with permission from Crawley, C. D.; Hawkridge, F. M., Biochem. Biophys. Res. Comm. 1981, 99, 516. Copyright 1981, American Chemical Society. Reference (92)).

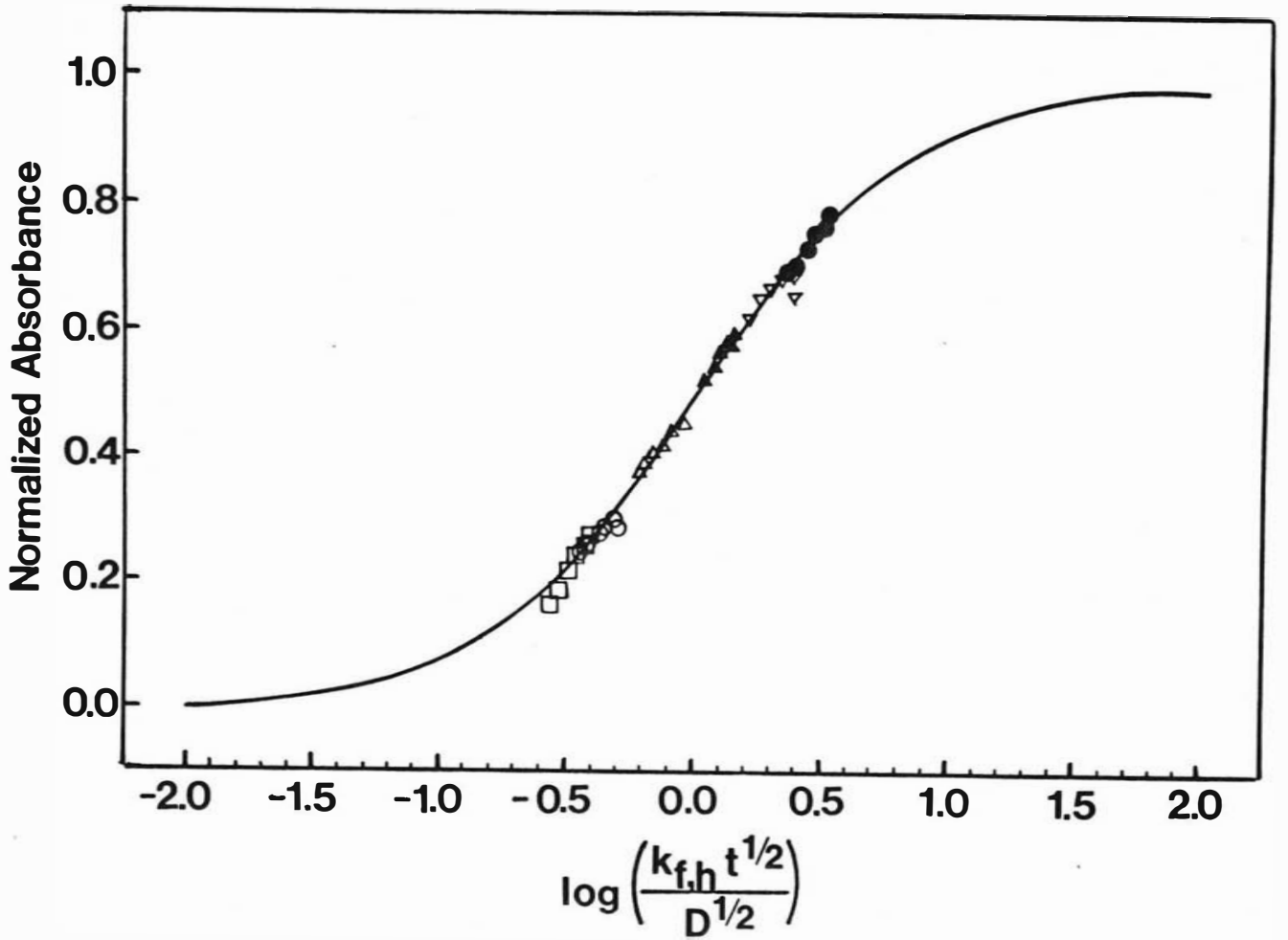
Normalized Absorbance
1.0
0.8
0.6
0.4
0.2
0.0
-2.0
-1.5
-1.0
-0.5
0.0
0.5
1.0
1.5
2.0
log (k_f,h t^1/2 / D^1/2)

-101, Fd appears to exhibit quasi-reversible behavior at the MVMG surfaces. Therefore the experimental results were treated and presented in accordance with the quasi-reversible model, for $\alpha \simeq 0.5$. Working curves at each overpotential were computer generated from the theoretical relations presented, and the new rate parameters were extracted. A comparison of data is summarized in Table IV and the graphical presentation of log k vs η for selected data analyzed by both treatments is shown in Figure 23. A summary of the overall results for the reduction of Fd at four different modified gold grid electrodes is given in Table IV.

2. SnO_2 (F) semi-conductor electrodes

An absorbance vs. time transient for the behavior exhibited by Fd at tin oxide electrodes is shown in Figure 24. Fd was electroactive at the plain and "modified" SnO_2 surfaces. However transients observed at these surfaces do not behave in a fashion characteristic of a freely diffusing reactant. Absorbance-time behavior does not correspond to the calculated theoretical values. A sharp increase in absorbance was detected at the onset of each potential step application. Afterwards, the absorbance increased somewhat but leveled off to a constant value smaller in magnitude than that predicted for the spectroscopic concentration. The behavior seemed characteristic of species adsorbing to the surface of the electrode. The sharp spike in absorbance occurred too rapidly to be attributed to reactant diffusing to the electrode given the diffusion coefficient of Fd. Also the decline in the absorbance at longer times could be explained as product accumulation onto the

TABLE IV

Summary of Results Obtained for the Irreversible and Quasi-reversible Treatment of the Reductive Electron Transfer Kinetic Data at the MVMG Minigrid Electrode

IRREVERSIBLE KINETIC CASE

[Ferredoxin] μM	$k^{\circ\prime}_{f,h}$ (cm/sec) α correlation coefficient
78.5	$4.9\ (\pm.2) \times 10^{-5}$ $0.78 \pm (0.18)$ 0.93
117.8	$6.3\ (\pm0.1) \times 10^{-5}$ $0.46 \pm (0.09)$ 0.96
123.9	$6.8\ (\pm0.1) \times 10^{-5}$ $0.47 \pm (0.07)$ 0.98

continued

TABLE IV (continued)

117.8	$8.1\ (\pm 0.1) \times 10^{-5}$ $0.67 \pm (0.06)$ 0.98
Overall Results	$6.5\ (\pm 1.3) \times 10^{-5}$ $0.60 \pm (0.16)$

QUASI-REVERSIBLE KINETIC CASE

[Ferredoxin] μM	$k^{o'}_{f,h}$ (cm/sec) α Correlation Coefficient
78.5	$9.8\ (\pm 0.24) \times 10^{-5}$ $0.50 \pm (0.003)$ 0.8

continued

TABLE IV (continued)

117.8	$8.9\ (\pm 0.06) \times 10^{-5}$ $0.36 \pm (0.1)$ 0.90
123.9	$8.5\ (\pm .07) \times 10^{-5}$ $0.42 \pm (0.01)$ 0.96
117.8	$1.9\ (\pm 0.05) \times 10^{-4}$ $0.39 \pm (0.07)$ 0.99
Overall Results	$1.16\ (\pm 0.5) \times 10^{-4}$ $0.42 \pm (0.06)$

Figure 23. Comparison of the log k vs. η behavior for selected transients treated using the irreversible and quasi-reversible theories for reduction at the MVMG mini-grid electrode.

Fd = 117.8 x 10^{-6} M, 0.2 M NaCl, pH 7.5

a) Irreversible case: slope = 9.1 (±0.02) x 10^{-3} mV^{-1}; intercept = -3.98 ± (0.02) cm/sec; correlation coefficient = 0.997.

b) Quasi-reversible case: slope 6.7 (±0.07) x 10^{-3} mV^{-1}; intercept = -3.72 ± 0.05) cm/sec; correlation coefficient = 0.994.

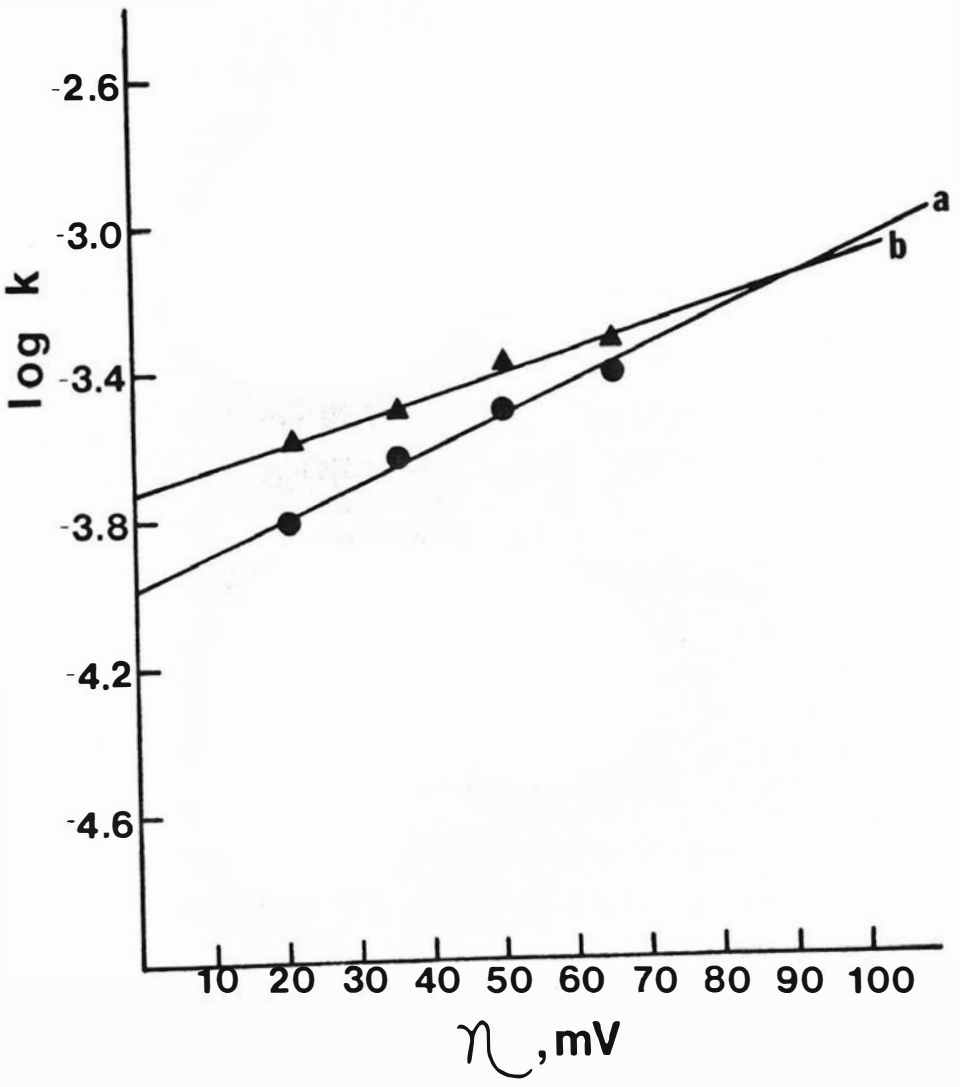
-2.6
-3.0
-3.4
-3.8
-4.2
-4.6
log k
a
b
10 20 30 40 50 60 70 80 90 100
η, mV

Figure 24. Absorbance-time transient for Fd at the plain SnO_2 electrode for η = 300 from 0 to 36 seconds.

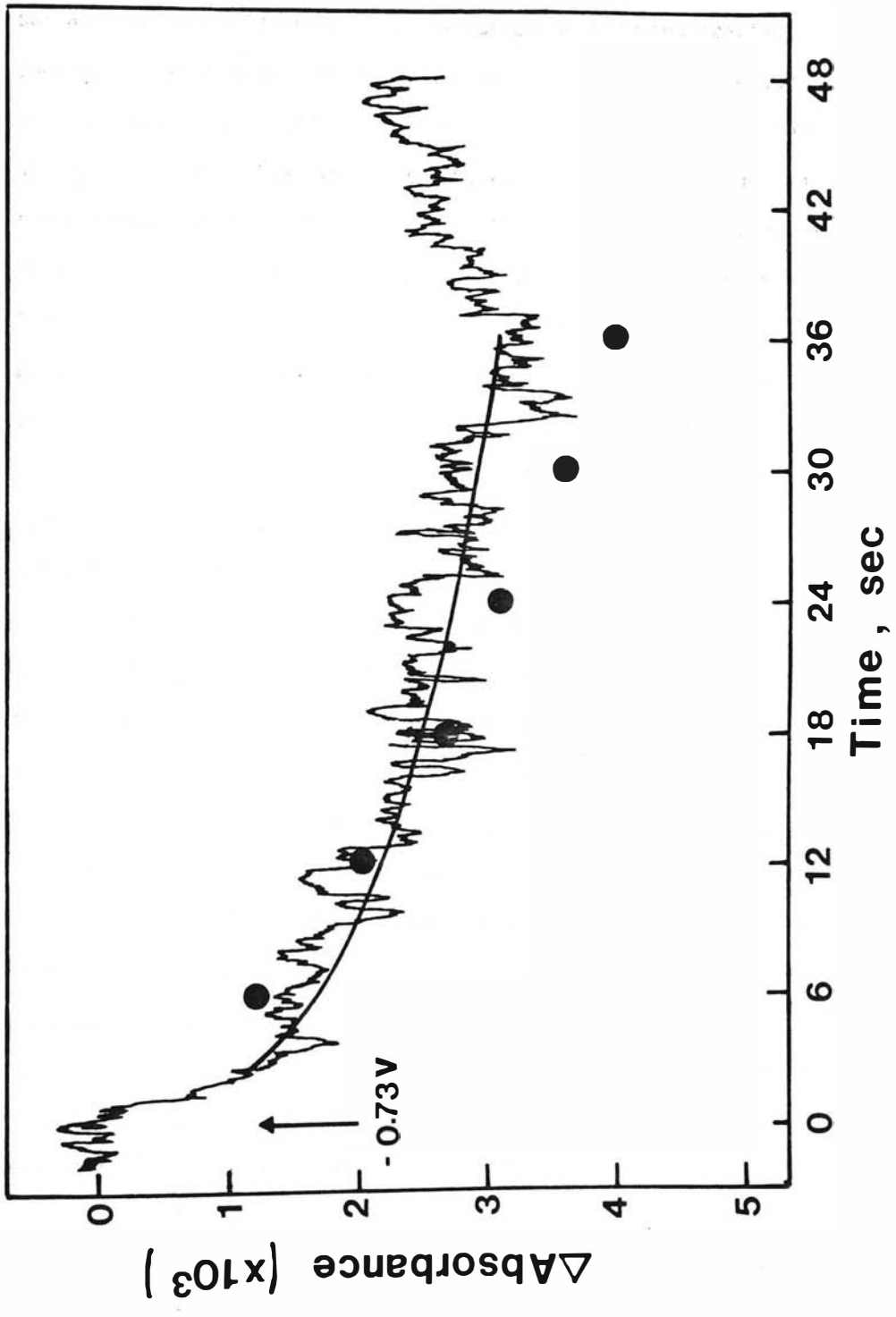
ΔAbsorbance (x10³)
0
1
2
3
4
5
- 0.73 V
0
6
12
18
24
30
36
42
48
Time, sec

surface, which would prevent the diffusion of incoming reactant species. The adsorbed species would not be attributed to a completely denatured layer of Fd since only the native species should absorb at 420 nm. The "spike" is observed in each transient and the magnitude of the signal is a function of the applied potential. It would seem that the native species undergoes adsorption/desorption behavior forming a seemingly native layer on the surface which prevents further reduction of the electroactive bulk species. Further studies on the behavior of Fd at these surfaces should yield mechanistic insights. However the observed behavior was not amenable to evaluation using the current theory developed by Albertson and coworkers (76). This point will be addressed later.

More negative potentials were required at SnO_2 electrodes to effect diffusion controlled behavior. For MVMG electrodes, potentials ranging from -425 to -525 mV were applied as opposed to -475 to -725 mV at SnO_2 which corresponds to $-46 < \eta < -296$. However, transients obtained between -625 to -725 mV were approximately the same order of magnitude in absorbance.

Absorbance changes at lower over-potentials were detected for the SnO_2 "modified" surface, as low as -275 mV. However the spike in absorbance became progressively more severe as the experiment progressed. After several transients were taken, absorbance increase attributable to incoming species decreased until no significant change resulted after the initial spike.

3. Intrex-G (MPOTE)

Ferredoxin was not electroactive at this surface. Upon appli-

cation of -525 mV, an absorbance increase occurred which is not characteristic of reduced Fd. On returning to the positive rest potential, the absorbance did not decrease, but remained the same. Upon application of -475 mV, further absorbance increases resulted with subsequent leveling.

These electrodes are made by sputtering very thin films (ca. 1000 Å) of gold onto polyester sheets. This film deteriorates with the production of significant amounts of hydrogen on the surface (84). These electrodes exhibit similar response as plain gold metal electrodes. For a pH 7.5 buffered solution significant hydrogen current is not generated until around -625 mV. However deterioration seemed evident here at -475 mV. The increase in absorbance and subsequent loss of activity may be attributed to stripping of gold from the electrode surface and/or subsequent adsorption of protein on the surface. The presence of the protein could also have resulted in the shifting of the hydrogen overpotential to more positive potentials.

4. MVMG Disk electrode

The disk potential, E_d, was varied with rotation rates to yield kinetic and diffusion controlled currents. The predicted diffusion controlled currents, I_d, can be calculated from the Levich equation:

$$i = 0.620\ nFAD_o^{2/3}\ \nu^{-1/6} C^b\ \omega^{1/2}$$

for C^b = 152 μM Fd. A comparison of the theoretical and experimental currents is given:

	50	100	200	500	1000	f(RPM)
Theoretical	2.24	3.17	4.48	7.08	10	
Experimental	2.55	3.35	4.40	6.17	7.9	

where E_d is -525 mV and I_d is in microamperes. From Equation (38), a plot of $1/i$ vs $\omega^{-\frac{1}{2}}$ is linear. This relationship is depicted in Figure 25, where background current contributions from protein adsorption and supporting electrolyte have been subtracted. The dependence of the rate constants on overpotential is shown in Table V and log k vs η is plotted in Figure 26.

B. Oxidative Kinetics

1. MVMG minigrid electrode

The log k vs η behavior is depicted in Table VI and plotted in Figure 27. Mass transfer limiting behavior seems to be predominant at overpotentials of 84 mV and greater, therefore only potentials of that and below were used in the least squares analysis. The plot is linear and A vs $t^{\frac{1}{2}}$ for 84 mV is also linear. However, the normalized absorbance-time transients do not fit the working curve as well and α is anomalously greater than 1 (see Figure 28). This may possibly be due to effects of any O_2 present in the system. As previously mentioned cyclics were not taken during these experiments to detect O_2 concentrations due to the detrimental effects observed on the activity and lifetime of the electrode in the presence of the protein. Also the electrode surface may have altered from maintaining the potential at a comparatively negative value

Figure 25. Current versus rotation rate as a function of overpotential at the Au ring-disk electrode.

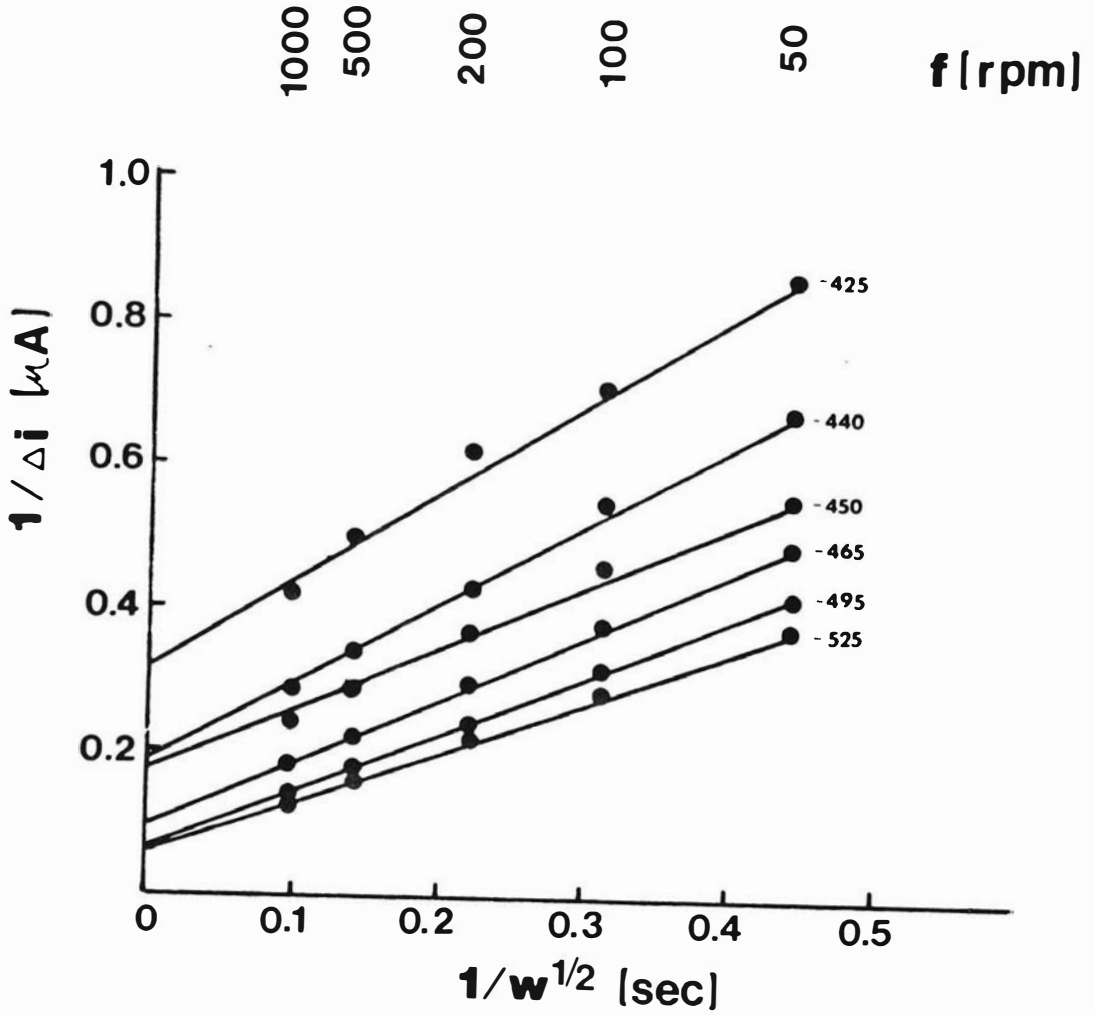
1000
500
200
100
50
f [rpm]
1.0
0.8
0.6
0.4
0.2
1/Δi [μA]
-425
-440
-450
-465
-495
-525
0
0.1
0.2
0.3
0.4
0.5
1/w^1/2 [sec]

Figure 26. Log k vs. η plot for Fd at the MVMG ring-disk electrode: slope = 8.07 (±0.08) x 10^{-3} mV^{-1}; intercept = -3.98 ± (0.04) cm/sec; correlation coefficient = 0.97.

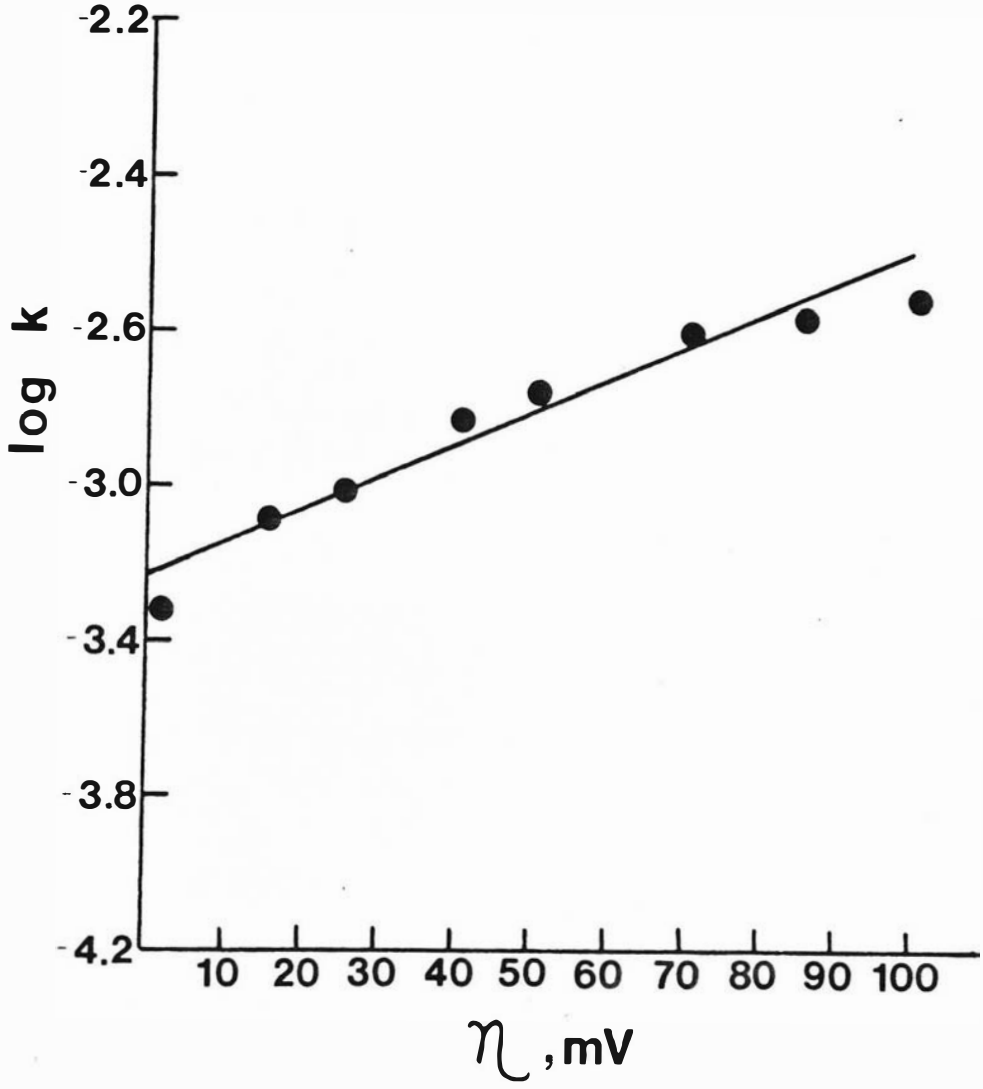
-2.2
-2.4
-2.6
-3.0
-3.4
-3.8
-4.2
log k
10 20 30 40 50 60 70 80 90 100
η, mV

Figure 27. Linear log k vs. η behavior for the oxidation of Fd at the MVMG minigrid electrode: slope = 1.98 (±.0002) x 10^{-2} mV^{-1}; intercept = -4.35 ± (0.01) cm/sec; correlation coefficient = 0.999.

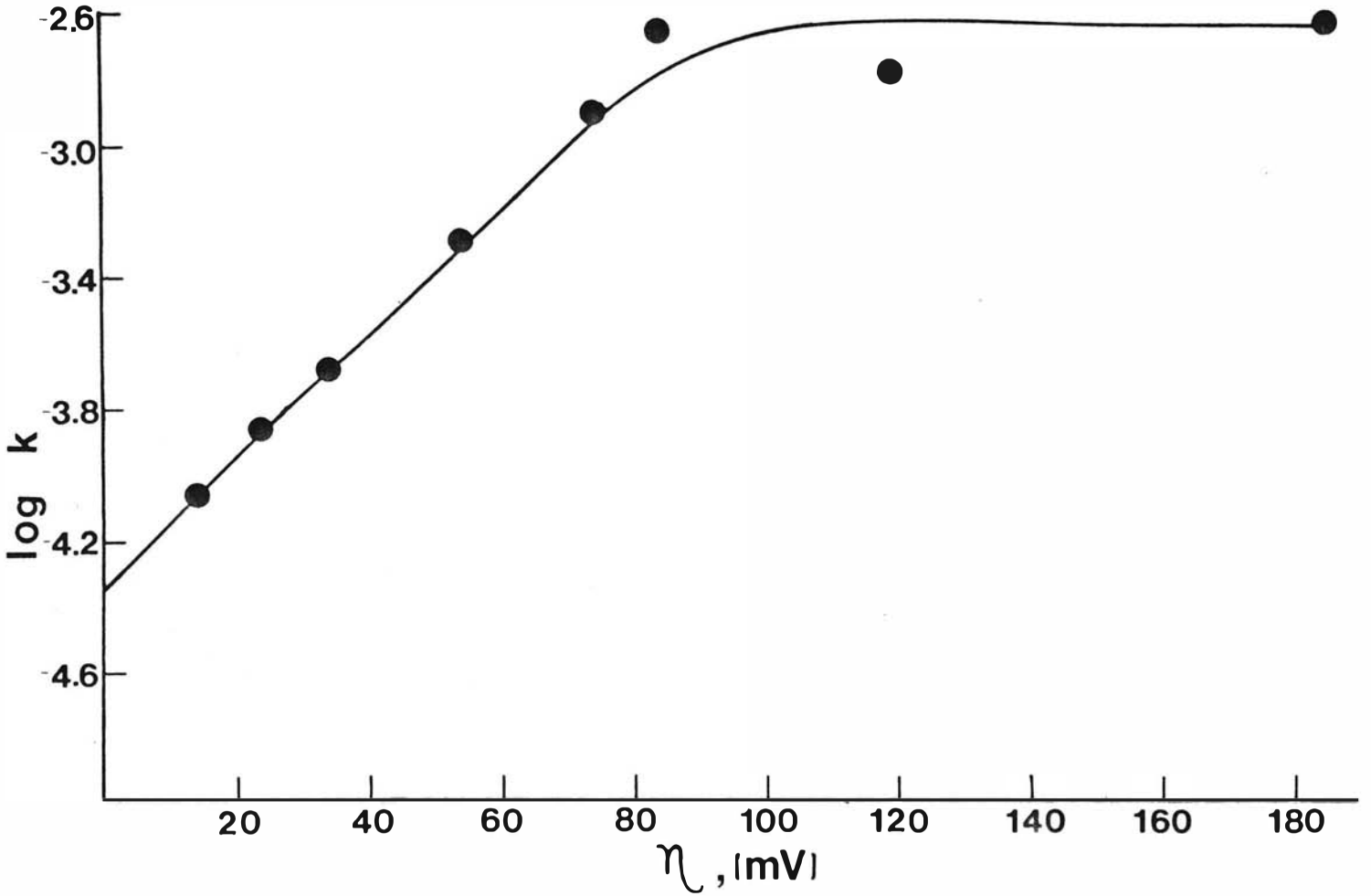
-2.6
-3.0
-3.4
-3.8
-4.2
-4.6
log k
20
40
60
80
100
120
140
160
180
η, [mV]

TABLE V

Dependence of the Heterogeneous Electron Transfer Rate Constants on Overpotential at the Methyl Viologen Modified Gold Rotating Disk Electrode

η (mV)	$k_{f,h}$ cm/sec
-101	3.1 (±.003) x 10^{-3}
- 86	2.77 (±.005) x 10^{-3}
- 71	2.53 (±.004) x 10^{-3}
- 51	1.77 (±.004) x 10^{-3}
- 41	1.46 (±.005) x 10^{-3}
- 26	9.51 (±.01) x 10^{-4}
- 16	8.02 (±.01) x 10^{-4}
- 1	4.7 (±.02) x 10^{-4}

Solution contained 152 μM ferredoxin, pH 7.5 tris buffer, 0.2 M NaCl. Rate constants were calculated from current measurements obtained at five different rotation rates for each applied overpotential. Error limits in parenthesis are indicative of the standard error in the intercept of linear regression analysis of $1/i$ vs. $1/w^{\frac{1}{2}}$.

TABLE VI

Heterogeneous Electron Transfer Rate Constants for the Oxidation of Spinach Ferredoxin at a Methyl Viologen Electrochemically Modified Gold Minigrid Electrode

η (mV)	$k_{f,h}$ (cm/s)
14	$8.5\ (\pm.2) \times 10^{-5}$
24	$1.4\ (\pm.2) \times 10^{-4}$
34	$2.1\ (\pm.2) \times 10^{-4}$
54	$5.1\ (\pm.1) \times 10^{-4}$
74	$1.2\ (\pm.1) \times 10^{-3}$
84	2.2×10^{-3}

Solution contained 161 μM ferredoxin, pH 7.5 tris buffer, 0.2 M NaCl. Rate constants are mean values of at least 3 transients at each overpotential, except at η = 74 and 84 which are representative of two and one transients respectively.

Figure 28. Normalized absorbance working curve fit for the oxidative kinetics of Fd at the MVMG minigrid electrode.

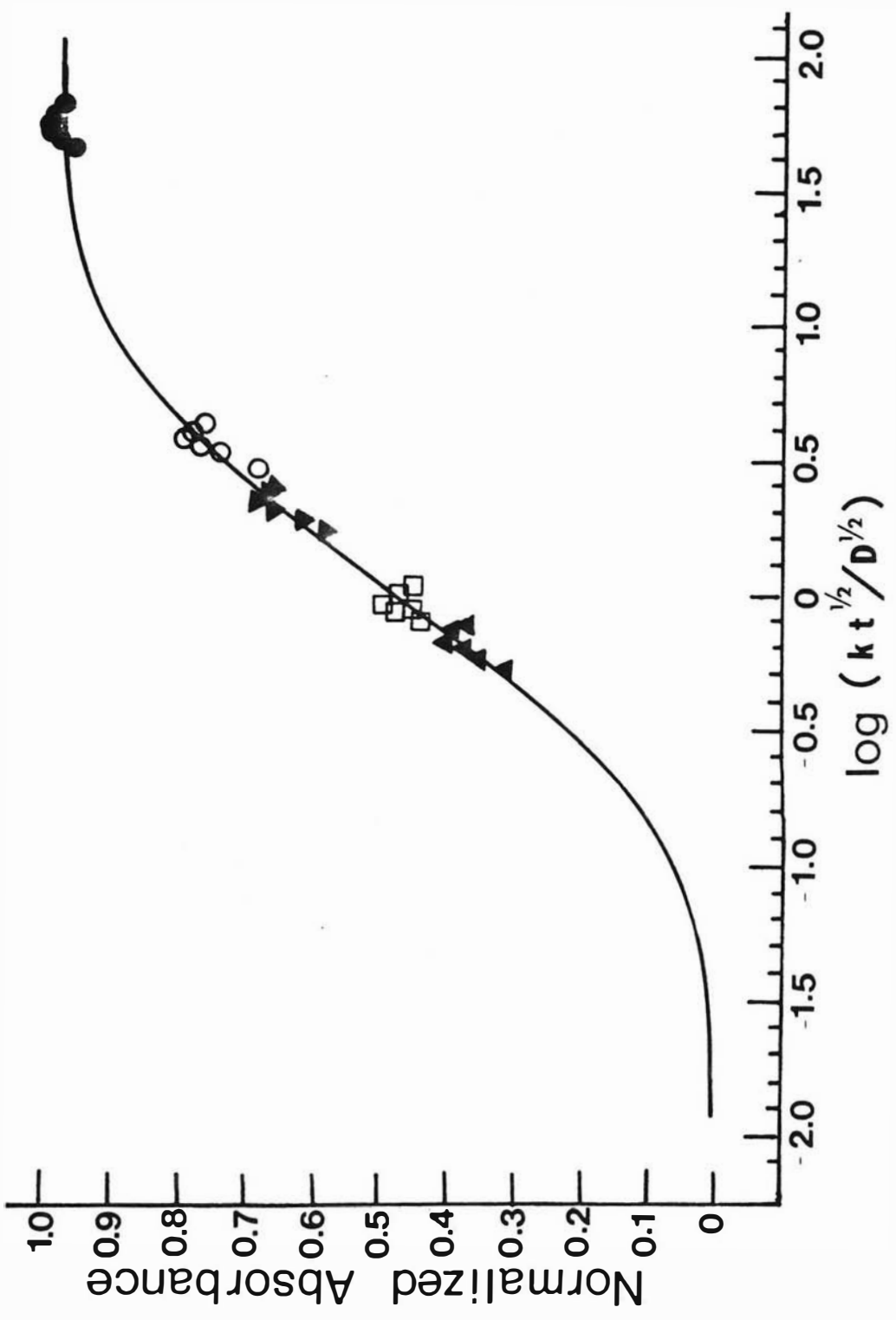
Normalized Absorbance
1.0
0.9
0.8
0.7
0.6
0.5
0.4
0.3
0.2
0.1
0
-2.0
-1.5
-1.0
-0.5
0
0.5
1.0
1.5
2.0
log (k t ½ / D ½)

for such a long period of time.

2. MVMG Ring-Disk electrode

Currents detected at the ring were small and sporadic. Limiting currents were not attainable, which either suggests that the modification at the ring was not effective or that the currents were not sufficient in magnitude to detect a trend after background currents were subtracted. Higher concentrations of Fd may be required to compensate for the smaller electrode area and hence smaller currents observed at the ring.

CHAPTER VI

DISCUSSION

Voltammetric measurements on proteins is a recent field which is becoming more prevalent. Kinetic determinations on biological molecules reacting homogeneously with various types of electrochemical mediators is well established (87, 88). However, reports of direct reduction of proteins at solid electrode surfaces are not as common (89-91). No previous studies are cited wherein the direct heterogeneous electron transfer kinetics of spinach ferredoxin are determined. To date only the MVMG electrodes have been effective in electrolyzing Fd directly without evidence of severe denaturation or adsorption. The spectroelectrochemical techniques have now been established. However, electrode surfaces must be developed or found which facilitate electron transfer with biological molecules. This area of work is just beginning to develop. Until one is able to simulate conditions by reproducing the cell environment, information describing the behavior of the species at artificial surfaces, which may or may not be a valid assessment of its behavior in vivo, should be pursued. However, the first step is to establish a model system from which one may postulate certain physiological aspects of the molecule under simulated conditions before one can concentrate on constructing the reaction environment. Such a system does seem presently to involve these electrodes, though variables concerning the heterogeneous kinetics and better adherence to model conditions can be optimized.

For spectroelectrochemical measurements, one requires an electrode surface which is electroactive and optically transparent to light of the wavelength of interest. The theory for single potential step chronoabsorptometry is only valid for cases which exhibit semi-infinite linear diffusion to a planar surface. Earlier model systems initially utilized planar oxide coated glass electrodes or metal deposited thin film electrodes (93). The gold minigrid surface is electroactive. However, it can only be considered planar once certain criteria have been established (93).

This condition is not met with the modified grid used in these experiments until 25 seconds after potential step application. The optical transparency of the grid is attributed to its perforated character wherein the gold itself is not transparent, but light is transmitted through the holes in the cross section of the grid. The electrode does not exhibit true planar character until sufficient time has elapsed to allow "hole filling" by diffusing electroactive species. For optical measurements, this criterion is exemplified by linear A vs $t^{\frac{1}{2}}$ behavior under diffusion controlled conditions. Petek and co-workers (93) have examined this behavior in minigrids of various hole dimensions from 2000 lines per inch (lpi) to 100 lpi. They report a relation from which one may estimate the time elapsed before the grid exhibits planar character.

$$0.50 = \text{erf}\ (x/2D^{\frac{1}{2}}t^{\frac{1}{2}}) \qquad (39)$$

where D is the diffusion coefficient of the product species and X is one-half the grid hole size.

For example, conditions of semi-infinite linear diffusion would become evident in a matter of milliseconds using 2000 lpi gold mesh for a species having $D = 10^{-5}$ cm^2/sec. Experiments conducted at these grid sizes would then allow one to measure transient behavior for Fd at shorter times. However, the percent optical transparency of the electrode decreases with hole size.

Another problem attendant to the grid is manifest in its lack of rigidity. If the grid is not placed perfectly flat on the surface of the backplate, electroactive species found in pockets of solution behind the electrode can diffuse to the surface, thus contributing to the flux. In cases where strictly double sided diffusion predominates, the predicted absorbance would be doubled. However, should there be contributions from double sided behavior in experiments designed to monitor single sided behavior, then the normalized absorbance would be greater than predicted producing added uncertainty and discrepancy in the calculated rate constant for different experiments.

Due to these complications with the grid the Intrex-G (MPOTE) and fluoride doped tin oxide (SnO_2) electrodes were tried though they also presented attendant problems.

The Intrex-G electrode is fairly rigid and optically transparent and would be ideal if the surface would be amenable to electrochemical modification with methyl viologen. However, modification conditions require potentials sufficiently negative to produce large amounts of hydrogen current which would strip the gold coating from the plastic surface.

The behavior observed at the SnO_2 electrode is interesting from a mechanistic viewpoint, though, as pointed out previously it is not amenable to analysis using Butler-Volmer formalism. It would seem that electron transfer is effected through a reversibly adsorbed layer of undenatured protein. Adsorption of protein to electrode surfaces is a widely cited phenomenon and has been postulated as a mechanism for electron transfer in these molecules (63, 70, 94, 95). Strong irreversible adsorption was reported for Fd by Kuznetsov (63) at mercury electrodes which resulted in denaturation via bonding of the S-S and S-H bonds to the surface. In some cases, after monolayer coverage of the surface was achieved, the resultant current indicated a hindrance to further charge transfer (63, 70). Bowden et al. (96) have postulated a mechanism involving charge transfer through an adsorbed layer of protein which would account for similarities in the rate of electron transfer observed for cytochrome c at various electrode surfaces. Spectroscopic behavior of Fd at SnO_2 appears to reflect characteristics akin to that observed with Fd at mercury and cytochrome c at various electrode surfaces. Optical evidence supports the immediate adsorption of protein to the surface and subsequent electron transfer, though, to a limiting degree. Large denaturation does not seem apparent in comparison to that observed at mercury, but this layer does seem to inhibit further charge transfer through the protein fabric in contrast to the conductive characteristic of the adsorbed cytochrome c layer. Adsorption is not spectroscopically apparent for cytochrome c at SnO_2 surfaces and the absorbance-time behavior is as

predicted by the theoretical relations.

Adsorption of Fd may occur at the minigrid surfaces though this could not be probed optically since the gold grid surfaces are not transparent to light. It does seem to occur at the gold disk surfaces due to the differences in background currents observed in buffer solutions for disks used before and after contact with the protein. However the extent of adsorption is not as severe since it does not appear to hinder further charge transfer.

Rate constants for ferredoxin have been narrowed to within half an order of magnitude using a theory which covers over nine orders of magnitude. This is reasonable in light of the high dependence of the technique on the ability to produce reproducible surfaces which is a procedure probably not yet optimized in this laboratory.

Reproducibility is also compromised in the Fd work due to the low molar absorptivity of the band monitored which forces one to monitor signals with very low signal to noise ratios. Because of such a large amount of uncertainty inherent in the signal more transients are required for averaging which also extends the length of time for each experiment. As the required time increases several complications may become evident: 1) oxygen may diffuse into the system, 2) Fd absorbance may decrease due to partial denaturation which would decrease the sensitivity of the measurement, 3) the electrode surface could alter resulting in a loss or decrease in activity, and 4) convective effects may become evident. These problems would be alleviated somewhat by using higher concentrations of Fd which are presently not commercially available.

For the gold disk experiments the above complications from optical effects are not apparent. Compared to absorbance measurements at the milliabsorbance unit level, the microampere currents measured in the gold disk Fd experiments exhibit more favorable signal-to-noise behavior. However, unlike transmission experiments which are species selective, current measurements are sensitive to all faradaic reactions occurring in the system. Because of this, background currents must be measured in the presence of buffer alone which may not account for any electroactive impurities present in the protein solution. Both techniques are unaffected by nonfaradaic charging currents.

For the gold disk experiments the above complications from optical effects are not apparent. Unlike absorbance measurements which are typically limiting at milli absorbance units, current recorders are sensitive to microamperes with much more favorable signal to noise behavior. However, unlike transmission experiments which are species selective, current measurements are sensitive to all faradaic reactions occurring in the system. Because of this, background currents must be measured in the presence of buffer alone which may not account for any electroactive impurities present in the protein matrix. Both techniques are unaffected by non-faradaic charging currents.

CHAPTER VII

CONCLUSION

The utility of electrochemical measurements at the MVMG surfaces in ascertaining the heterogeneous kinetic parameters of electron transfer has been demonstrated and is the first such data reported for soluble spinach ferredoxin. Homogeneous rate constants have been determined in the presence of small molecule mediators using various electrochemical (98) and spectroscopic methods (41, 99). However, Fd reacts at membrane bound sites in vivo and a heterogeneous model for this process should offer a better simulation of the true reaction environment.

Observation of the relative rates and behavior of Fd as determined by transient and steady state techniques at these electrodes resulted in the following: 1) small differences in the rate of electron transfer were detected on varying time scales; 2) behavior indicative of ferredoxin adsorption on to the electrode is evident; 3) relatively large heterogeneous rates of electron transfer occur in comparison with other biological molecules studied at these surfaces; and 4) similar rates of oxidation and reduction are observed at the MVMG minigrid surface. Comparative studies of this type have not been conducted on the protein in its native environment, though general implications can be made concerning the mechanism at these surfaces.

The similarity in reaction rate for the transient and steady state experiments support electon transfer as the rate controlling

step in the reaction. If protein conformational changes or complexation are involved, they occur before electron transfer on the time scale of these experiments. Adsorption of the protein onto the surface is evident, though electron transfer can be effected through the adsorbed layer. The magnitude of the rate constant in comparison with that observed for cytochrome c at these surfaces would suggest the existence of a redox accessible reactive site in the protein matrix akin to that evident in cytochrome c. Oxidation also seems to occur via a mechanism similar to reduction.

The kinetic dependence of the reaction on factors such as ionic strength, pH and concentration should yield information on electrostatic effects on the rate or specific binding sites in the molecule. Additional experiments should be conducted at shorter time scales in order to detect the presence of transient pre-steps in the mechanism of oxidation or reduction. Thermodynamic parameters can also be obtained from temperature controlled studies at both the RRDE and minigrid surfaces.

This work has demonstrated the viability of the electrochemical techniques utilized in studying the reactions of Fd and similar molecules. This approach should allow for more indepth studies as described above which would give insight into the mechanism of electron transfer in these biologically important molecules.

REFERENCES

1. Sanadi, D. R., Ed. "Chemical Mechanisms in Bioenergetics", American Chemical Society: Wash., D.C., 1977.

2. Milazzo, G. Experientia (1980), 36, 1243.

3. Berg, H. Experientia (1980), 36, 1247.

4. Bockris, J. O. "Bioelectrochemistry", Keyzer, H.; Gutman, F., Eds.; Plenum Press: New York, 1980; pp. 5-17.

5. Cope, F. W. "Bioelectrochemistry", Keyzer, H.; Gutman, F., Eds.; Plenum Press: New York, 1980; pp. 297-327.

6. Wilson, D. F. Biochim. Biophys. Acta (1980), 616, 371.

7. Lamprecht, I.; Zotin, A. I. "Thermodynamics of Biological Processes", Walter de Gruyter: New York, 1978.

8. White, A.; Handler, P.; Smith, E. L.; Hill, B. L.; Lehman, I. R. "Principles of Biochemistry", McGraw-Hill: New York, 1978; p. 303.

9. Bard, A. J.; Faulkner, L. R. "Electrochemical Methods", John Wiley and Sons: New York, 1980.

10. Bauer, H. "Electrodics", John Wiley and Sons; New York, 1972; p. 33.

11. Simionescu, C. I.; Percec, V. Experientia (1980), 36, 1264.

12. Evans, M. G.; Gergely, J. Biochim. Biophys. Acta (1949), 3, 188.

13. McCarty, R. E. Photochem. Photobio. Rev. (1980), 5, 1.

14. Boardman, N. K. "Bioelectrochemistry", Keyzer, H.; Gutman, F., Eds; Plenum Press: New York, 1980; p. 100.

15. Losada, M.; Whatley, F. R.; Arnon, D. I. Nature (1961), 190, 606.

16. Arnon, D. I.; Tsujimoto, H. Y.; McSwain, B. D. Biochemistry (1964), 51, 1274.

17. Arnon, D. I.; Tsujimoto, H. Y.; Tang, G. M. S. FEBS Letters (1980), 120, 119.

18. Ke, B.; Shuvalov, V. A.; Dolan, E. "Frontiers of Biological Energetics", Dutton, P. L.; Leigh, J. S.; Scarpa, A., Eds., Vol. I, Academic Press: New York, 1978; p. 234.

19. Bouges-Bocquet, B. Biochim. Biophys. Acta (1980), 590, 223.

20. Hiyama, T.; Fork, D. C. Arch. Biochem. Biophys. (1980), 199, 488.

21. Fajer, J.; Davis, M. S.; Forman, A.; Klimov, V. V.; Dolan, E.; Ke, B. J. Am. Chem. Soc. (1980), 102, 7145.

22. Schneeman, R.; Krogmann, D. W. J. Biol. Chem. (1975), 250, 4965.

23. Arnon, D. I.; Whatley, R. R.; Allen, M. B. Nature (1957), 180, 182.

24. Arnon, D. I. Naturwissenschaften, (1969), 56, 295.

25. Arnon, D. I. Science, (1965), 149, 1460.

26. Shin, M.; Arnon, D. I. J. Biol. Chem. (1965), 240, 1405.

27. Ke, B.; Bulen, W. A.; Shaw, E. R.; Breeze, R. H. Arch. Biochem. Biophys. (1974), 162, 301.

28. Orme-Johnson, W. H. Ann. Rev. Biochem. (1973), 42, 159.

29. Lovenberg, W., Ed. "Iron-Sulfur Proteins", Vol. I-III; Academic Press: New York, 1973-1977.

30. Malkin, R.; Rabinowitz, J. C. Ann. Rev. Biochem. (1967), 36, 113.

31. Buchanan, B.; Arnon, D. I. Adv. Enz. Rel. Areas Mol. Bio. (1970), 33, 119.

32. Nomenclature Committee of the International Union of Biochemistry, Biochim. Biophys. Acta (1979), 549, 181.

33. Tagawa, K.; Arnon, D. I. Nature, (1962), 195, 537.

34. Gibson, J. F.; Hall, D. O.; Thornley, J. H. M.; Whatley, F. R. Proc. Nat. Acad. Sci. (1966), 56, 987.

35. Petersson, L.; Cammack, R.; Rao, K. K. Biochim. Biophys. Acta, (1980) 622, 18.

36. Palmer, G.; Dunham, W. R.; Fee, J. A.; Sands, R. H.; Hzuka, T.; Yonetani, T. Biochim. Biophys. Acta (1971), 245, 204.

37. Ochiai, E. "Bioinorganic Chemistry", Allyn and Bacon: Boston, 1977; pp. 168-217.

38. Carter, C. W.; Kraut, J.; Freer, S. T.; Alden, R. A. J. Biol. Chem. (1974), 249, 6339.

39. Matsubara, H.; Sasaki, R. M.; Chain, R. K. J. Biol. Chem. (1968), 243, 1725.

40. Matsubara, H.; Sasaki, R. M. J. Biol. Chem. (1968), 243, 1732.

41. Armstrong, F. A.; Henderson, R. A.; Segal, M. G.; Sykes, A. G. J. Chem. Soc.; Chem. Commun. (1978), 1102.

42. Tagawa, K.; Arnon, D. I. Biochim. Biophys. Acta (1968), 153, 602.

43. Wilson, D. F. Arch. Biochim. Biophys. (1967), 122, 254.

44. Wada, K. J. Biochem. (1979), 86, 1747.

45. Petering, D.; Fee, J. A.; Palmer, G. J. Biol. Chem. (1971), 246, 643.

46. Rawlings, J.; Siiman, O.; Gray, H. B. Proc. Nat. Acad. Sci. (1974), 77, 125.

47. Ogawa, K.; Tsukihara, T.; Tahara, H.; Katsube, Y.; Matsu-ura, Y.; Tanaka, N.; Kakudo, M.; Wada, K.; Matsubara, H. J. Biochem. (1977), 81, 529.

48. Kunita, A.; Koshibe, M.; Nishikawa, Y.; Fukuyama, K.; Tsukihara, T.; Katsube, Y.; Matsuura, Y.; Tanaka, N.; Kakudo, M.; Hase, T.; Matsubara, H. J. Biochem. (1978), 84, 989.

49. Mayerle, J. J.; Denmark, S. E.; Depamphilis, B. V.; Ibers, J. A.; Holm, R. H. J. Am. Chem. Soc. (1975), 95, 1032.

50. Adman, E. T. Biochim. Biophys. Acta (1979), 549, 107.

51. Sarai, A. Biochim. Biophys. Acta (1980), 589, 71.

52. Teo, B.; Shulman, R. G.; Brown, G. S.; Meixner, A. E. J. Am. Chem. Soc. (1979), 101, 5624.

53. Cowan, D. O.; Pasternak, G.; Kaufman, F. Proc. Nat. Acad. Sci. (1970), 66, 837.

54. Stombaugh, N. A.; Sundquist, J. E.; Burris, R. H.; Orme-Johnson, W. H. Biochemistry (1976), 15, 2633.

55. Stankovich, M. T. Anal. Biochem. (1980), 109, 295.

56. Chien, Y. W. J. Pharm. Sci. (1976), 65, 1471.

57. Orme-Johnson, W. H.; Beinert, H. Anal. Biochem. (1969), 32, 425.

58. Ke, B.; Hawkridge, F. M.; Sahu, S. Proc. Nat. Acad. Sci. (1976), 73, 2211.

59. Kuwana, T.; Szentrimay, R.; Yeh, P. "Electrochemical Studies of Biological Systems" Sawyer, D. T., Ed.; American Chemical Society: Wash., D.C., 1977; pp. 143-169.

60. Salmon, R. T.; Hawkridge, R. M. J. Electroanal. Chem. (1980), 112, 253.

61. Rickard, L. H.; Landrum, H. L.; Hawkridge, F. M. Bioelectrochem. Bioenerg. (1978), 5, 686.

62. Weitzman, P. D. J.; Kennedy, I. R.; Caldwell, R. A. F.E.B.S. Letters (1971), 17, 241.

63. Kuznetsov, B. A.; Mestechkina, N. M.; Shumakovich, G. P. Bioelectrochem. Bioenerg. (1977), 4, 1.

64. Kiselev, B. A.; Kazakova, A. A.; Yevstigneyev, V. B.; Gins, V. K.; Mukhin, Y. N. Biofizika (1976), 21, 35.

65. Dalton, H.; Zubieta, J. Biochim. Biophys. Acta (1973), 322, 133.

66. Hill, C. L; Renaud, J.; Holm, R. H.; Martenson, L. E. J. Am. Chem. Soc. (1977), 99, 2550.

67. Bianco, P.; Haladjian, J. Biochem. Biophys. Res. Commun. (1977), 78, 323.

68. Ikeda, T.; Toriyama, K.; Senda, M. Bull. Chem. Soc. Jpn. (1979), 52, 1937.

69. Kakutani, T.; Toriyama, K.; Ikeda, T.; Senda, M. Bull. Chem. Soc. Jpn. (1980), 53, 947.

70. Scheller, F.; Prumke, H. J.; Schmidt, H. E., Mohr, P. Bioelectrochem. Bioenerg. (1976), 3, 328.

71. Landrum, H. L.; Salmon, R. T.; Hawkridge, R. M. J. Am. Chem. Soc. (1977), 99, 3154.

72. Stargardt, J.; Hawkridge, R. M.; Landrum, H. L. Anal. Chem. (1978), 50, 930.

73. Bowden, E. F.; Wang, M.; Bailey, J. W.; Hawkridge, F. M.; Blount, H. N. J. Electrochem. Soc.; submitted.

74. Bockris, J.; Reddy, A. "Modern Electrochemistry" Vol. II, Plenum Press: New York, 1970; Chapters 8-9.

75. Bruckenstein, S.; Miller, B. Accts. Chem. Res. (1977), 10, 55.

76. Albertson, D. El; Blount, H. N.; Hawkridge, F. M. Anal. Chem. (1979), 51, 557.

77. Bancroft, E. E.; Blount, H. N.; Hawkridge, R. M. Adv. Chem. Ser. (1982), submitted.

78. Adams, R. N. "Electrochemistry at Solid Electrodes", Marcel Dekker: New York, 1969.

79. Albery, W. J.; Hitchman, M. L. "Ring-Disk Electrodes", Clarendon Press: London, 1971.

80. Napp, D. T.; Johnson, D. C.; Bruckenstein, S. Anal. Chem. (1967), 4, 481.

81. Hawkridge, F. M.; Kuwana, T. Anal. Chem. (1973), 45, 1021.

82. Shu, F. R.; Wilson, G. S. Anal. Chem. (1976), 48, 1676.

83. Davies, C. W.; James, A. M. "Dictionary of Electrochemistry", John Wiley and Sons: New York, 1976.

84. Cieslinki, R.; Armstrong, N. R. Anal. Chem. (1979), 57, 565.

85. Bowden, E. F.; Hawkridge, F. M.; Blount, H. N. Bioelectrochem. Bioenerg. (1980), 7, 447.

86. Albertson, D. E. M.S. Thesis, University of Delaware, Newark, DE, 1980.

87. Dasgupta, S.; Ryan, M. D. Bioelectrochem. Bioenerg. (1980), 7, 587.

88. Wei, I.; Ryan, M. D. Anal. Biochem. (1980), 106, 269.

89. Yeh, P.; Kuwana, T. Chem. Lett. (1977), 1145.

90. Eddowes, M. J.; Hill, H. A. O.; Uosaki. K. J. Am. Chem. Soc. (1979), 101, 7113.

91. Eddowes, M. J., Hill, H. A. O. J. Am. Chem. Soc. (1979), 101 4461.

92. Crawley, C. D.; Hawkridge, F. M. Biochem. Biophys. Res. Commun. (1981), 99, 516.

93. Petek, M.; Neal, T. E.; Murray, R. W. Anal. Chem. (1971), 43, 1069.

94. Scheller, F.; Janchen. M.; Etzold, G.; Will, H. Bioelectrochem. Bioenerg. (1974), 1, 478.

95. Scheller, F.; Strnad, G.; Neumann, B.; Kuhn, M. Bioelectrochem. Bioenerg. (1979), 6, 117.

96. Bowden, E. F.; Hawkridge, F. M.; Blount, H. N. Adv. Chem. Ser., (1982), submitted.

97. Scheller, F. Bioelectrochem. Bioenerg. (1977), 4, 490.

98. Dasgupta, S. R., Ph.D. Dissertation, Marquette University, Milwaukee, Wisconsin, 1980.

99. Rawlings, J.; Wherland, S.; Gray, H. B. J. Am. Chem. Soc. (1977), 99, 1968.

Vita